INFLUENZA A VIRUS MATRIX PROTEIN M1 :
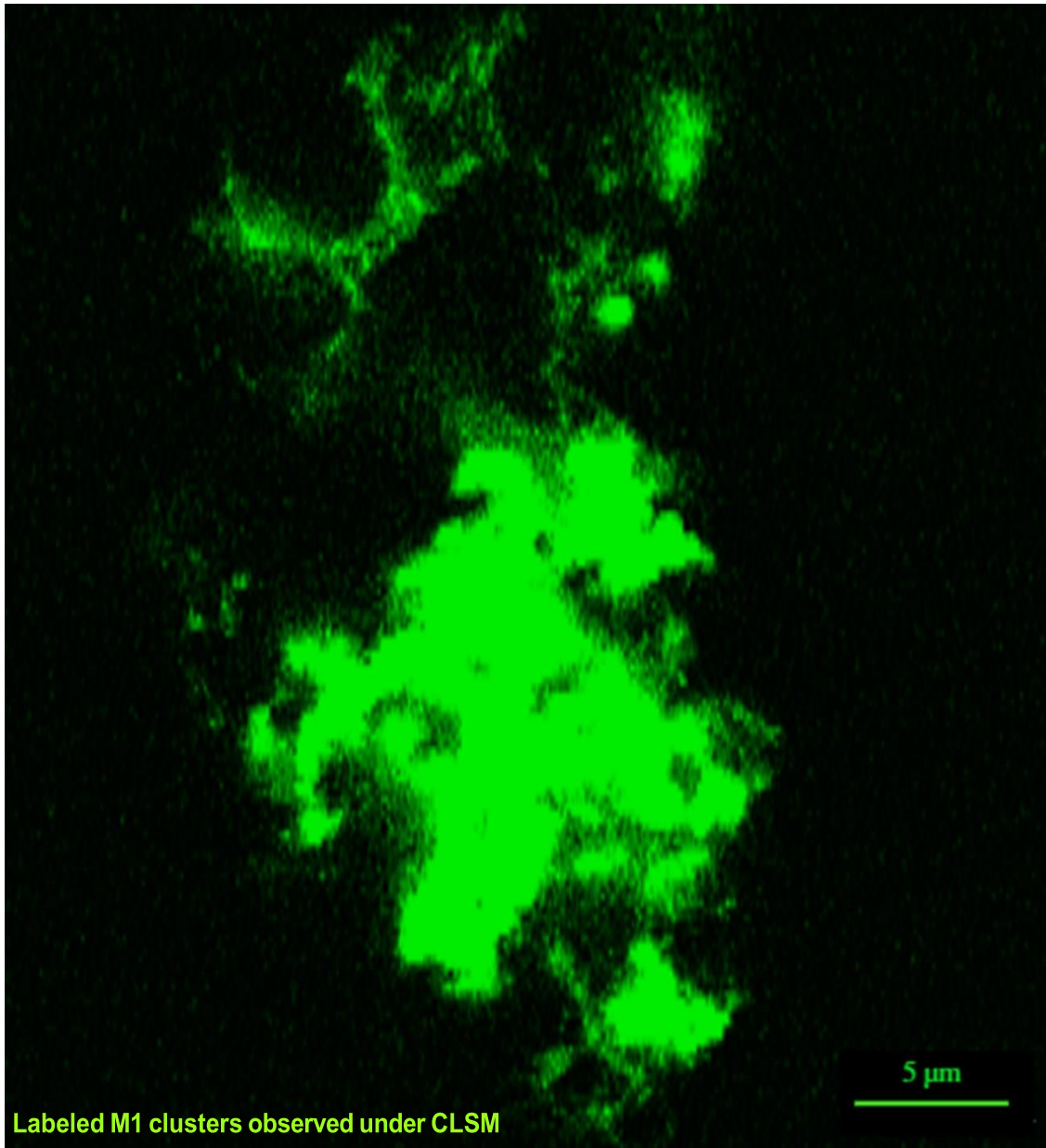
Structural determinants of membrane binding and protein-induced deformation

Labeled M1 clusters observed under CLSM

5 µm

ISMAIL DAHMANI

Influenza A virus matrix protein M1 :
Structural determinants of membrane binding and protein-induced deformation

Univ.-Diss.
zur Erlangung des akademischen Grades
"doctor rerum naturalium"
(Dr. rer. nat.)
in der Wissenschaftsdisziplin " Molekulare Biochemie "

Eingereicht an der
Mathematisch-Naturwissenschaftlichen Fakultät
Institut für Biochemie und Biologie
der Universität Potsdam

Vorgelegt von
ISMAIL DAHMANI
September 2020

Ort und Tag der Disputation: Potsdam, 10. Februar 2021

Hauptbetreuer:
Prof. Dr. Salvatore Chiantia

Gutachter:
PD Dr. Michael Veit
Dr. Oleg V. Batishchev

III

To avoid the discontinuity for reading, the references are added at the end of each paragraph in an order corresponding to the beginning and the end of each paragraph.

Parts of this research have already been published:

1. Höfer, C. T.; Di Lella, S.; **Dahmani, I**.; Jungnick, N.; Bordag, N.; Bobone, S. et al. (2019a): Structural determinants of the interaction between influenza A virus matrix protein M1 and lipid membranes. In: Biochimica et Biophysica Acta (BBA) - Biomembranes 1861 (6), S. 1123–1134. DOI: 10.1016/j.bbamem.2019.03.013.I. (In this work I performed SPR analysis of M1 binding to membrane model represented by a lipid monolayer.)

2. **Dahmani I**, K. Ludwig, S. Chiantia, (2019). Influenza A matrix protein M1 induces lipid membrane deformation via protein multimerization. In: Bioscience Reports 39 (8). DOI: 0.1042/BSR20191024.

3. Dey, Pradip; Bergmann, Tobias; Cuellar-Camacho, Jose Luis; Ehrmann, Svenja; Chowdhury, **Dahmani I**, Haag R, Azab W, Mohammad Suman, Zhang, Minze. (2018): Multivalent Flexible Nanogels Exhibit Broad-Spectrum Antiviral Activity by Blocking Virus Entry. In ACS nano 12 (7), pp. 6429–6442. DOI: 10.1021/acsnano.8b01616. (In this work I performed SPR analysis of NP binding.)

4. Kolyvushko O, Latzke J, **Dahmani I**, Osterrieder N, Chiantia S, Azab W. (2020). Differentially-Charged Liposomes Interact with Alphaherpesviruses and Interfere with Virus Entry. In Pathogens. 9, 359 DOI: 10.3390/pathogens9050359 (In this work I performed SPR and CSLM analysis of virus binding to lipids).

Parts of this thesis have been presented at the following conferences:

1. Oral Talk. Biennial Meeting. German Biophysical Society, Düsseldorf, Germany, September 2018.

2. Oral Talk. DPG Spring Meeting, Regensburg, Germany, April 2019.

3. Poster. First European & 10th German BioSensor Symposium (EBS/DBS), Potsdam, Germany, March 2017.

4. Poster. DGfB-Membrane Models for Biophysics, Drübeck, Germany, March 2018.

5. Poster. Molecular Biophysics Meeting, Hünfeld, Germany, April 2019.

Table of Contents

List of Abbreviations

Arf1	adp-ribosylation factor 1
C2 domain	conserved domain 2
CL	cardiolipin
CLSM	confocal laser scanning microscopy
COPI / COPII	coatomer protein complex i/ii
cryo-ET	cryogenic -electron tomography
cryo-TEM	cryogenic transmission electron microscopy
DOPC	1,2-dioleoyl-sn-glycero-3-phosphocholine
DOPS	1,2-dioleoyl-sn-glycero-3-phospho-l-serine
DOTAP	1,2-dioleoyl-3-trimethylammonium-propane
ESCRT	endosomal sorting complex required for transport
F-BAR	fes/cip4 homology-bin/amphiphysin/rvs protein
FCS	fluorescence correlation spectroscopy
FRAP	fluorescence recovery after photobleaching
Gag	group-specific antigen
GMAP-210	Golgi microtubule-associated protein 210
HA	hemagglutinin protein
HCV NS4B	hepatitis c virus non-structural protein 4b
HPA	hydrophobic adsorption
HPP	hydrophobic planar alkyl layer
I-BAR	inverse bin/amphiphysin/Rvs protein
ISAV	influenza salmon anaemia virus
ITO	indium tin oxide
L_D phase	lipid-disordered phase
L_O phase	liquid-ordered phase
LUVs	large unilamellar vesicles
M1	matrix protein 1

M2	matrix protein 2
N&B	number and brightness
NA	neuraminidase protein
N-BAR	n-terminal amphipathic helix-containing bin/amphiphysin/rvs
NEP	nuclear export protein
NLS	nuclear localization signal or sequence
NS2	non-structural protein 2
PA	polymerase acidic
PA	phosphatidic acid
PB1/2	polymerase basic protein 1/2
PBD	polybasic domain
PE	phosphatidylethanolamine
PG	phosphatidylglycerol
PHE	2-(4-(3-(4-acetyl-3-hydroxy-2-propylphenoxy)propoxy) phenoxy acetic acid
PI 3-P	phosphatidylinositol trisphosphate
PI 2-P	phosphatidylinositol biphosphate
PIPs	phosphatidylinositides
POPC	1-palmitoyl-2-oleoyl-glycero-3-phosphocholine
POPS	palmitoyl-2-oleoyl-sn-glycero-3-phospho-l-serine
PtdA	phosphatidic acid
PtdIns 3-kinase	phosphatidylinositol 3-kinase
RICS	raster image correlation spectroscopy
RU	resonance units
SAR1	secretion associated Ras-related GTPase 1A
SEC	size exclusion chromatography
SF9	spodoptera frugiperda 9
SFV nsp1	semliki forest virus (sfv) non-structural protein 1 (nsp1)
SLBs	supported lipid bilayers

SOPC	1-stearoyl-2-oleoyl-sn-glycero-3-phosphocholine
SNARE	soluble n-ethylmaleimide-sensitive factor attachment protein receptor
SPR	surface plasmon resonance
SV-AUC	sedimentation velocity analytical ultracentrifugation
vRNA	viral RNA
VP40	viral protein 40
vRNP	viral ribonucleoprotein

Abstract

Influenza A virus (IAV) is a pathogen responsible for severe seasonal epidemics threatening human and animal populations every year. During the viral assembly process in the infected cells, the plasma membrane (PM) has to bend in localized regions into a vesicle towards the extracellular side. Studies in cellular models have proposed that different viral proteins might be responsible for inducing membrane curvature in this context (including M1), but a clear consensus has not been reached. M1 is the most abundant protein in IAV particles. It plays an important role in virus assembly and budding at the PM. M1 is recruited to the host cell membrane where it associates with lipids and other viral proteins. However, the details of M1 interactions with the cellular PM, as well as M1-mediated membrane bending at the budozone, have not been clarified.

In this work, we used several experimental approaches to analyze M1-lipids and M1-M1 interactions. By performing SPR analysis, we quantified membrane association for full-length M1 and different genetically engineered M1 constructs (i.e., N- and C-terminally truncated constructs and a mutant of the polybasic region). This allowed us to obtain novel information on the protein regions mediating M1 binding to membranes. By using fluorescence microscopy, cryogenic transmission electron microscopy (cryo-TEM), and three-dimensional (3D) tomography (cryo-ET), we showed that M1 is indeed able to cause membrane deformation on vesicles containing negatively-charged lipids, in the absence of other viral components. Further, sFCS analysis proved that simple protein binding is not sufficient to induce membrane restructuring. Rather, it appears that stable M1-M1 interactions and multimer formation are required to alter the bilayer three-dimensional structure through the formation of a protein scaffold.

Finally, to mimic the budding mechanism in cells that arise by the lateral organization of the virus membrane components on lipid raft domains, we created vesicles with lipid domains. Our results showed that local binding of M1 to spatial confined acidic lipids within membrane domains of vesicles led to local M1 inward curvature.

I Introduction

1. Membranes

1.1 General structure of lipids

Hundreds of phospholipids forming the plasma membrane (PM) of mammalian cells are classified regarding the degree of saturation (unsaturated, saturated), length of their acyl chains, and the characteristics of the head groups. The most important lipids in animal cells are considered to be the glycerophospholipids (Figure 2). This includes phosphatidylcholine (POPC/SOPC), phosphatidylethanolamine (PE), phosphatidylserine (POPS), phosphatidylinositol (PI), phosphatidylglycerol (PG). Figure 1 represents the general chemical structure of these lipids. The second-largest class of PM lipids is represented by the sphingolipids, unlike glycerophospholipids, they contain sphingosine instead of glycerol (Castillo et al. 2016).
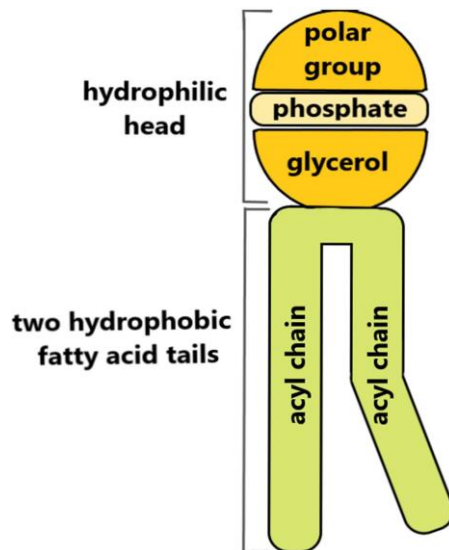
Figure 1 General schematic chemical structure of phospholipids

The glycerol backbone forms the central basic part of glycerophospholipids. Acyl chains (tails) that can differ in length and degree of saturation are attached to the sn-1/ sn-2 hydroxyl groups. Different hydrophilic head groups are bound to the glycerol backbone through phosphodiester bonds at the sn-3 position. These head groups confer unique biophysical characteristics that allow differentiating between the different phospholipid classes.

lipid abbreviation	Rhodamine-DOPE	POPS	DOPS	DPPG	DOTAP	DOPC	DSPC
net charge (pH=7)	0	-1	-1	-1	+1	0	0

lipid abbreviation	PI4P	PI3P	PI(4,5)P2
net charge (pH=7)	-2	-2	-4
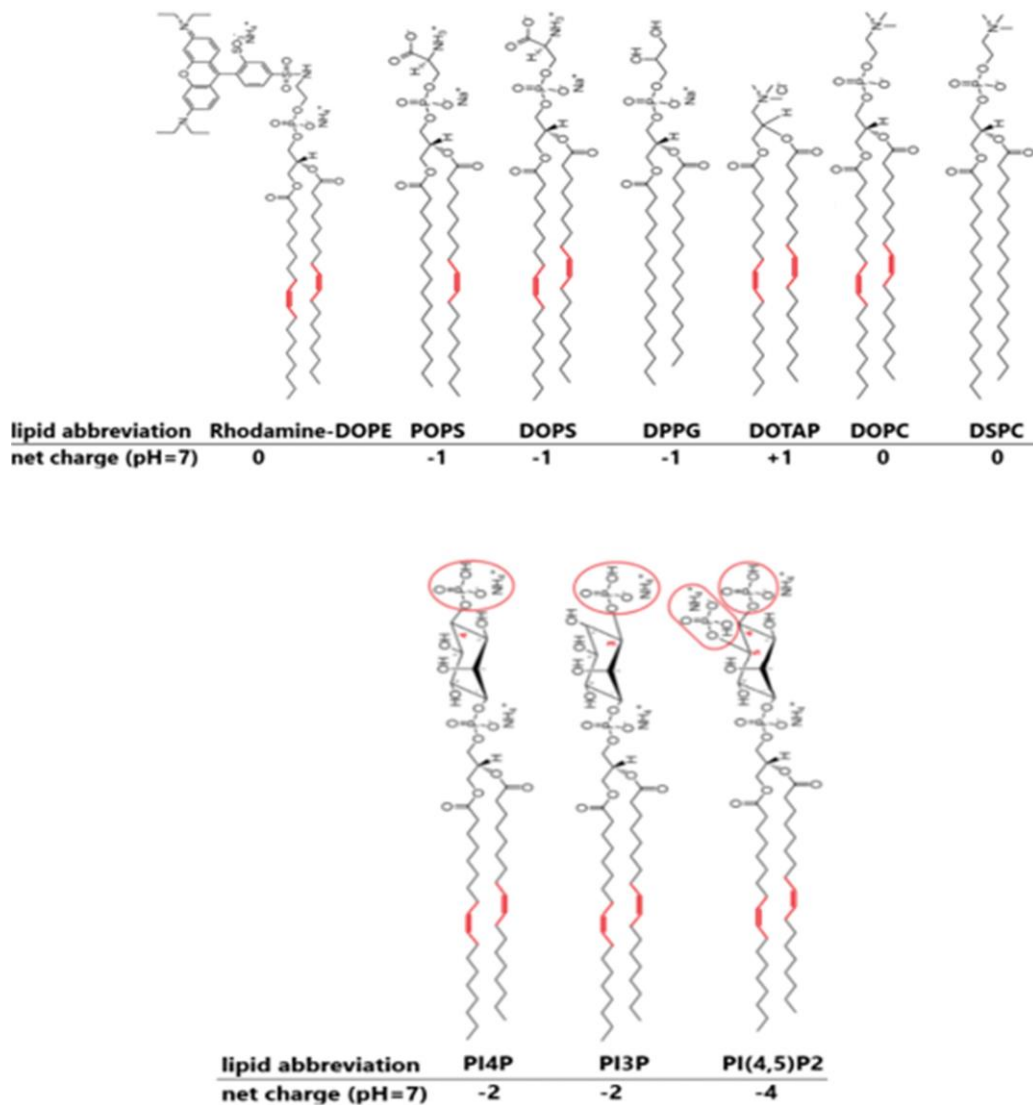
Figure 2 Detailed chemical structure of glycerophospholipids. Chemical structures of common glycerophospholipid molecules with indicated headgroup, glycerol, and acyl chain components. Red lines in the acyl chain represent the double bonds (adapted from (Luchini and Vitiello 2019; Muftuoglu et al. 2016).

The unsaturated phospholipids possess one or more *cis* double bond on the acyl hydrocarbon chains that creates a rigid bend (kink) with a 30° torsion angle on the tails. This bend disturbs the attractive van der Waals forces and prevents the hydrophobic interaction between neighboring acyl chains which interfere with the tight packing of the phospholipids. The decreased packing makes the bilayer less ordered and causes an increase in membrane fluidity (rotational and lateral diffusion mobility). The saturated phospholipids (no double bonds) possess straight acyl hydrocarbon chains that allow strong van der Waals and hydrophobic interactions which are more favorable for their packing. This increased packing makes the membrane more ordered, stable, and less fluid. Figure 3 shows acyl chain characteristics in the presence or absence of double bonds or the effect of temperature on their conformation (Saeedimasine et al. 2019; Pichler und Emmerstorfer-Augustin 2018; Balleza 2012; Casares et al. 2019). Furthermore, besides the degree of saturation, a longer chain in comparison to shorter tails increases van der Waals interactions.
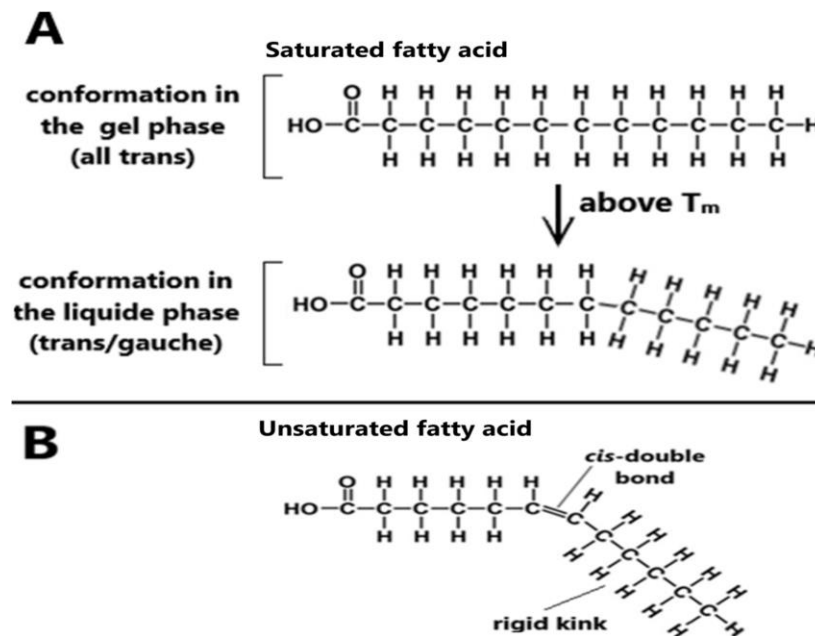
Figure 3 Detailed chemical structure of acyl chains. **A**) High melting temperature lipids (tends to have long/saturated tails). In the gel phase, acyl chains of saturated lipids adopt all-*trans* conformation. Increasing temperature causes rotation isomerization between *trans* and *gauche* conformations.
B) Low melting temperature lipids tend to have unsaturated tails. The double bonds introduce a rigid kink..

1.2 Cholesterol

Cholesterol is a non-phospholipid and very non-polar membrane component. It is considered the main sterol in mammalian cells. Cholesterol has a vital role and is highly enriched in the PM (30-40%) compared to the other intracellular membranes (van Meer und Kroon 2011).

Its structure consists of large hydrophobic and small hydrophilic domains. The small hydrophilic hydroxyl group (-OH) is in contact with the aqueous environment. It can interact with the polar group of the neighboring phospholipids through stabilizing hydrogen bonds. Figure 4 represents the schematic chemical structure of cholesterol (Olsen et al. 2013; Ohvo-Rekilä et al. 2002; Gater et al. 2013).
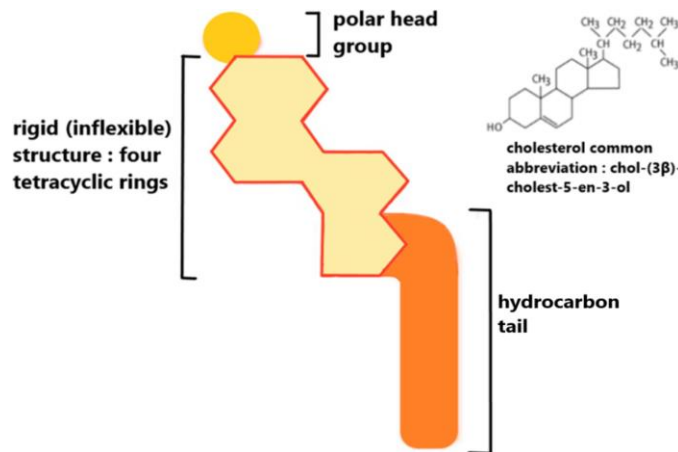
Figure 4 General schematic chemical structure of cholesterol (adapted from Vella 1994).

The large hydrophobic domain is divided into two parts, the first one includes a short thermally flexible, hydrocarbon tail. The second part includes a long rigid hydrophobic chain. Its structure consists of a tetracyclic ring [bulky steroid- ring] that adopts a *trans* conformation. The smooth α-face of the ring allows a tight attractive van der Waals and hydrophobic interactions with the acyl-chain methyl groups of the phospholipids. Cholesterol shows a strong preferential

interaction and packing with saturated lipids and weak interaction with the unsaturated ones. In the presence of cholesterol, the hydrocarbon chain of the saturated lipids becomes fully extended and rigid (Subczynski et al. 2017; Pandit et al. 2008; Ermilova und Lyubartsev 2018).

Recent work showed that cholesterol has also a high affinity for SOPS (1-stearoyl-2-oleoyl-sn-glycero-3-phospho-L-serine), while low interaction is reported with DOPS, POPS, PLPS (Martinez-Seara et al. 2008; Róg et al. 2007; Hac-Wydro und Wydro 2007; Breidigan et al. 2017; Maekawa und Fairn 2015).

Cholesterol is the main modulator of the PM physicochemical properties, its presence can change the basic mechanical characteristics of the lipid bilayer like fluidity, bending rigidity (less deformable), bilayer thickness, and membrane lateral tension. Secondly, by fitting into the spaces between phospholipids, cholesterol decreases membrane permeability to small water-soluble molecules due to the so-called condensing effect that increases order and packing of lipids. However, the cholesterol effect on PM biomechanics in mammalian cells showed totally inverse effects in comparison to artificial PM vesicles made of pure lipids. In fact, studies showed that cholesterol depletion in cells increased membrane rigidity and decreased lateral diffusion of lipids, while in pure lipid cholesterol enrichment increased membrane rigidity (Byfield et al. 2004; Oh et al. 2009; Sun et al. 2007; Zhang et al. 2019; Needham et al. 1990; Khatibzadeh et al. 2013).

1.3 Plasma membrane anionic lipids

Acidic (anionic) glycerophospholipids, particularly phosphatidylserine (PS), phosphatidic acid (PtdA), (PG), cardiolipin (CL), phosphatidylinositides (PIPs) and its phosphorylated derivatives (PI(4)P, PI(4,5)P$_2$, PI(3,4,5)P$_3$) are exclusively restricted to the cytoplasmic leaflet of the PM and intracellular membranes in mammalian cells or bacteria. This enrichment favors the binding by electrostatic

interactions of polycationic proteins or the specific binding of proteins containing a PS or inositol binding domain (ex C2 domain) (Hammond et al. 2012; Balla 2013; Yeung et al. 2008; Cho und Stahelin 2006; Hammond und Balla 2015; Moravcevic et al. 2012; Heo et al. 2006; Leventis und Grinstein 2010; McLaughlin und Murray 2005; McLaughlin et al. 2002; Wang et al. 2002).

Due to their basic surface, many viral matrix proteins, including M1, VP40, Gag can bind to the inner leaflet of the infected cell or to membrane models enriched with anionic lipids (Bobone et al. 2017; Chukkapalli et al. 2013; Johnson et al. 2016; Ruigrok et al. 2000b; Datta et al. 2007).

1.3.1 Inositol lipids

The multivalent negatively charged phosphoinositides PIPs are represented at the PM of mammalian cells essentially by the divalent acidic lipids $PI(4,5)P_2$. They represent 0.5-1.0 % mol% of the phospholipids present in the PM inner leaflets and intracellular membranes. $PI(4,5)P_2$ net negative charge is -4 depending on pH and other factors (McLaughlin et al. 2002; Kutateladze 2010; Aloia et al. 1993; Chan et al. 2008; Maldonado und Blough 1980; Rusten und Stenmark 2006).

1.3.2 Phosphatidylserine

Phosphatidylserine has a single net negative charge ($z=-1$). In mammalian cells, PS is synthesized by two distinct PS synthases (PSS1/ PSS2) which exchange the polar head-group of existing phospholipids (PC or PE) by L-serine. PS is distributed widely among animals, plants, and microorganisms. In eukaryotes, PS is the most abundant anionic phospholipid in the PM cytosolic leaflet (15-20 mol%) (Luchini und Vitiello 2019; Leventis und Grinstein 2010; Vance 2008; Vance 1990).

In nature, palmitoyl-2-oleoyl-sn-glycero-3-phospho-L-serine (POPS) represents the main form of PS. It includes one shorter saturated acid chain (16:0-18:1). The 1,2-dioleoyl-sn-glycero-3-phospho-L-serine (DOPS) has two unsaturated acyl chains (18:1-18:1). For our work, we opted for DOPS as an alternative. Since it is more stable to oxidation and has similar physical properties to the naturally occurring brain PS (Luchini und Vitiello 2019; Bigay und Antonny 2012; 1,2-Dioleoyl-sn-glycero-3-phospho-L-serine, sodium salt - PubChem).

Recent experiments performed on asymmetric model membranes and cells showed that the physical interaction of cholesterol with PS (18:0/18:1) allowed asymmetric distribution of cholesterol and its retention on the same leaflet as for PS. Interestingly this led to the formation of L_O domains enriched with both cholesterol and PS. In parallel, PS depletion caused cholesterol asymmetry loss and domain disappearance. These results could suggest that besides the role played by enzymes in the membrane transport of cholesterol between the leaflets, the asymmetric distribution of cholesterol is depending on the distribution of lipids like PS or saturated lipids (Maekawa und Fairn 2015).

1.4 Membrane domains and the "lipid raft" concept

The different lipids composing the PM may organize in two physical phases. The liquid-ordered phase (L_O phase) is stabilized by high levels of cholesterol and saturated lipids making it less fluid. The lipid-disordered phase (L_D phase) is formed by unsaturated phospholipids and is less enriched with cholesterol (more fluid).

The L_O phase within the PM of mammalian cells forms transient microdomains (10-200 nanometers large). These domains called lipid rafts may float freely and spread flatly on the surface of the PM. The raft domains correspond to the lateral segregation of saturated lipids like sphingomyelin (SM) and glycosphingolipids

such as gangliosides (GT1b, GM1). The driving force behind lateral phase separation and raft domain formation is due to the strong attraction between saturated lipids and cholesterol. The disordered tails of the unsaturated lipid create a difference in the average dipole density between the two domains which leads to an effective repulsion between them. (Bavari et al. 2002; Sezgin et al. 2017; Farnoud et al. 2015; Olsen et al. 2017; Heberle et al. 2011; Allender und Schick 2006; Veatch et al. 2003; Wang et al. 2015; Subczynski et al. 2017; Pandit et al. 2008; Ermilova et al. 2018; Eggeling et al. 2009; Ekyalongo et al. 2015).

Rafts domains have been implicated in a large number of physiological functions in cells that include intracellular signaling and trafficking, protein sorting, membrane fusion, virus budding (Simons et al. 1997; Takeda et al. 2003; Gassart et al. 2003; Brown und London 1998; Helms und Zurzolo 2004; Hanzal-Bayer und Hancock 2007; Diaz-Rohrer et al. 2014; Alonso und Millán 2001).

Lipid rafts in cells have been identified as detergent-resistant membranes (DRMs) since they remain intact and resist extraction with nonionic detergents (Brown 2006). However, direct observation of rafts in biological membranes is not possible since these domains are small in size and have a transient dynamic behavior (Crane und Tamm 2004; Hoekstra et al. 2003; Nayak et al. 2004; Veit und Thaa 2011; Barros et al. 2016; Simons et al. 2000).

Meanwhile, artificial raft-like domains could be obtained with bigger size when using GUVs made from a mixture of unsaturated phospholipids and fully saturated lipids in the presence of cholesterol. These raft-like domains are supposed to be a good model to simulate the inhomogeneous organization in cell PMs and to study their behavior with standards fluorescence microscopy (Simons und Sampaio 2011; Brown 2006; Wang et al. 2015; Magee et al. 2003).

The apical PM of polarized cells contains more cholesterol/sphingolipids in comparison to the basolateral surface. This creates areas on the PM called budozones which are potential sites for influenza virus budding (Gerl et al. 2012).

1.5 Mechanical properties of the membrane

Membrane dynamical and elastic properties are important for a wide range of biological functions such as budding and egress of viruses, endocytic membrane fusion, fission, cell division and movement, the clustering of cell signaling proteins, organelle shaping, etc (Deseri und Zurlo 2013; Lipowsky 2014; Dimova 2014).

As observed with simulation studies or when using artificial membrane systems, bending rigidity and surface tension are supposed to be the primary forces opposing the lipid bilayer deformation. The physical reason that explains the elastic behavior of the lipid bilayer is that bending causes an increased distance between the lipid's head groups and the exposition of the hydrophobic core to water which is energetically unfavorable. For this reason, the dominant shape with the lowest energy arising from the three-dimensional disposition of lipids corresponds in most cases to a vesicle. To overcome membrane resistance to bending (curving) and stretching, a larger localized force has to be applied to bring the missing energy needed to deform the membrane locally. The external factors that can curve the bilayer could arise from mechanical pulling/pushing forces or the lateral tension that could be applied by bound proteins, lipids asymmetry, small molecules, or by osmotic pressure (Lipowsky 2014; Dimova 2014; Alimohamadi 2018; Doktorova et al. 2017; Waugh et al. 1992; Guckenberger und Gekle 2017; Marsh 2007).

Vesicles or cell membranes can either be curved toward the lumen or either curved away from it. When a positive curvature arises on the inner leaflet, the corresponding outer leaflet will undergo a negative curvature. If we assume that each leaflet is treated as an independent elastic plate, thus we can consider that, during bilayer curvature, when the outer monolayer is stretched the opposite inner monolayer is compressed (Jarsch et al. 2016b).

In our work, we consider the membrane vesicle curvature as being negative if the bilayer is locally bent away from the side in which the protein is bound and positive if it is bent toward the protein side.

1.5.1 The bending rigidity modulus

The bending rigidity or the elastic modulus (κ) is a measure of the energy required to bend the membrane. This parameter describes a mechanical characteristic of the membrane (stiffness) which depends on the membrane composition (Helfrich 1973).

Membranes made with lipid mixtures of unsaturated phospholipids and cholesterol show a lower bending modulus while membranes including lipids with saturated acyl chains and cholesterol have a higher bending modulus. For fluid membranes, the bending modulus can vary between 10-100 $k_B T$ (k_B is the Boltzmann constant and T is the absolute temperature). However, in general, for biological lipid bilayers, it's usually estimated to be ~20 $k_B T$ (Marsh 2007; Waugh et al. 1992; Guckenberger und Gekle 2017; Jarsch et al. 2016a; Helfrich 1973; Roux et al. 2005; Pan et al. 2009; Marsh 2006).

1.6 Mechanisms of membrane curvature

Lipid membranes are deformable and fluidic by nature. The tendency of the membrane to bend rather than to stretch or compress in presence of applied force or due to lateral line tension is reasonably explained by the natural behavior of the lipid bilayer to conserve its surface area. To determines the minimum energy configuration of a membrane, a constraint is implemented using a Lagrange multiplier (representing membrane tension for the incompressibility constraint). There are several proposed mechanisms to explain lipid or proteins mediated positive or negative curvature at the PM (Shin et al. 2012; Brown 2012).

These mechanisms can either be intrinsic to the membrane bilayer (lipid composition, presence of integral protein) or can be brought by extrinsic factors like protein binding.

At least four mechanisms are reported: scaffolding, crowding, wedging effect, heterogeneous distribution of different lipids.

1.6.1 Scaffolding mechanism

Membrane curvature mediated by scaffolding can either arise by binding of the shaped protein or by a protein that forms shaped oligomers after binding.

1.6.1.1 Shaping proteins

Many peripheral proteins can show an individual intrinsic curved shape with a rigid hydrophilic part that interacts with the membrane by electrostatic interactions or via adaptors. Such cases include the coatomer protein family (COPI and COPII) and the classical Bin–Amphiphysin–Rvs (BAR) domain. For example, the (F-BAR, I-BAR) proteins can sense and create membrane curvature and they are disposed of in a specific way to form a dimer that exhibits an intrinsic "banana" shape.

These proteins are often recruited via their positively charged residues at sites enriched with PS and/or PIP2/PIP3. Then the bound proteins can cause membrane curvature (either positive or negative) by imposing their crescent rigid shape on the membrane surface.

Figure 5 shows an example of how rigid proteins with intrinsic curvature can peripherally bind to membrane rich with anionic lipids.
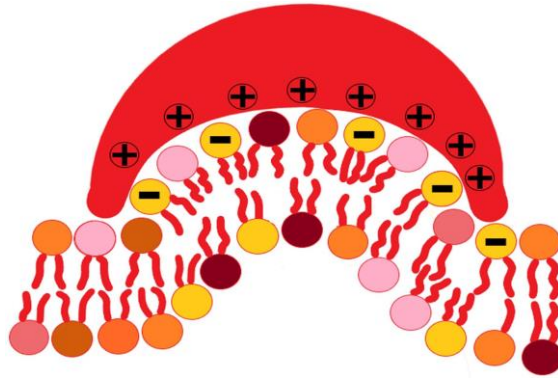
Figure 5 Membrane curvature mediated by shaping proteins. BAR-domain proteins bind on membranes via their basic-charged amino acid residues then generate curvature that fellow the geometries corresponding to the structures of the membrane-binding surface (nanoscopic scaffolding).

The sufficient contacts through strong Coulomb interactions due to the presence of polybasic domains in the concave region allow the protein to impose their shape for molding the membrane into either a positive or negative curve (Frost et al. 2008; McMahon und Gallop 2005; Schweitzer und Kozlov 2015; Zimmerberg und Kozlov 2006; Mim und Unger 2012; Gallop et al. 2006; Peter et al. 2004; Henne et al. 2007; Itoh et al. 2005; Dharmalingam et al. 2009).

1.6.1.2 Scaffolding via protein oligomerization

Other peripheral proteins with a spherical or slightly curved shape have the capacity to oligomerize upon binding to the membrane. The binding could be either directly with lipids via electrostatic interaction (for some proteins partial insertion of the amphipathic helices is required) or indirectly via adaptor proteins that link them to membranes. Then the formed oligomer complexes create a kind of rigid coat (scaffold) up to a micrometer scale with a specific shape (curved positively or negatively). Following that, the membrane part bound to it undergoes deformation by following the contour of the coat (molding effect). To deform a membrane by scaffolding, the energetic gain upon coat formation has to

be at least equal to the energetic cost required for membrane deformation (Henrich et al. 2017; Hu et al. 2008; Simunovic et al. 2015; Farsad et al. 2003).

Examples of such proteins that multimerize to bend the membrane include the HIV Gag protein, COPI/COPII protein complexes, caveolins, or clathrin triskelion that mediate endocytosis. The dynamin family proteins also multimerize into spirals (helical oligomers) to form organelles with tubulated morphology. Cytoskeletal filamentous proteins such as septins can also polymerize at curved membranes and promote membrane tubulation alone or in the presence of actin/ microtubules. Besides their individual capacity to bend membrane, BAR domain proteins (F-BAR, I-BAR, N-BAR) can also further oligomerize to allow tubulations and vesiculation.
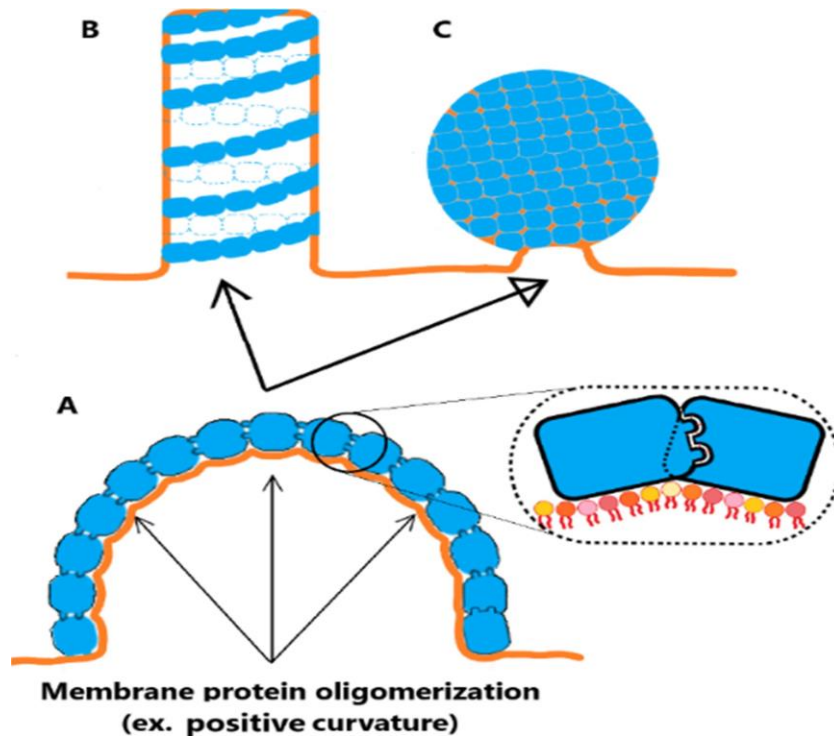
Figure 6 Membrane curvature mediated by protein oligomerization. After their biding, the proteins oligomerize by the coordinated assembly to form a scaffold or a lattice structure that imposes a force to bend the membrane. **A**) An example of membrane budding (ex-positive curvature) mediated by protein oligomerization. (**B, C**) The multimerized proteins can organize into a superstructure forming either helices or spheres. Such examples (with positive curvature) include the formation of intracellular carriers related to clathrin or the COPI/ COPII coat protein complexes or extracellular carriers related to the virus budding (with negative curvature).

Figures 6 and 7 represent different ways of membrane deformation due to protein oligomerization (Peter et al. 2004; Dick and Vogt 2014; Antonny 2011; Dawson et al. 2006; Beber et al. 2019; Bertin et al. 2010; Garcia et al. 2011; Bertin et al. 2008; Antonny et al. 2005).
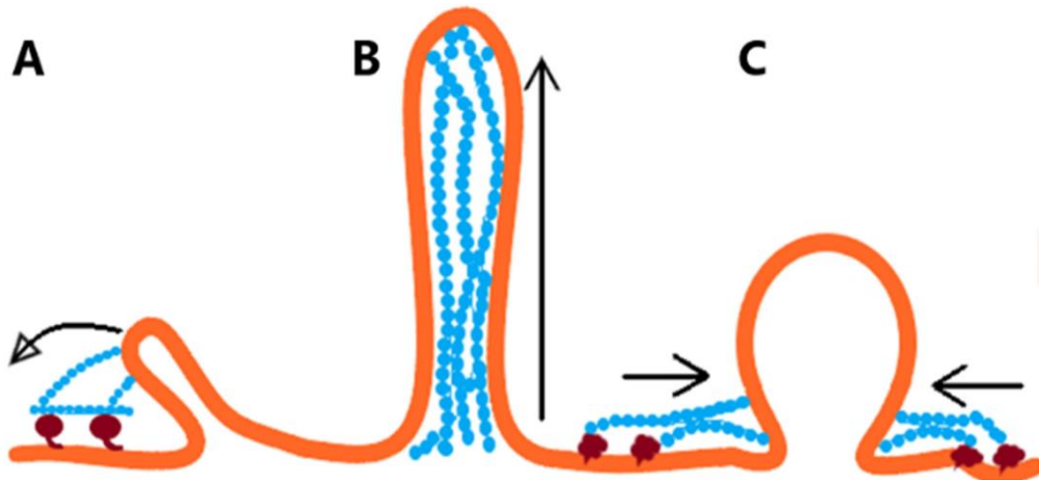
Figure 7 Membrane tubulations mediated by protein cytoskeleton polymerization in the presence of motor proteins. Actin cytoskeleton polymerization outside the membrane. The pulling forces are exerted on the tip of a tube (ex-filamentous viruses budding). **B**) Actin cytoskeleton polymerization inside the membrane. The stretching/pushing forces are exerted on the extremity of a tube (ex-lamellipodia/ filopodia/ protrusions). **C** Actin cytoskeleton polymerization outside the membrane. The pushing forces are exerted on the boundary (ex-clathrin mediated endocytosis).

1.6.2 Crowding mechanism

Proteins attached to the membrane surface at high density generate steric confinement. Then the induced lateral pressure driven by protein-protein thermal lateral collisions leads to membrane spontaneous bending. This mechanism was demonstrated by studying the binding of monomeric hydrophilic proteins to GUVs. GFPs bound via their His-tag and locally confined on membrane domains of GUVs caused membrane tubulations by steric crowding. Figure 8 shows a simple presentation of such protein crowding mediated

membrane curvature (Stachowiak et al. 2010; Stachowiak et al. 2012; Busch et al. 2015; Zhao et al. 2013; Chen et al. 2016; Ford et al. 2002). However, it is not clear if such protein confining concentrations can be achieved on PM of cells to reach the required level for steric-induced membrane bending (Kozlov et al. 2014).
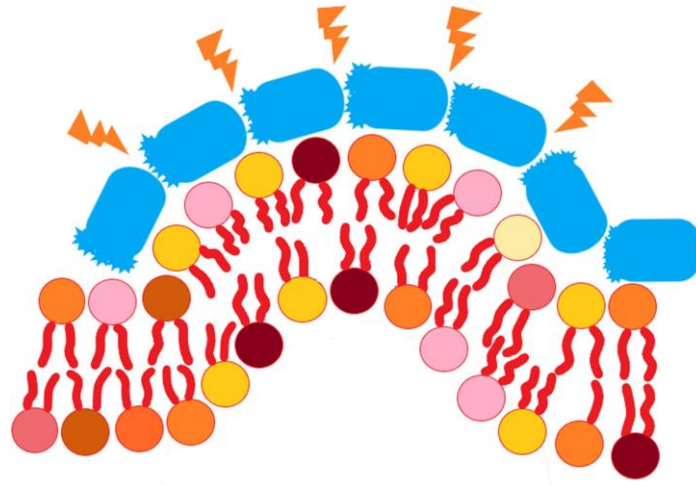
Figure 8 Membrane curvature generated by protein crowding. Proteins binding and localization at high density create lateral pressure that forces the bilayer to bend due to steric effect (orange triangles represent the energy arising from the proteins collision).

1.6.3 Wedging mechanism

Another effective way of inducing local membrane curvature is by asymmetric insertion of amphipathic helical (AHs) domains in the membrane that create a wedging effect. This curvature could either be positive or negative depending on the shape of the inserted domain. Many non-transmembrane proteins have peptide sequences that are in a disordered state (unfolded) when present in the solution. However, after their binding to the PM, the concerned peptide sequences can fold into α-helices. The created α-helices are characterized by one hydrophobic protein motif and one polar face giving them an amphipathic character. The hydrophobic side of the helix penetrates and competes for space between the lipid head groups. Then its partition between the acyl chains induces

an in-plane compression that forces the displacement and lateral expansion of the neighboring lipids and, in parallel, creates tension in the opposing leaflet. These processes lead to membrane deformation (McMahon and Gallop 2005; Ford et al. 2002; Lee 2005; Drin and Antonny 2010; McMahon and Boucrot 2015).

However, other studies suggested that the wedge effect by insertion itself is not sufficient to induce membrane curvature as it must be supported by protein clustering or oligomerization. This was assumed due to the fact that the force induced by single insertion may dissipate shortly on either side of the insertion. Thus, to efficiently deform the membrane many localized insertions are required to create asymmetry in the lipid bilayer (Campelo et al. 2008; Kirchhausen 2012; Voeltz et al. 2006).

Such examples of proteins that mediate curvature by hydrophobic insertion include the epsin family members, the matrix protein M2, VP40 matrix protein, ESCRT, SNARE, ARF/Sar1 small GTPases, α-synuclein, caveolins (CAV), the C2 domain proteins (Synaptotagmin-1 and Doc2B), Amphipathic Lipid Packing Sensor (ALPS) and finally the islet amyloid polypeptide (IAPP) that favor the formation of curvature followed by membrane disruption and permeabilization (Drin and Antonny 2010; Cui et al. 2011; Vanni et al. 2013; Takei et al. 1999; Farsad et al. 2001; Richnau et al. 2004; Adu-Gyamfi et al. 2013; Isas et al. 2015; Gallop et al. 2006; Jao et al. 2010; Lai et al. 2012; Krabben et al. 2011; Schmidt et al. 2013; Jackson 2010; Manca et al. 2019; Soni et al. 2013; Buchkovich et al. 2013).

Many membranes amphipathic helices (m-AH) present on proteins can behave as sensors of lipid packing defects present on curved surfaces. This facilitates their insertion in the hydrophobic membrane interior and allows further membrane deformation. Few examples of such proteins include the N-BAR domains present on the proteins (amphiphysin endophilins, nadrin) as well the F-BAR domains of syndapin. Figure 9 represents examples of the different cases that lead to membrane curvature by insertion (Drin et al. 2007; Kegulian et al. 2015).

Several of the proteins mentioned above are implicated in the membrane fusion or fission processes. The curvature promoted by fusogenic proteins leads to lipid mixing, while in the case of fission, the inserted protein cause lipid demixing (Furukawa and Mima 2014; Chernomordik and Kozlov 2008; Khelashvili et al. 2009; Heimburg et al. 1999).
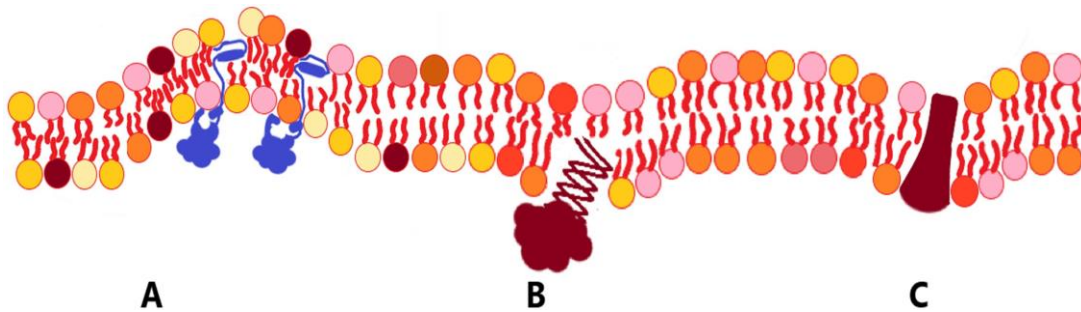
Figure 9 Membrane curvature mediated by insertion of hydrophobic or amphipathic protein motifs generate an area mismatch between the inner and the outer leaflet leading to local membrane curvature.

A-B) Peripheral membrane proteins with amphipathic helices. **A**) The helix hydrophobic side with the conical shape insert until reaching the opposite leaflet leads to negative curvature (ex VP40 matrix protein). **B**) The Helix with inverted conical shape causes positive curvature (ex α- synuclein, Epsin, Arf1, SAR1, GMAP-210, N-BAR(amphiphysins), SFV nsp1, HCV NS4B). **C**) Membrane-p- rotein integration that acts as a wedge to cause either positive or negative curvature (ex-ion channels or receptors, Flavivirus NS4A.

1.6.4 Lipid driven membrane curvature

The elastic and mechanical properties of the membrane are sensitive to the composition and the heterogeneous distribution of the lipids within it. The simplest approach to understand the lipid role in membrane budding involves a consideration of the lateral packing and the transverse asymmetry between the two sides of the bilayer.

Lipids can have different molecular intrinsic shape depending on the size of their head groups and their acyl chain characteristics (length, saturation, number of

tails). For example, PC, PS, SM, PG, digalactosyldiacylglycerol (DGDG) have cylindrical or slightly truncated cone shapes (cross-sectional areas of the head group and lipid backbone are quite similar).

Ceramide, Diacylglycerol (DAG), unsaturated fatty acid——UFA, monogalactosyldiacylglycerol (MGDG) diphosphatidylglycerol (DPG), cholesterol, dioleoylglycerol (DOG), unsaturated PE, PtdA, CL have a cone shape (small head cross-section as compared to hydrophobic tails (McMahon and Boucrot 2015).
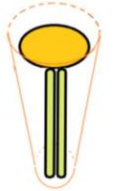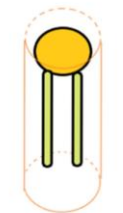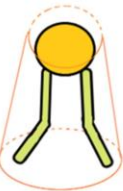
Lipid type	Molecular shape	Characteristics
Inverted conical lipids such as lysolipids, PIPs.		Larger head group than tail cross-sectional area (show preference for positive curvature).
Cylindrical shaped lipids, such as PC, PS-Ca^{++}, SM, PG, DGDG.		Equal head group and tail cross sectional areas (no curvature preference).
Conical lipids like ceramide, DAG, MGDG, DPG, cholesterol, DOG, unsatur-PE, PA-Ca^{++}, CL		The tails are larger than the head group cross sectional area (show preference for positive curvature).

Figure 10 Molecular shapes of different lipids. The occupied volume by the head group and acyl chains determines the molecular shape of the lipids which influence the collective and the physical membrane properties.

Finally, other lipids like detergents, lysolipids (ex lyso-PC), PIPs are considered inverted cone-shaped lipids (the cross-sectional area of the polar head group is larger than the acyl chains). Figure 10 shows the geometry exhibited by some

lipid molecules (Frolov et al. 2011; Janmey and Kinnunen 2006; Gruner et al. 1985; Israelachvili et al. 1980)**.**

1.6.4.1 Membrane curvature mediated by the asymmetric disposition of lipids

The ability of lipids to promote either zero, positive or negative spontaneous curvature in membranes is determined by their tendency to impose their own shape between the inner and the outer leaflets. Membrane with a charged surface due presence of anionic or cationic lipids can also undergo curvature due to the strong repulsion in the bilayer plane between the polar heads groups of similar charges (Hirama et al. 2017). Figure 11 represents the different cases of membrane curvature mediated by lipids.
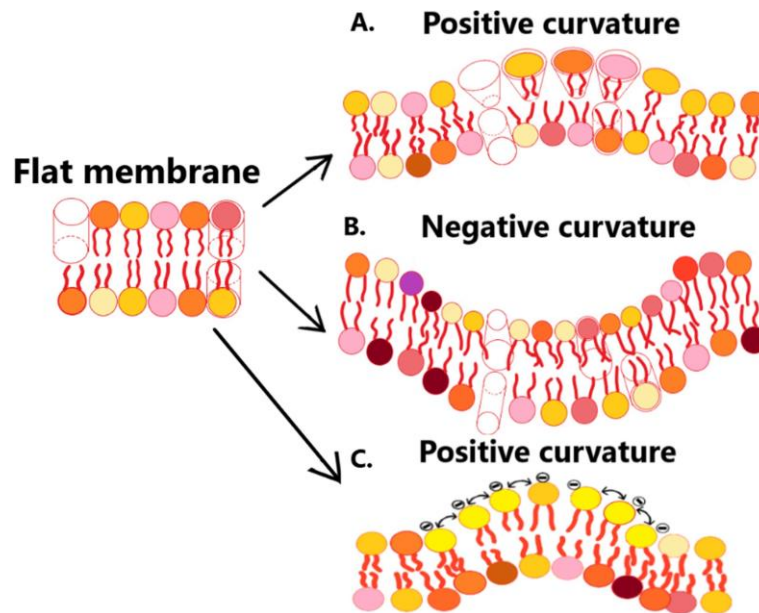
Figure 11 Local spontaneous membrane curvature generated by the asymmetric disposition of lipids.
In this context, this depends on the characteristics of the head group, as well as the acyl chain of the membrane constituents. **A-B**) Schematic representation of membrane bending based on the intrinsic lipid structures. **A**) Cone-shaped lipids impose their intrinsic shape to create positive curvature.
B) Inverted conical-shaped lipids create negative curvature as does the insertion of cholesterol.
C) Membrane curvature resulting from anionic phospholipids head groups repulsion (adapted from (Hirama et al. 2017)).

In cells, this unequal distribution of lipids between the two sides of the bilayer can be caused by the action of head-group-modifying enzymes such as phosphatidylinositol 3-kinase (PtdIns *3*-kinase) or by the flippases, floppases, and scramblases. These enzymes can actively shuttle lipids across the membrane (McMahon and Gallop 2005; Israelachvili and Wennerstroem 1992; Ritacco et al. 2011; Boal 2012; Cooke et al 2006; Hankins et al. 2015; Sanyal and Menon 2009).

1.6.4.2 Membrane curvature mediated by the unequal lateral distribution of lipids

It is known that the L_O domains have a larger thickness than cholesterol-poor L_D domains. This difference is mainly due to the fact that saturated lipids with their straight acyl chain and all-trans conformation have higher apparent perpendicular length while the surrounding unsaturated lipids with their kinked tail and increased gauche conformation are thinner which creates a hydrophobic mismatch (Pan et al. 2008; Marquardt et al. 2016; Halling et al. 2008).

In this case, the acyl chains of the statured lipids present at the L_O-L_D phases borders become exposed to water. The energetically cost resulting from hydrophobic mismatch combined with steric attractive interactions and difference of the packing density between membrane lipids create a lateral line tension. Then to decrease line energy and reduce the contour length of the raft domains at the boundary, a bulge out of the membrane is created, producing a bent lipid raft. This outward budding phenomenon was observed experimentally in GUVs with multiple domains. The tendency of the borderline around a domain to become shorter makes the domain bulge out and finally bud off.

Figure 12 schematizes the bilayer adaptation to the hydrophobic mismatch at the raft interface (Simons and Sampaio 2011; Pike 2009; Tsukamoto et al. 2014;

Schuck and Simons 2004; Klemm et al. 2009; Kuzmin et al. 2005; Wallace et al. 2006; García-Sáez et al. 2007; Baumgart et al. 2003).
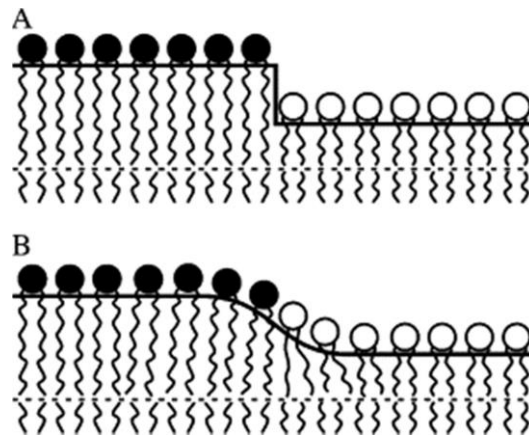
Figure 12 Schematic representation of the raft boundary. A) The difference of thickness between the L_O (black circles)-L_D (white circles) phases leads to a hydrophobic mismatch. **B**) Monolayer deformation arises at the raft boundary to decrease line tension and the lipids acyl chains exposure to water (Kuzmin et al. 2005).

2. Biophysical techniques used in this work

2.1 Surface Plasmon Resonance (SPR)

2.1.1 Principle of the SPR analysis

Surface Plasmon resonance (SPR) is a powerful technique that allows real-time quantitation of interactions and determination of binding kinetics without any further labeling. Different kinds of binding processes can be studied via SPR such as protein-lipids, protein-protein, and even protein-drug interactions (Stahelin 2013; Frostell et al. 2013).

The SPR technique is based on the complex optical phenomenon of the attenuated total reflection via the Kretschmann configuration. First, a light beam (monochromatic p-polarized light e.g. laser) passes through a prism and reaches a metal surface (usually gold). When photons reach the interface, the shifting of the resonance angle depends on changes in the refractive index (RI) of the medium on the non-illuminated side of the chip. This change is in direct proportion to the mass concentration of macromolecules attached to the metal surface in real-time (Tang et al. 2010).

The SPR machine uses a photo-detector array for measuring the very small variation in the plasmon resonance angle. This variation is quantified in resonance units or response units (RUs). 1 RU represents a shift of 10^{-4} degrees. 1000 RU is equivalent to a change in sensor surface protein or DNA concentration of about 1 ng/mm^2, if we assume that the sensor chip matrix coating is ~100 nm thick this represents 10 mg/ml in the bulk protein concentration (Kolomenskii et al. 1997; Zhang and Oglesbee 2003; Löfås et al. 1991).

First, one of the interaction partners represented by the ligand is immobilized on the biosensor chip surface. Then the analyte flows over it. When the interaction happens between the ligand and the analyte, the dynamic change of the SPR angle can be detected and assayed for measuring the level of binding response. The binding at equilibrium which corresponds to the steady-state plateau is reached when the rate of binding equals the rate of dissociation and no variation of the signal is observed within time. Finally, the signal decreases when the running buffer replaces the analyte and the formed ligand-analyte complex dissociates.

SPR results are presented as a set of sensorgrams, which correspond to the plot of SPR signal (response in resonance units RU) versus time.

2.1.2 Data acquisition and analysis

The kinetic measurements involve repeated injections of the analyte at different concentrations over the same ligand and measuring the level of binding in time. Before each new analyte injection, the ligand surface regeneration is performed by complete removal of the previously bound analyte using an adequate regeneration buffer that does not affect the ligand binding. The response is observed in the sensorgrams as a sharp drop in RU after analyte dissociation and a return to the initial baseline.

Then the obtained sensorgrams data can be fitted to a kinetic binding model. The most used one is the Langmuir model. This model considers all the binding sites to be similar and that only one analyte binds to one ligand molecule (1:1 reversible reaction). However, we must notice that the Langmuir model does not take into consideration the mass transport of the analyte between the bulk flow and surface (O'Shannessy et al. 1993).

The fitting of the sensorgrams to this model allows the calculation of the association k_a (in the unit of $M^{-1}s^{-1}$) and dissociation k_d (in the unit of s^{-1}) rate constants and determination of the equilibrium dissociation constant K_D also named binding affinity (in the unit of M). The K_D values are calculated by plotting the collected set of binding level values corresponding to the maximum response (R_{eq}) obtained for each C_x versus protein concentration. The K_D represents the concentration of analyte A at which 50% of the binding sites for the ligands are occupied.

2.2 Scanning FCS (sFCS) on GUVs

Fluorescence correlation spectroscopy (FCS) is an exquisitely sensitive technique that allows in real-time, fast temporal (microseconds) and high spatial (a few

hundred nanometers) resolution analysis. It is mainly used for the quantification and analysis of fluorophore dynamics. For that, a laser beam is focused on a small diffraction-limited spot using an adapted objective. A pinhole serves to obtain small fixed detection or observation volume (0.1-0.5 femtoliter). This volume, named the confocal volume, corresponds to 200–300 nm width in the x-y direction and 500-12000 nm height in the vertical axis (Elson 2011; Grünwald et al. 2005; Berland et al. 1996). During FCS experiments, the fluorescence emitted from small concentrations (nanomolar to the micromolar range) of fluorescently labeled samples diffusing over time (due to Brownian or directed movement) in and out the laser-illuminated observation volume is analyzed.

We have to notice that the observation volume is not illuminated homogeneously (as described by a Gaussian ellipsoid (Chen et al. 1999b)), thus the produced photon count follows a Poisson distribution. For that reason, the optimal positioning of the sample (e.g. plasma membrane) within the observation volume center is critical for accurate determination of the molecular brightness.

The fluctuations generated by the sample fluorophores are selected by means of an emission filter (bandpass filter) and the fluorescence intensity as a function of time is recorded by single-photon detectors.

FCS analysis allows us to acquire many physical parameters that concern: the average number of fluorescent particles (N_p), correlation time (τ_D), average intensity, interactions among components (cross-correlation), the number of photon counts per molecule/particle (CPM/CPP).

Before sample analysis, calibration of the point spread function (PSF) can be acquired by calculating the autocorrelation function $G(t)$ of a fluorophore with a determined diffusion coefficient (Dix et al. 2006).

To overcome the bleaching of molecules that occurs during the measurements we use corrective calculations. The removal of unexpected fluorescent spikes is also performed during data analysis.

2.2.1 The diffusion coefficient

The diffusion coefficient (D) is defined as the rate of movement. It depends on the viscosity of the environment and the size (hydrodynamic radius) of the molecule. The diffusion coefficient can be calculated as in equation 1, where ω_0 is the diameter of the detection volume.

The diffusion time or the average dwell time (τ_D) represents the average time required for fluorescently labeled particles to traverse the radial dimension of the observation volume. This parameter is defined as the lag time where the amplitude of the smoothed autocorrelation curve drops to 50% of its initial value in a defined time.

Fluorescent-tagged proteins that move more quickly through the confocal detection volume (small diffusion time) and thus show a faster correlation decay have a low oligomeric state, while high oligomeric state proteins show slower diffusion rates (longer diffusion times) and thus remain in the focal volume for an extended period.

$$D = \omega_0^2 / 4\,\tau_d$$

Equation 1

The relation between the diffusion rate of protein and oligomeric state is described by the following formula, $\dfrac{D_k}{D_1} = k^{-\frac{1}{3}}$, where k is the number of monomers composing the oligomer protein. However, we have to notice that due to its limited resolution, the FCS does not allow us to distinguish between diffusion rates of two proteins differing by factor below 1.6. In other words, by applying the equation above, the limit resolution of FCS allows us to resolve at least only between a monomer and a tetramer (Meseth et al., 1999).

2.2.2 Molecular brightness

The brightness is the parameter that indicates a sample oligomeric size by determining the number of fluorescent molecules within the protein complex. Brightness (B) expressed as counts per second per molecule (CPSM) is defined as the ratio of variance σ^2 to the mean intensity μ (factor of dispersion). Brightness values are calculated by dividing the average photon count rate (k) (fluorescence intensity trace per particle) by the number of fluorescent molecules as indicated in equation 2.

$$B=\langle F(t)\rangle/N$$

Equation 2

Figure 13 represents a global illustration of the sFCS analysis mechanism and diffusional/oligomeric parameters determination for labeled M1 bound to GUVs.
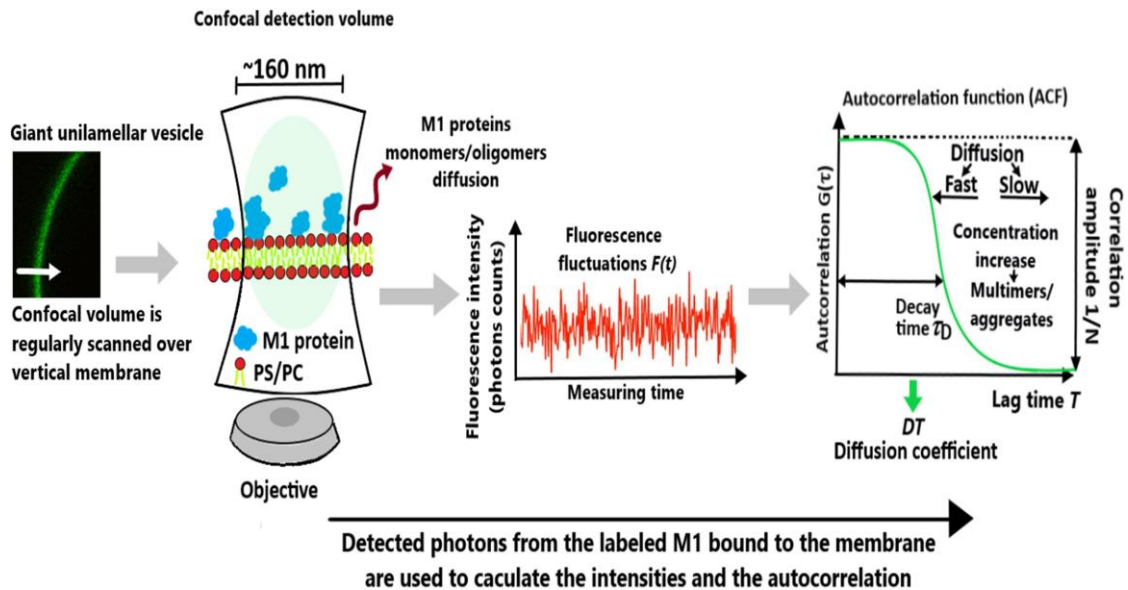

Figure 13 Schematic representation of labeled M1 bound to GUVs analysis by scanning fluorescence correlation spectroscopy (sFCS).

3. Influenza A virus

Influenza viruses belong to the Orthomyxoviridae family. These enveloped viruses are considered to be the most widespread pathogens. They are characterized by their fast binding to cells and uptake into compartments to hide from the host immune system (Batishchev et al. 2016; Nara et al. 2010).

There are three types of influenza viruses (A, B, and C). Both types A and B are considered to be major respiratory pathogens. Type C cases are clinically less relevant (Taubenberger and Morens 2008).

Like most enveloped viruses, the infection cycle in cells includes an early stage (entry process) and a late stage that requires trafficking and assembly of its viral components to the budding site. The budding process is characterized by the induction of an outward membrane bulge. Later, the formed bud is snipped from the cellular membrane by scission to allow new virions release (Londrigan et al. 2015; Frensing et al. 2016).

Influenza A virus (IAV) infections rank among the major global health problems. The virus can infect humans and birds, as well as different kinds of mammals, such as equines, whales, seals, swine, mink, etc. Aquatic birds represent the wildlife reservoir of the virus. The disease is endemic in all populations. The virus is typically highly active and spreads easily during the winter period in crowded and enclosed spaces (Griot and Hoop 2007).

Given that the IAV is the most medically important, from an anthropocentric point of view, it will be the type of Influenza that we will focus on in our study.

The IAV lipid envelope derived from the host cell PM contains two surface integral glycoproteins forming spike-like projections: the hemagglutinin protein (HA) and neuraminidase protein (NA). In addition, a transmembrane ion channel (M2) is also present in the envelope of the virus (Jin et al. 1997; Zhang et al. 2000). The inner M1 protein shell present below the lipid envelope forms the

viral capsid. M1 is presumed to interact simultaneously with the viral ribonucleoproteins (RNP), the lipid envelope, and with the cytoplasmic tails of HA and NA (Zhang et al. 2000; McCown and Pekosz 2005). Figure 14 represents the IAV structural organization.

The IAV genome consists of eight separate negative-sense single-stranded RNA segments encoding for at least 10 viral proteins: The positively charged nucleoprotein (NP) can bind and coat the viral RNA (vRNA) by electrostatic interaction to form the viral ribonucleoprotein (vRNP) complex. This coating is important for genome packaging but also is necessary to protect the RNA from cellular nuclease digestion. NP exhibits multiple NLS sites for nuclear import. It has also been reported that NP allows nuclear export of vRNPs by directly interacting with CRM1(chromosomal maintenance 1) without the involvement of M1 and NEP (Elton et al. 1999; Tao et al. 2012; Chenavas et al. 2013; Melen et al. 2003; Cros et al. 2005; Neumann et al. 1997; Elton et al. 2001; Yu et al. 2012).
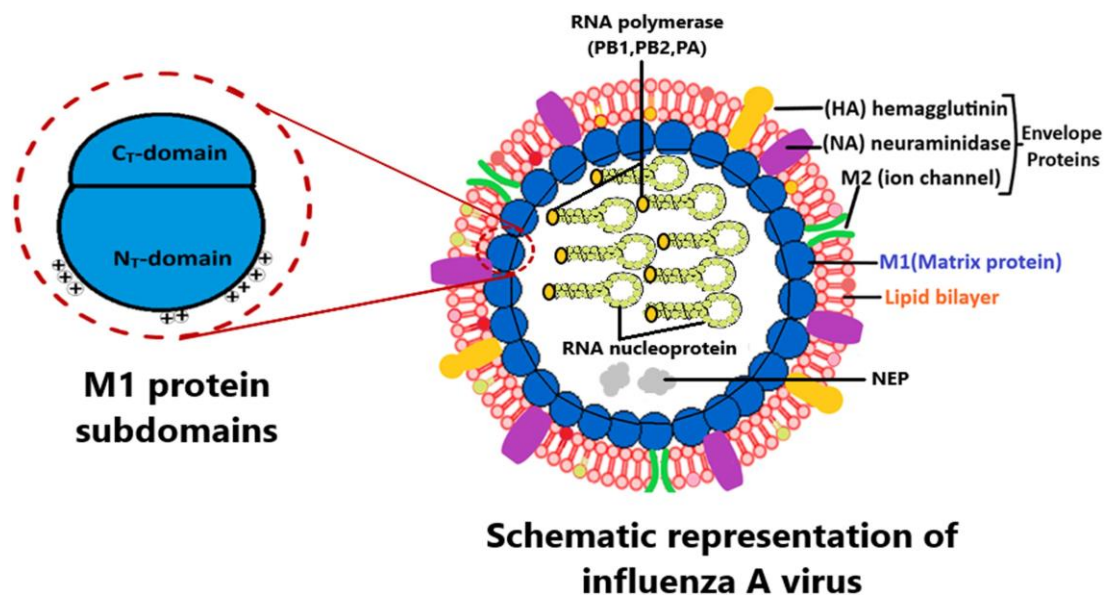
Figure 14 Schematic structure of the IAV. The three envelope proteins: the ion channel matrix protein 2 (M2), hemagglutinin (HA), and neuraminidase (NA). The matrix 1 protein (M1) binds via its N-terminal domain to the viral envelope and forms an inner layer. The nucleoprotein (NP) encapsulating the eight single-stranded RNAs attached to the polymerase complex (PB1, PB2, PA). The non-structural protein 2 (NS2) also called NEP is also present in low numbers.

The IAV RNA polymerase complex (RdRp) is composed of three subunits: polymerase basic protein 1 and 2 (PB1/PB2), polymerase acidic protein (PA). Their function is to cleave the host cell mRNA with capped oligonucleotide sequences to use them as a primer for synthesizing the new viral mRNA (Honda et al. 2001).

3.1 Influenza A virus (IAV) strains

IAVs show a high genetic variation leading to antigenic shift or drift. The antigenic drift is due to the accumulation of point mutations causing minor and gradual structural antigenic changes, while the antigenic shift is due to the introduction of new NA and/or HA subtypes (another host species may cross into the human) leading to major antigenic changes. Both HA and NA frequently undergo genetic modifications decreasing the effectiveness of the host immune response. IAV viruses are further divided into subtypes based on antigenic variants and structural properties of the two surface glycoproteins HA and NA. There are 18 different variants of HA (H1 to H18) and 11 different variants of NA (N1 to N11). This gives a total of 198 possible different combinations. Only two IAV subtypes (H1N1 and H3N2) are currently circulating in the human population (Wikramaratna et al. 2013; Noda and Kawaoka 2010; Weber and Elliott 2002; Lloren et al. 2017).

IAV entry is initiated by the activated HA protein binding to sialic acid receptors present on the surface of the host cell. This triggers virus internalization inside the endosome by either receptor-mediated endocytosis or macropinocytosis. It was recently demonstrated that IAV entry and fusion are rather a quick process and arise in a short time (~10 min) (Dou et al. 2017; Dou et al. 2018).

3.2 IAV envelope components

3.2.1 Neuraminidase

Neuraminidase (NA) is a 60Å long polypeptide chain forming a homo-tetramer. Each monomer consists of 470 amino acids. NA structure includes an ectodomain (catalytic head), a stalk region, a transmembrane region, and a cytoplasmic tail. Spherical IAVs (~120 nm) diameter contain around 40-50 NA copies, which is 5-7 times less comparing to HA. NA is a multifunctional protein, its roles involve virus movement, binding, and release from infected cells. NA has an exosialidase activity that allows it to recognize and cleave the α-ketosidic linkage between the terminal sialic (N-acetylneuraminic) acid residues and the remaining carbohydrate residues. The optimal activity of NA occurs at a pH (5.5–6.5) in presence of Ca^2+ (Mountford et al. 1982; Lentz et al. 1987; McKimm-Breschkin 2013; Gong et al. 2007; Ward et al. 1983; Moules et al. 2010).

This activity could help virus movement to evade the defensive layer (enriched with sialylated "decoy" receptors) present on the respiratory tract airway mucus (gel-forming mucins) or the cellular glycocalyx cilia. After penetration through the mucus barrier, the virus targets the epithelial cells underlying the respiratory epithelium (Shtyrya et al. 2009; Kesimer et al. 2009; McAuley et al. 2017; Yang et al. 2014).

Upon its attachment to the target cell, NA facilitates the virus rolling by repeated binding and release steps from the endocytic inactive sites present over the cell surface until reaching a functional receptor (the active site that allows multiple HA-sialic interactions) that allows irreversible binding and efficient endocytosis. For many IAV strains, the desialylation of HA is necessary to allow its cleavage by proteases and to activate fusogenic activity (Yamamoto-Goshima and Maeno 1994; Li et al. 1993).

Finally, NA activity allows also the prevention of HA mediated self-aggregation or clumping of the newly released virions that have been sialylated as part of the glycosylation processes within the host cell (Böttcher et al. 2006; Romero-Beltran et al. 2016; Yang et al. 2014; Su et al. 2009; Guo et al. 2018; Du et al. 2019; Air 2012).

NA inhibitors drugs that can mimic the transition state of bound sialic acid residues like oseltamivir (Tamiflu®), zanamivir (Relenza®) and peramivir (EU: *Alpivab*®) or Oxocarbenium are used to block NAs active site, to inhibit virus entry and slow down the release of newly formed virions (Pizzorno et al. 2012; LeGoff et al. 2012).

3.2.2 Hemagglutinin

HA is the most abundant envelope glycoprotein and is also considered the most determinant for virus virulence. Each IAV contains around 300-400 HA. This makes an equivalent density of around 1 glycoprotein/120 nm^2. HA is expressed as a single inactive (fusion incompetent) precursor designated as HA_0. Before its trimerization, HA_0 undergoes several posttranslational modifications including glycosylation, S-acylation (palmitate, stearate), disulfide bond formation in the host. Each HA_0 monomer consists of two disulfide-linked polypeptides subunits (HA_1/HA_2). The subunit HA_1 known as the head (about 320 amino acids) is composed of anti-parallel beta-sheets and includes the membrane-distal sialic acid receptor-binding site (RBS), the antigenic binding site, and the HA_1/HA_2 cleavage site (Harris et al. 2006; Wasilewski et al. 2012; Schulze 1997; Kim et al. 2018; Chen et al. 2005; Mair et al. 2014).

To acquire the ability of binding to sialic acids and the fusogenic capacity (by the generation of the hydrophobic N-terminal fusion peptide HA_2), the HA_0 requires cleavage-activation by an appropriate host endoprotease. This cleavage could

arise either during transport by furin to the trans-Golgi-network (TGN) or by the human airway trypsin-like protease (HAT) expressed by epithelial cells (Fontana and Steven 2015; Blijleven et al. 2016; Böttcher-Friebertshäuser et al. 2010; Baron et al. 2013).

During the virus assembly, HA_0 associate probably with sphingolipid-cholesterol rafts via its transmembrane domains. Then clustering and concentration of HA arise probably by the lateral mobility of these lipids at the budding site (Takeda et al. 2003; Nayak et al. 2004; Hess et al. 2007; Leser and Lamb 2005; Hess et al. 2005; Scheiffele et al. 1997; Ohkura et al. 2014; Makarkov et al. 2019).

The HA_1 subunit is mainly responsible for virus attachment to the cell. The binding pocket on HA_1 recognizes the host cell sialic acid moieties linked to complex glycans on glycoproteins/glycolipids. The specificity of the HA-SA interaction is an important determinant that affects cell and host tropism, interspecies adaptation pathogenicity, and transmissibility. HA_1 avidity for the sialic acid α-Galactose must be strong enough to allow a good and fast binding before NA can cleave receptors. The ~300–400 HA trimers per virion could help the virus to form several connections that allow a stable interaction (Du et al. 2019; Steinhauer 1999; Kido 2015; Graaf and Fouchier 2014; Matrosovich et al. 1993; Suzuki et al. 2000; Russell et al. 2006; Ibricevic et al. 2006; Bradley et al. 2011; Stevens et al. 2006; Yamada et al. 2006). After attachment, IAV entry is mediated by clathrin-mediated endocytosis involving the adaptor protein Epsin-1 and dynamin for virus pinching off. IAV uptake could also be mediated by raft-dependent endocytosis (Suzuki et al. 2000; Childs et al. 2009; Trebbien et al. 2011; Verma et al. 2018; Vries et al. 2011) or in other cases by macropinocytosis (Roy et al. 2000; Rust et al. 2004; Sieczkarski and Whittaker 2002).

After virus uptake in the endosome, the HA pocket protonation cause repulsive electrostatic interactions that lead to the dissociation of the clamp formed by the HA_1 from the HA_2 subunit. Then membrane-embedded HA_2 subunits undergo large irreversible conformational rearrangements. Later the fusion peptide (FP)

exposition via functional loop-to-helix transition leads to an extended coiled-coil. During this transition, the formed extended amphipathic fusion peptide (or loop) projects and shoots out like a harpoon (about 100 Å) toward the target and inserts into the host endosomal membrane to form a trimer that bridges the two membranes. As the interior of the endosome continues to acidify (pH~5), the 23 amino-acid fusion peptide (HAfp23) refold to the final lowest energy conformation (the stable form) and bends back on itself so that it looks like a hairpin with TMD and FP at the same end. The helical hairpin has also the characteristic to adopt an inverted wedge shape structure (small hydrophilic head region and relatively bulky hydrophobic region) that induces negative curvature and close contact between the viral envelope and endosomal membranes. Further contact between the two bilayers combined with the high negative curvature will promote hemifusion between the virus and the endosome. Finally, when fusion arises, post-fusion hairpin drives the pore formation leading to the release of the viral content into the host cell (Lakadamyali et al. 2004; Chen et al. 1999a; Xu and Wilson 2011; Hoffman et al. 1997; Yu et al. 2002; Lin et al. 2014; Huang et al. 2009; Gruenke et al. 2002; Bullough et al. 1994; Lorieau et al. 2012; Ghosh et al. 2015; Lorieau et al. 2011; Smrt et al. 2015; Worch 2014).

3.2.3 Matrix protein 2 (M2)

The IAV integral membrane protein M2 (97 amino acids) is formed of an externally oriented N-terminal domain (ectodomain -amino acids 1-24) that can be recognized by the immune system. The transmembrane domain (a.a 25-43) has an ion channel activity that allows virus uncoating, while the cytoplasmic domain (a.a 44-97) allows interaction with the M1- RNP complex. At a late stage of the assembly process, the M2 formed clusters are recruited and localized on the periphery of the lipid rafts which correspond to the budding site edge (Schmidt et al. 2013; Yu et al. 2012; Gerhard et al. 1997; Treanor et al. 1990; Wang et al. 2011;

Rossman and Lamb 2011; Chen et al. 2008; McCown and Pekosz 2006; Iwatsuki-Horimoto et al. 2006; Su et al. 2018; Wohlgemuth et al. 2018). Simulations and experimental observations confirmed that M2 displays also linactant properties in membranes with phase-separated lipid mixtures. Experiments performed on GUVs showed that M2 tends to be completely excluded from the L_o and was localized only in L_D with subsequent over-representation at the border between L_D and L_O domains. The M2 exclusion from the Lo phase is due to the fact that the lipids in this phase are too rigid and highly packed. The preference for M2 to localize at the lipid microdomains edge is due to the $M2_{AH}$ insertion. In fact, after binding to the PM, M2 forms rapidly an α-helix, that can sense positive curvature created by lipids defects at the microdomains boundaries. Following that, M2 inserts deeply into the bilayer further amplifying membrane positive curvature by the wedging mechanism. Then, the membrane neck at the budding site undergoes more constriction leading to subsequent virion scission (Schmidt et al. 2013; Yu et al. 2012; Wang et al. 2011; Rossman and Lamb 2011; Grantham et al. 2010; Iwatsuki-Horimoto et al. 2006; Su et al. 2018; Wohlgemuth et al. 2018; Madsen et al. 2018; Martyna et al. 2017; Martyna et al. 2016; Ho et al. 2016; Rossman et al. 2010b; Rossman et al. 2010a; Kozlov et al. 2010). M2 has a strong positive selective pressure induced by drugs or due to the host immune response and tropism since it is a major antigen marker (Furuse et al. 2009).

3.3 IAV Matrix protein 1(M1)

3.3.1 M1 protein structural characteristics and evolution

The IAV matrix protein (M1) is quite a small protein (60 Å long) encoded by the viral RNA segment 7. It consists of 252 amino acids and 27.9 kDa MW (calculated for A/FPV/Rostock/34 strain). With approximately 3000 copies per virion, M1 is the most abundant protein among all the IAV components. M1 organizes in a helical manner to form the secondary structure. The α-helices are separated by linker sequences that create two major domains: The N-terminal domain and the C-terminal domain (Arzt et al. 2001; Safo et al. 2014; Ruigrok et al. 1989; Ruigrok et al. 2000a; Harris et al. 1999; Calder et al. 2010)**.**
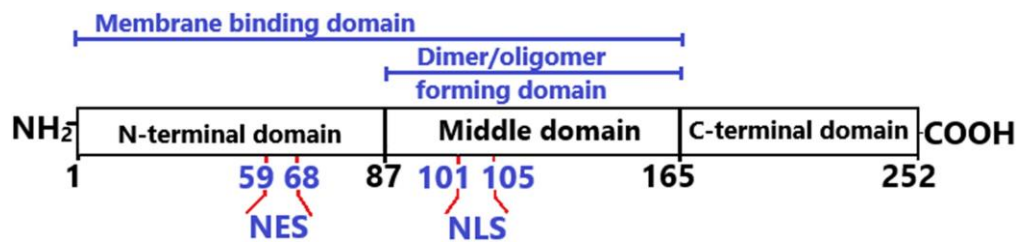

Figure 15 M1 protein functional domains organization. The membrane-binding regions on the N-terminal and the middle domains concern the arginine triplet (aa 76-77-78) neighboring the nuclear export signal (NES) and the polybasic region (aa 95-105) that include also the nuclear localization sequence (NLS).

The N-terminal domain (165 a.a, N_{1-165}) nine α-helices (H1-H9) linked by eight loops. This domain includes also the middle domain linked by the helix H5 to the first part of the N-terminal domain.

The C-terminal domain (87 amino acids, $C_{166-252}$) is connected to the N-terminal domain by the loop L9. The N-terminal domain has several functions and is considered as a target of any potential anti-influenza agents. Figure 15 represents the M1 different domains disposition (Noton et al. 2007; Liu et al. 2009; Sha and Luo 1997b; Harris et al. 2001; Shtykova et al. 2013; Shishkov et al. 2011; Fujiyoshi et al. 1994).

Despite multiple attempts of crystallization and X-ray diffraction analysis, the three-dimensional crystal structure for M1 (isolated from virus particles or recombinant obtained from bacteria) was determined only for the N-terminal domain (N_{1-165}). This is because the C-terminal region was digested or detached during crystallization. This cleavage could arise at the protease-sensitive loop L9 between glutamine 164 and methionine 165 due to contaminating proteases present in the solution. However, other studies suggested that this difficulty to keep the M1 C-terminal part arises from its intrinsic disorder which prevents the growth of diffraction-quality crystals. Alternative methods based on tritium bombardment, small-angle X-ray or neutron scattering (SAXS or SANS), circular dichroism spectroscopy (CD) are more suitable for 3D structural analysis of proteins with flexible regions in solution or *in situ* (inside virions). Using such methods, it was possible to show that the full M1 has an elongated shape (vary between 6-10 nm in solution) while the NM1 fragment is characterized by a dense globular structure and compact core. The full M1 contains 72% α-helices while β-strands are not included, similarly, the crystal structure analysis showed that NM1 is 70% α-helical. The C-terminal domain was predicted to have two regions: the first region contains four α-helices and represents 31% of the structure, while the second region (69%) contributes more to the flexibility of M1. This region is formed of weakly structured and extended motif, forming a random-coil tail that gives an elongated shape (Safo et al. 2014; Ruigrok et al. 2000a; Shishkov et al. 2011; Sha and Luo 1997b; Shishkov et al. 1999; Shtykova et al. 2017; Kordyukova et al. 2019; Arzt et al. 2004; Mertens and Svergun 2010; Ali et al. 2000; Ksenofontov et al. 2011; Shishkov et al. 2009; Zhang et al. 2017). Recently the first full-length crystal structure of the matrix protein from the ISAV virus (orthomyxovirus of fish) has been resolved. The ISAV M1 has high similarities with the IAV M1, where eight of the nine α-helices in the IAV (fluorescein-specific anticalin) M1 N-terminal domain can be matched to those in ISAV-M1. The crystal structure analysis of the full-length ISAV-M1 protein showed that the C-terminal domain is connected to the N-terminal domain

through a flexible linker. The ISAV-M1 C-terminal domain is made of four α-helices stabilized and packed as a tight helical bundle (α9–α12). The structural integrity is further strengthened by a salt bridge between residues E122 and R153 of two adjacent α-helices (Gao etal. 2015).

While the other IAV proteins (HA, NA) are known to mutate at a very high rate, M1 has one of the most conserved amino acid sequences among virus proteins. In fact, segment M shows a slow evolutionary rate into host-specific lineages and is very often used to diagnostic all IAVs. We have to notice also that the M gene from human IAVs is not interchangeable among subtypes while the avian IAVs is interchangeable (Furuse et al. 2009; McCauley and Mahy 1983; Mosier et al. 2016; Vivek Darapaneni 2015; Heiny et al. 2007; Ito et al. 1991; Acharya et al. 2010; Wang et al. 2006).

Mosier et al. comparison of 742 amino acids sequences obtained from the NCBI IAV M1 Database and representing a large time interval (1925–2015), disparate geographic locations, hosts and strains (including the pandemic swine H1N1 and seasonal H3N2 and the highly pathogenic strain H5N1) showed 29.8% identity and 57.5% similarity, while M2 sequences showed only 2.1% identity and 20.6% similarity. The same study showed that M1 mutations are extremely rare at many positions and the lowest sequence identity was dominated by a few homologous amino acid residues. In another study, the comparison of 2836 amino acid sequences mainly from avian (40%), human (25%), and swine (22%) viruses showed that only 15% of the total residues for the M1 sequence were highly variable (Vivek Darapaneni 2015).

This high degree of conservation could mean that M1 is under low evolutionary selective pressures. This could imply that the M1 gene segment undergoes probably a strong negative selection to retain the same amino acid because any changes may lead to nonfunctional protein. This assumption seems rational since we have to consider that M1 has a multifunctional role, thus any eventual change due to minor mutations on the M segment could be detrimental to the virus

replication or potentially lethal to the virus. This advantage for M1 can be expected to minimize the impact of selection pressures (either environmental, drug-induced, or due to the host's immune response), therefore the M1 from IAV might be a suitable target as influenza vaccines (IVs). However, some sites of M1 can undergo a higher selective pressure (positive selection) for amino acid substitution, these sites could be important in determining cell tropism and host adaptation of influenza virus and immune responses (Suzuki and Gojobori 1999; Sergei L. Kosakovsky Pond, Art F.Y. Poon, Simon D.W. Frost 2007).

3.3.2 M1 post-translational modifications (SUMOylation and phosphorylation)

The AIMP2 (aminoacyl tRNA synthetase complex interacting multifunctional protein 2) can SUMOylate the M1 at lysine 242 to protect it from proteasomal degradation. The SUMOylation favorites also M1 binding to the ribonucleoprotein (NP) and nuclear export. Any defect that impaired M1 SUMOylation caused vRNAs accumulation in the nucleus and a decrease in virion production. Further, it was also demonstrated that SUMOylation is important to modulate the assembly and morphogenesis of IAV (Wu et al. 2011; Han et al. 2014; Pal et al. 2011).

M1 has the potential to be phosphorylated by cellular kinases at the sites (S53A, S70A, S161A, S185A, Y132), previous studies showed that tyrosine 132 phosphorylation induces a large conformational change on the NLS that enhances the M1 binding capacity to the importin-α1 However, a new study showed that M1 phosphorylation is not required for its activity during assembly (Reinhardt and Wolff 2000; Wang et al. 2013; Yángüez et al. 2018).

3.3.3 Functional characteristics of M1

M1 is a multifunctional protein that plays essential roles in many aspects of the virus life cycle. These functions are represented by its ability to undergo self-assembly, to display bidirectional nuclear traffic through for the RNP complexes, then to further interact with PM and with the cytoplasmic tails of HA, NA, and M2. All these characteristics are crucial for coordinated and ordered assembly, trafficking, and budding of the virion (Ali et al. 2000; R T Avalos et al. 1997).

3.3.3.1 M1 interactions with lipids

The structure examination of M1 revealed an extensive amount of surface-exposed basic amino acids on the N-terminal domain that give the M1 a global positive net charge at neutral pH. Electron microscopy observation also revealed that M1 is bound peripherally to the virus lipid envelope. Two regions with positively charged amino acid residues have attracted distinct attention as potential zones that allow binding to anionic lipids mainly via electrostatic interaction. The first region concerns the arginine (aa 76-77-78), the second region concerns the polybasic region (aa 95-105). (Rossman and Lamb 2011; Ruigrok et al. 2000a; Sha and Luo 1997b; Brevnov et al. 2015; Arzt et al. 2001; Kretzschmar et al. 1996).

In recent work, SPR analysis of M1 interactions with a negatively charged surface showed that the binding of M1 at low pH (pH4) remained rather strong as at neutral pH. This could lead to the suggestion that acidic conditions are not affecting the electrostatic interaction of M1 with membrane lipids (Brevnov et al. 2015).

The arginine triplet (aa 76-77-78) present on the helix 5 allows M1 membrane targeting and attachment as well as its incorporation into the virions. Recent studies

showed that single arginine-to-alanine substitution at position 77 or 78 is sufficient to cause aberrant virus budding (Das et al. 2012; Kerviel et al. 2016).

The polybasic region (aa 95-105) present on helix 6 includes the positively charged amino acids (Lys95, Lys98, Arg101, Lys102, Lys104, Arg105). A Polybasic region knockout M1 showed altered membrane association, while the residues 93 and 94 neighboring this region form a cholesterol recognition amino acid consensus (CRAC) domain that gives M1 a raft/cholesterol-binding capacity (Nayak et al. 2004; Höfer et al. 2019b; Liu and Ye 2004; Tsfasman et al. 2015).

3.3.3.2 M1 protein multimerization (dimerization and capsid formation)

Protein M1 monomer surface screening showed that one face has a continuous patch of positively charged amino acids while the opposite face is negatively charged and includes the motif residues (Glu8, Glu23, Glu29, Asp30, Asp38, Glu44). It has been reported previously that M1 dimerization is mediated by the middle region 91-158 aa, while another study suggested that it is mediated by the C-terminal part (residues 181–193). The adjacent M1-M1 binding could be mediated through a combination of electrostatic interaction, hydrophobic forces, and hydrogen bonds (Batishchev et al. 2016; Zhang et al. 2015).

Crystal structure analysis of both full length and the N-terminal domain of M1 showed that it always forms a dimer at both acidic and neutral pH, but in each case the orientation of the monomers is different. This dimeric state was also confirmed by analyzing recombinant expressed and purified M1 in a solution using size exclusion chromatography and sedimentation velocity analytical ultracentrifugation (SV-AUC) (Sha and Luo 1997a).

At neutral pH, when acidic and basic amino acids of M1 exist mainly in their ionized forms, the two monomers are oriented to interact in a face-to-back fashion. In this case, the NLS region and the neighboring patch of positively

charged residues at one side of monomer (Lys95, Lys98, Arg101, Lys102, Lys104, Arg105, Arg134, plus Asp94) interact with the patch of negatively charged residues (Glu8, Glu23, Glu29, Asp30, Asp38, Glu44 plus Lys35) located at the backside of the other monomer by electrostatic interaction (Zhang et al. 2015).

At acidic pH (5.0 or lower), M1 monomers reorient to form dimers deposed in a face-to-face fashion. In this case, the two sides interact via hydrophobic interactions. The amino acids involved in this dimerization belong to the helices H6 and the outermost α-helices (H9 and loops L9) and concern the Asn82, Arg101 Asn133 on one side and Asn82, Asp94, Gly88 the other side. However, in another work, M1 mutant with a knockout NLS (basic residues were replaced by alanines) remained in a dimeric form at low pH. This shows that a.a. present on the NLS interface are not the only contributor to the dimer formation (Sha and Luo 1997a).

Other studies report that the IAV M1 or the M1 N-terminal domain remains in a monomeric state in solution at low pH or even a neutral pH as shown using analytical ultracentrifugation, SAXS, and atomic force microscopy (AFM). Similarly, recent analysis on the full-length M1 from Influenza C virus by size exclusion chromatography (SEC) and SAXS measurements demonstrated that the M1 remains in a monomeric state (Saletti et al. 2017; Zhirnov 1992).

The tendency of viral matrix proteins for self-assembly and oligomerization has been observed in several cases including Influenza, HIV, Nipah, and Ebola viruses. Many techniques like RICS, FCS, AFM, SEC, Bio-layer interferometry (BLI), and SV-AUC confirmed the intrinsic property and biologically determined tendency of the recombinant M1 to oligomerize into helix-like structures. This arises at neutral pH either in solution or when bound to negatively charged mica surfaces or anionic lipids. This tendency of M1 to multimerize was also confirmed in cells expressing M1 using quantitative microscopy approaches like N&B, FCS. In parallel, electron microphotographs observation of the M1 layer directly isolated from the IAV shell showed that M1 form elongated flexible ribbons and

41

small coils (Batishchev et al. 2016; Ruigrok et al. 1989; Ruigrok et al. 2000a; Harris et al. 2001; Shtykova et al. 2013; Hilsch et al. 2014; Ono et al. 2000).

The main function of the M1 capsid is to protect the functional integrity of the virus components from external influence. The M1 capsid also enforces the viral envelope shape by supporting the structural stability and the mechanical strength by forming the skeleton of the scaffold (Nayak et al. 2004; Rossman and Lamb 2011; Nayak et al. 2009).

The IAV capsid is made of M1 homo-oligomers organized in a single dense layer (6 nm thick). The M1 proteins are arranged in a lattice of rods densely packed that form a rigid three-dimensional structure with helical symmetry below the viral lipid envelop. Depending on the helical arrangement, it can either form a spherical or filamentous shape. In fact, the range of the helical pitch (the height of one complete turn of the helix) along the length of the filamentous particles is different from the one in the spherical particles. It was also demonstrated that M1 is less ordered at the poles of filamentous viruses than in the middle, this is supposed to make the layer more flexible. (Ruigrok et al. 2000a; Calder et al. 2010; Harris et al. 2001; Dadonaite et al. 2016; Chlanda and Zimmerberg 2016; Archetti 1955).

Initial reports showed that M1 alone was capable to drive the assembly and production of immature virus-like particles (VLPs) by itself. When overexpressed alone in fibroblast cells (COS-1 Line) using a vaccinia virus or in SF9 insect cells using recombinant baculovirus, M1 formed VLPs with similar size and morphology as for influenza virions. These observations indicate that when targeted to the PM, M1 may be sufficient to induce budding on the cell membrane and allow particle release without the need for the other viral components. It is also possible that the above-mentioned expression system causes overexpression of M1 and nonspecific release of extracellular microvesicles such as exosomes that are enriched with M1 protein. However, similar results (budding or vesicles release) could not be reproduced via the transfection based system in

mammalian cells (Chlanda et al. 2016; Archetti 1955; Vijayakrishnan et al. 2013; Gómez-Puertas et al. 2000; G Mez-Puertas et al. 1999; Latham et al. 2001; Chlanda et al. 2015; Wang et al. 2010; Chen et al. 2007).

3.3.4 pH and PHE drug-induced M1 protein disassembly

3.3.4.1 pH-dependent disintegration of the M1 capsid

It is known that the IAV exposure to low pH inside the endosomal compartment causes M1 capsid disintegration. In fact, at acidic conditions (pH ~5.0 or lower), the M1 protein carboxyl groups become almost completely protonated (pKa = 5.2). This allows the protein to bear a higher positive charge, under these conditions and due to the opposite charge of each monomer, M1-M1 electrostatic interaction is converted to repulsive forces that facilitate the dissociation of the M1 shell. The CryoET observation of the IAV incubated at pH 4.9 for 30 minutes showed M1 capsid disappearance. This was used to isolate M1 from assembled virions. Similarly, M1 analysis in solution showed that it forms oligomers at neutral pH and dissociates into dimers or monomers under acidic conditions as mentioned earlier (Safo et al. 2014; Shishkov et al. 2011; Brevnov et al. 2015; Fontana and Steven 2013; Pinto et al. 1992; Zhirnov 1990; Fontana et al. 2012; Schowalter et al. 2009).

During the process of virion internal acidification, the endosomal maturation pathway arises in two distinct steps. In the first step, the virion core is weakly acidified (pH ~6.5 to 6.0) by protons influx and K^+ (or Na^+) efflux. This leads to the weakening of M1-M1 interactions and probably M1 capsid de-oligomerization. M1-RNP interactions are also disrupted leading to vRNP dissociation from the M1 layer while M1 remains bound to lipids (Shishkov et al. 2011; Brevnov et al. 2015; Fontana and Steven 2013; Pinto et al. 1992; Zhirnov 1990; Fontana et al. 2012; Leiding et al. 2010; Manzoor et al. 2017; Helenius 1992;

Shimbo et al. 1996; Chizhmakov et al. 1996; Edinger et al. 2014; Stauffer et al. 2014; Pielak and Chou 2010; Lee 2010; Bui et al. 1996; Ye et al. 1999).

3.3.4.2 M1-M1 interaction inhibitor (PHE drug):

The L-165041 compound abbreviated as PHE was originally used as a selective agonist of the nuclear transcription factor-peroxisome proliferator-activated receptor β /δ (PPARβ /δ). PHE is a small molecule with a hydrophobic character (represented in Figure 16). This drug belongs to the protein-protein interaction (PPI) inhibitors compounds.

Molecular Weight:	402.443 g/mol
Chemical Formula $C_{22}H_{26}O_7$	
Topological polar surface area	102.29
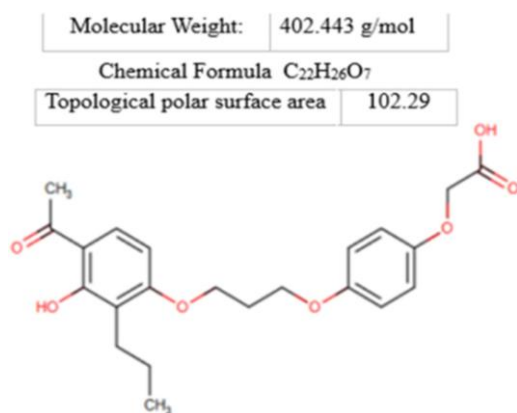
Figure 16 General Chemical Structure of the L-165041 compound (PHE drug) adapted from (PubChem).

Mosier et al. selected the PHE molecule by screening thousands of drugs belonging to the PPI inhibitors family. The PHE molecule was identified as the first M1 targeting compound. Experimental analysis showed that it can disturb the hydrophobic M1-M1 interaction by acting as a wedge to destabilize its self-association and thus disturb M1 layer formation at pH 7.0. Following molecular modeling analysis and virtual screening using a blind docking technique, it was estimated that the PHE molecule has 41 potential binding sites on M1. These sites

are mainly targeting the hydrophobic pocket or the patch present on the M1-M1 interface. These hydrophobic sites are found adjacent to the negatively and positively charged faces. Mosier et al also found that the PHE reduces the thickness of the M1 layer and inhibited *in ovo* propagation of multiple IAV strains including H1N1(WSN/33), pandemic H1N1, H3N2, and H5N1, in a dose-dependent manner. Using Bio-layer Interferometry (BLI) analysis they also confirmed that PHE binds M1 and prevents its oligomerization (Mosier et al. 2016).

3.4 Virion morphology

IAVs are highly pleomorphic with shapes varying from spherical to filamentous. The spherical/ovoid one has a diameter ranging from 100 to 130 nm with spikes. The strains A/Puerto Rico/8/1934 H1N1, A/WSN/1933 (H1N1) show for example spherical morphology. The filamentous virions can reach up to 20 µm in length like in the case A/Udorn/1972 H3N2 strain (Mosley and Wyckoff 1946; Seladi-Schulman et al. 2013; Elleman and Barclay 2004; Badham and Rossman 2016).

Observation of IAVs clinical and veterinary isolates, obtained from lung sections or the respiratory tract cells, showed a mixture of different shapes but with filamentous form predominance. These isolates remain filamentous after few passages in embryonated chicken eggs (ECEs) or epithelial cells such as Madin-Darby canine kidney (MDCK). Nevertheless, after several passages, many of these filament-producing strains produced only spherical virions. The loss of the filament-forming phenotype is probably due to virus adaptation to the laboratory/handling conditions, but this also depends on the infected cells type. Inversely, when spherical laboratory-adapted strains (ex A/Puerto Rico/8/34 [H1N1]) are passaged in guinea pigs they regain their filamentous phenotype. This could be explained by the fact that the natural (i.e. *in vivo*) conditions are

more adequate for the formation of the filamentous virion. (Rossman and Lamb 2011; Vijayakrishnan et al. 2013; Seladi-Schulman et al. 2013; Elleman et al. 2004; Bourmakina and García-Sastre 2005; Nakajima et al. 2010; Choppin and Tamm 1960; Hayase et al. 1995; Elton et al. 2013; Itoh et al. 2009; Kilbourne and Murphy 1960; Shortridge et al. 1998; Rossman et al. 2012).

3.4.1 Viral factors affecting virion morphology

3.4.1.1 Role of M1

M1 is a major genetic determinant of morphological phenotypes. Many studies demonstrated that single or double induced mutations located all over the protein (aa 30, 41, 76, 77, 78, 87, 92, 95, 98, 101, 102, 104 and 105, 157 aa 169, 183, 185, 198, 204, 207, 209 ,85-231,93 and 94, 218) caused a variation in virus shape. Structural analysis showed that most of these mutations are located on the positively charged face of the helix six domain region and are implicated in M1-M1 interactions. We have to notice that some of these mutations can also accumulate accidentally during the repeated virions passaging (Safo et al. 2014; Calder et al. 2010; Harris et al. 2001; Chlanda and Zimmerberg 2016; Seladi-Schulman et al. 2013; Elleman and Barclay 2004; Bourmakina and García-Sastre 2005; Campbell et al. 2014b; Burleigh et al. 2005; Campbell et al. 2014a; Roberts et al. 1998).

In parallel, IAVs incubated at low pH (4.9) show a loss of the filamentous morphology. Thus, it is possible that by affecting M1-M1 interactions in acidic conditions, the viral lipid envelope adapts the spherical form since it is the lowest energy form for lipids (Calder et al. 2010).

3.4.1.2 Role of the envelope glycoproteins

The surface glycoproteins (HA, NA, M2) play also a role in determining the IAV morphology, this could be either due to specific mutations or to the heterogeneous distribution of these proteins over the virus. Electron microscopy observation of filamentous virions showed NA clustering at one of the virus extremities, while the viral ribonucleoprotein was packed on the opposite extremity inside the virion. In parallel, earlier studies demonstrated that the deletions in the cytoplasmic tail of HA or NA affected virus morphology (Jin et al. 1997; Zhang et al. 2000; Rossman and Lamb 2011; Grantham et al. 2010; Iwatsuki-Horimoto et al. 2006; Rossman et al. 2010a; Calder et al. 2010; Nayak et al. 2009; Bourmakina and García-Sastre 2003; Roberts et al. 1998; Bouvier and Palese 2008; Bialas et al. 2014).

Similarly, mutations on the $M2_{AH}$ C-terminus or partial deletion of the M2 tail converted a filamentous virus to the spherical one. Inversely filamentous viruses were obtained from spherical forms after truncation of the C-terminus part (residue 70). The same effect was also observed when monoclonal antibodies were used to block M2. It was also suggested that the M2 delayed abscission can further stabilize the formed complex at the site of budding to allow the continued clustering of M1 and thus the elongation required for the formation of the filamentous form (Chen et al. 2008; Grantham et al. 2010; McCown and Pekosz 2006; Iwatsuki-Horimoto et al. 2006; Roberts et al. 2013; Rossman et al. 2010b; Rossman et al. 2010a; Kolpe et al. 2019; Wharton et al. 1994).

3.4.1.3 Role of the envelope lipid composition

The viral envelope lipid composition can also affect morphology. It was suggested that during budding, the filamentous viruses require the formation of larger raft microdomains that make the envelope more rigid. A recent study showed that a protein usually causing vesicular inward buds in GUVs made from unsaturated lipids caused rigid tubulation when the GUVs were made from saturated lipids. This led to the conclusion that membrane rigidity can make the membrane form filaments (Yu et al. 2018).

3.4.2 Cellular factors affecting virion morphology

Cell polarity and actin cytoskeleton networks play an important role in determining virus morphology. It was shown that the cell depolarization due to disruption of actin or microtubules by the use of inhibitors showed a reduction of filamentous virions production by the infected cells and an increase of the spherical/slightly elongated particles. This led to the conclusion that microtubule motor proteins can provide the mechanical force and the membrane tension that allows tubule formation during budding. However, it is also possible that lipid rafts declustering due to the disruption of the actin cytoskeleton could be the other reason explaining the loss of filamentous virions production (Zhang et al. 2000; Fujiyoshi et al. 1994; Roberts and Compans 1998; Roberts et al. 1998; Simpson-Holley et al. 2002; Sun and Whittaker 2007; Cheung and Poon 2007; Scheiffele et al. 1999).

3.5 Mechanism of IAV virus assembly and budding (role of lipid rafts)

Like other viruses, the assembly mechanism and budding of IAV is an extremely diverse, dynamic, and multi-step process, involving host and viral factors. It also implicates a complex web of interactions among viral proteins. This requires trafficking and concentration of the viral components at specific regions of the PM corresponding to the budding site. During the first step of this process, the host PM is bent into a vesicle towards the extracellular side in an area referred to as the budozone, then the particle produced after scission form either spherical (80-120 nm) or filamentous virions (1-20 µm). It is supposed that the induction of lipid bilayer bending is driven by the energetically favorable self-assembly of the capsid protein M1 and the pre-assembled viral surface spike glycoproteins (HA, NA, M2) (Badham and Rossman 2016). Even though this point has been investigated in cells, it is not clear what is the major force driving the IAV components recruitment and clustering on the budding site. IAV assembly may be orchestrated mainly by the M1 since it can interact simultaneously with other viral components and with the PM.

In the second step of budding, the neck formed at the budozone edges undergoes narrowing (radius decreases). This narrowing is probably due to the lateral line tension exerted by the PM surrounding the budozone area. We have also to notice that the positive curvature mediated by the M2 localized at the boundaries of bud could also contribute further to this narrowing shortly before scission (Veit and Thaa 2011; Nayak et al. 2004; McMahon and Gallop 2005; Rossman and Lamb 2011; Chen et al. 2008; Martyna et al. 2017; Rossman et al. 2010b; Calder et al. 2010; Fujiyoshi et al. 1994; Kordyukova et al. 2019; Nayak et al. 2009; Badham and Rossman 2016; Göttlinger 2010; Rossman and Lamb 2013; Chabanon et al. 2018).

Figure 17 describes the proposed steps of M1 mediated assembly and budding.
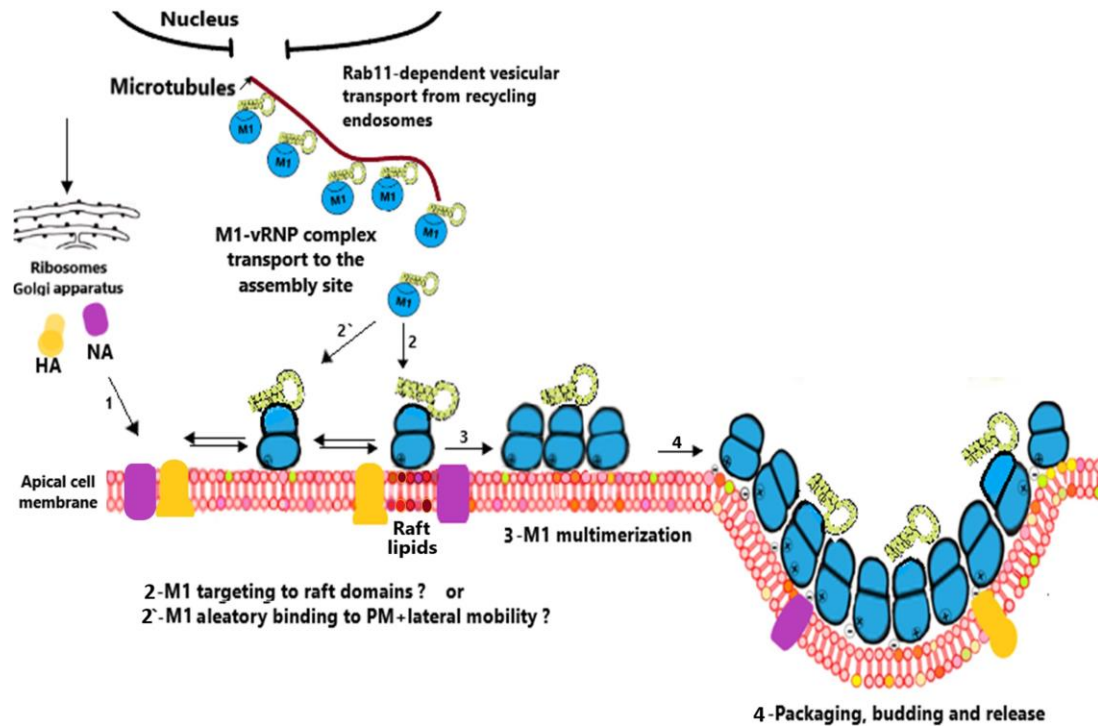
Figure 17 Proposed mechanism of IAV assembly and budding.
1) The viral mature glycoproteins HA and NA, as well as the ion channel protein M2 are transported by the trans-Golgi secretory pathway to the budding site. Later they associate via their transmembrane domains to the lipids rafts on the apical membrane. **2/2`**) M1 proteins are transported via the RNPs complexes to the budding site in a microtubule-dependent manner on Rab-11 positive recycling endosomes. **2**) M1 binds to the cytoplasmic tails of HA and NA. **2`**) M1 binds randomly to the anionic lipids. **3**) M1 can undergo lateral mobility on the PM that allows its clustering and in parallel the lateral sorting of anionic lipids. **4**) Budding starts following M1, HA, and NA clustering, while M2 protein can be localized at the edge of the bud.

3.5.1 Role of lipid rafts in virus assembly

In previous studies, lipidomic analysis of the apical PM isolated from uninfected cells and the one extracted from the IAV envelope was performed (Gerl et al. 2012; Simons and Gerl 2010). The comparison between them showed that the viral envelope is enriched with sphingolipids, cholesterol, PE and PS, but contains less PC. This enrichment with saturated lipids suggests that virus assembly and budding could occur at preexisting raft microdomains present at the apical PM in the infected cells. This also fits with the fact that the influenza virus envelope glycoproteins (HA, NA) show a high affinity for cholesterol/sphingolipid-rich rafts.

However, other studies showed that cholesterol and sphingolipids are not essential for influenza HA colocalization and clustering during assembly (Nayak et al. 2004; Leser and Lamb 2005; Scheiffele et al. 1999; Ivanova et al. 2015; Barman et al. 2001; Barman and Nayak 2007; Polozov et al. 2008; Wilson et al. 2015; Kraft 2016).

Therefore, this hypothesis is controversial and needs re-evaluation. First, it is not clear if these lipid rafts are preexisting or are formed by clustering of the virus components during assembly and budding. Second, it is not possible to determine if the raft lipids are on the inner or outer layer of the PM at the budding site. Third, since M1 is a non-raft-associated protein, its interaction with the cytoplasmic tail of the raft-clustered HA and NA is not sufficient to reach the high density required to form the M1 capsid. This is further confirmed by the fact that the M1 amount is at least 10 times higher than the one of HA. Finally, we have also to notice that the comparison in the above-mentioned studies considered the apical PM of uninfected cells as a control. Thus since the host lipid metabolism may change after infection, we could consider that the uninfected cells might not be the adequate control, as would be the case with the infected cells.

In another comparison, the same studies showed that the whole-cell lipid extracts isolated from infected cells have an increasing amount in PI and a decrease in PC in comparison to the uninfected cells (Yuan et al. 2019; Woods et al. 2016; Gerl et al. 2012; Simons and Gerl 2010).

We hypothesize that during assembly, M1 protein binds randomly to the anionic lipids present on the inner leaflet, and then undergoes lateral mobility which favors juxtaposed M1-M1 interaction. Simultaneously M1 could interact with the cytoplasmic tail of the previously bound NA and HA leading gradually to their self-assembly. Similarly, the concerned lipids with bound viral proteins may also undergo lateral sorting which leads to their clustering and their enrichment at the budding site.

A recent study on HIV assembly showed that the capsid Gag protein multimerization causes cholesterol and PIP_2/ selective lateral sorting which leads to their clustering and domain formation (Yandrapalli et al. 2016). This result could mean that HIV envelope enrichment with cholesterol and PIP_2 is mainly due to Gag-Gag interaction and their lateral mobility which concentrates and segregate specific lipids within the plane of the bilayer.

Thesis focus and scope of this research

In this work, we aim to study the role of Influenza A virus (IAV) matrix protein (M1) in membrane bending at the budozone area, during virus assembly. The main question is whether membrane curvature is solely mediated by M1 or requires also other IAV components to promote virus budding. Also, we wanted to investigate the nature of the forces driving membrane bending at the budding site, since there are several possible mechanisms known to cause lipid bilayer deformation.

Addressing these questions *in vivo* might prove very complex since in cells M1 interacts probably with preexisting clustered lipids via multiple IAV proteins. For this reason, we investigated M1-lipid interactions in a controlled environment, in order to clarify whether the protein has indeed the ability to induce curvature in lipid bilayers on its own.

We utilized different techniques to probe M1-lipids and M1-M1 interactions using model membranes containing anionic lipids. This included Surface Plasmon Resonance (SPR) for determining the apparent binding affinity to lipids for M1 or its derived constructs. Giant and small unilamellar vesicles (GUVs/ SUVs) were also analyzed using confocal and transmission electron microscopy. To quantify protein-protein interactions we performed fluorescence correlation spectroscopy (FCS) analysis.

Besides the known fact that M1 binds to anionic lipids, it is yet not established whether membrane composition could affect M1-induced membrane bending. Consequently, we investigated the effect of membrane enrichment with cholesterol or the presence of other substitute anionic lipids on M1 ability to bend the membrane of vesicles.

Also, the connection between M1-induced membrane bending and its localized binding and clustering has not been explored. With this in mind, we focus on

GUVs with laterally confined anionic lipids to observe if M1 binding could promote localized membrane deformation.

This thesis is submitted in partial fulfillment of the requirements for obtaining a Ph.D. degree in molecular biochemistry at the University of Potsdam. The present thesis contains work in the field of membrane-protein biophysics, with a focus on techniques to investigate protein-lipid interactions and membrane deformation.

The research has been carried out at the Cell Membrane Biophysics Group of Prof. Dr. Salvatore Chiantia, Institute of Biochemistry and Biology, University of Potsdam.

The experimental part has been performed in the period from April 2016 to June 2019.

II MATERIALS and METHODS

1 Chemicals and phospholipids

All lipids (i.e. dioleoyl-sn-glycero-3-phosphocholine (DOPC), 2-distearoyl-sn-glycero-3-phosphocholine (DSPC), 1,2-dioleoyl-sn-glycero-3-phospho-l-serine (DOPS), positively charged 1,2-dioleoyltriammonium-propane (DOTAP), 1,2-dipalmitoyl-sn-glycero-3-phospho-(1′-rac-glycerol) (DPPG), cholesterol and 1,2-dioleoyl-*sn*-glycero-3-phosphoethanolamine-*N*-Lissamine rhodamine B sulfonyl (Rhodamine-DOPE), 1,2-dioleoyl-*sn*-glycero-3-[(N-(5-iminodiacetic acid) succinyl] (nickel salt) (Ni-Tris-NTA DOGS) were obtained from Avanti Polar Lipids (Alabaster, AL, U.S.A). The transition temperature (Tm) of DPPG and DSPC is around 41°C and 55°C, respectively. Alexa Fluor 488 succinimidyl ester was obtained from Life Technologies (Darmstadt, Germany). PHE drug: 2-[4-[3-(4-acetyl-3-hydroxy-2-propylphenoxy) propoxy]phenoxy]acetic acid was purchased from Cayman Chemical (Ann Arbor, MI, U.S.A.). Ten-fold concentrated phosphate buffer (PBS, 100 mM phosphate buffer, 27 mM potassium chloride, and 1.37 M sodium chloride at pH 7.4) was from Alfa Aesar (Haverhill, MA, U.S.A.). Glucose and sucrose were from VWR Chemicals (Radnor, PE, U.S.A.). All other chemicals were purchased from ROTH (Karlsruhe, Germany), unless differently specified. Indium tin oxide (ITO)-coated coverslips, 20 × 20 mm, thickness #1, 8–12 Ohms resistivity, were purchased from SPI supplies (West Chester, PA, U.S.A.).

2 Methodology

2.1 Expression and purification of recombinant M1 constructs

For all experiments, we used four different constructs coding for the (M1, NM1, CM1, M1m) proteins that represent M1 wild-type, the N-terminal domain 1–164 aa (NM1), the C-terminal domain 165–252 aa (CM1), and a mutant lacking a polybasic sequence stretch (M1m), respectively (were kindly provided by Nadine Jungnick (Humboldt-Universität, Berlin, Germany)). In a separate analysis we also used three other constructs that represent M1 with single substitutions of the highly conserved arginine triplet with alanine at positions 76-77-78 (were kindly provided by Chris Höfer (Freie Universität, Berlin, Germany)).

The M1 used in this work is derived from the influenza FPV/Rostock/34 virus that was cloned into a pET15b plasmid. All the M1 protein constructs are carrying an N-terminal 6xHis-tag. The proteins were expressed in Rosetta Escherichia coli (DE3) pLysS-competent cells [*F–, ompT, hsdS$_B$ (r$_B$–, m$_B$–), dcm, gal, lacY1, λ (DE3), pLysS (Cm$_R$)*] grown in 1 l of LB medium (containing 0.2% glucose, 50 mg/ml chloramphenicol, 50 mg/ml ampicillin). Protein production was induced by addition of 0.3 mM IPTG during exponential growth for 3h at 37°C until reaching OD$_{600}$~0.7 (as described by (Hilsch et al. 2014)), then bacteria were harvested by centrifugation for 10 min at 1000 (xg) (Thermo Lynx 4000 F12-6 rotor, Thermo Fisher Scientific, Waltham, MA, United States) and the obtained pellets were stored at −80°C. Afterwards, bacteria pellets were resuspended in ice-cold lysis buffer (16 mM Na$_2$HPO$_4$, 3 mM KH$_2$PO$_4$, 500 mM NaCl, 5.4 mM KCl, 200 µg/mL DNase I, 300 µg/mL lysozyme, 1 mM PMSF, EDTA-free protease inhibitor cocktail, pH 7.4). The lysate was quickly frozen (15 min at −80°C) and incubated on a rotation shaker at 4°C for 30–60 min. Then all the following steps

were performed at 4°C. The bacteria were completely lysed using a French press (Glen Mills, NJ, U.S.A.) run at 1000 psi or sonicated on ice (5 x 20 s). The obtained bacterial lysate was clarified from cell debris by centrifugation at 66000 (xg) for 30 min (Thermo Lynx 4000, A27-8 rotor, Thermo Fisher Scientific, Waltham, MA, United States). The supernatant was incubated with a 2 ml TALON metal affinity resin for His-tag purification (Takara, Saint-Germain-end-Laye, France) in a tube using a rotation shaker for 30–60 min at 4°C. The suspension was loaded onto a column and the cleared lysate was allowed to flow through. To prevent unspecific protein and DNA binding to the resin, the column was washed with equilibration buffer (8 mM Na_2HPO_4, 1.5 mM KH_2PO_4, 500 mM NaCl, 2.7 mM KCl, pH 7.4) for another 10 min at 4°C on a shaker platform. The column was washed again 2-3 times using gravity flow with equilibration buffer, followed by an intermediate washing buffer composed of equilibration buffer with 60 mM imidazole. Protein was finally eluted with elution buffer (two-fold concentrated PBS with 180 mM imidazole, pH 7.4). The eluted fractions were collected and concentrations were determined by UV absorbance at 280 nm on an Agilent 8453 UV/VIS spectrophotometer (Agilent Technologies, Milford, MA, U.S.A.). Typical (maximal) protein concentrations were ~60 µM. SDS/PAGE was also performed to verify protein purity. Afterward, selected protein samples containing fractions were pooled and buffer exchanged with PBS buffer by SEC using PD-10 desalting columns that contain Sephadex G-25 (GE Healthcare, Munich, Germany). This step is important because the excess of high-salt and the imidazole in the elution buffer may affect M1 binding to the lipids and osmolarity of the vesicles. as well as to remove bulk responses caused by the difference of refractive index (RI) between sample and running buffer during SPR analysis. M1 derived constructs NM1, M1m, CM1 were also purified at pH 7.4 as described above. The elution buffer used for NM1 and M1m was the same as the one used for M1. However, the elution buffer used for CM1 was 1xPBS with additional 100 mM imidazole (pH 7.4).

For the M1 purification at pH 5, the intermediate washing buffer contained 20 mM imidazole (pH 6.5). The elution buffer contained 50 mM sodium acetate and 300 mM NaCl (pH 5). In both cases, proteins were immediately subjected to fluorescence labeling.

2.2 Protein labeling for fluorescence microscopy

Purified M1 constructs were conjugated with the primary amine-reactive dye Alexa Fluor 488 succinimidyl ester. For that freshly purified protein (in elution buffer) was incubated with a 10-fold molar excess of reactive dye for 12 h at 10 °C, pH 7.2. For simple imaging experiments, the protein dye mixture was directly used, without further separation. For quantitative experiments (e.g. sFCS experiments), the labeled protein (M1-Alexa488) was separated from the free dye using SEC (PD-10, GE Healthcare, Munich, Germany). The labeled protein was eluted with diluted PBS (pH 7.4) that matches the desired final osmolarity. Protein concentration and labeling efficiency were determined by absorbance at 280 and 490 nm, respectively. The maximum protein concentrations were typically $\sim$40 µM, while labeling efficiencies ranged between 0.1 and 0.15 dye/protein.

2.3 Lipid monolayers preparation from liposomes

Liposomes required for preparing the lipids monolayer were generated by mixing pure samples dissolved in chloroform in the desired molar ratios (70:30 DOPS: DOPC or 100 % DOTAP, 20:80 DOPS: DOPC, 10:90 PI4P: DOPC, 10:90 PI3P: DOPC) then the solvent was evaporated under a nitrogen stream. The lipid film was resuspended in PBS (pH 7.4) by vortexing and the obtained dispersion was sonicated using a bath sonicator (Emag Emmi 20 HC, Mörfelden-Walldorf, Germany) for 5mn.

Large unilamellar vesicles (LUVs) which are adequate for cryo-TEM were prepared by extrusion. For that, the desired lipids dispersion mixture (100 % DOPC, DOPC/DOPS (75/25), DOPC/DOPS (60/40)) prepared in PBS (pH 7.4) at concentration 2 mM total was vigorously vortexed for 2–5 min. The diameter of the obtained multilamellar vesicles was reduced by serially extruding the suspension 11-times through a 100-nm pore diameter polycarbonate membrane (Whatman, Maidstone, U.K.) with a hand-held extruder (Avanti Polar Lipids, Alabaster, U.S.A). Liposome size ($\sim$130 nm diameter) was measured via dynamics light scattering, using a Zetasizer HS 1000, (Malvern, Worcestershire, U.K.). The purified M1 (unlabeled) in elution buffer was diluted with deionized water to approximatively match the osmolarity of the liposome suspension ($\sim$2.6-fold dilution).

Phospholipid monolayers are simple model membrane systems that are perfectly suited to study the binding of peripheral proteins onto a membrane surface using an adapted sensor ship. The HPA sensor chip contains a self-assembled monolayer of long-chain alkanethiol groups that are covalently bound to its gold surface forming a hydrophobic layer to facilitate adsorption of liposomes. When injected over the surface, the liposomes rupture and fuse to form a supported lipid monolayer on the chip. This lipid monolayer generates a membrane-like environment where analytes in aqueous buffer interact with polar lipid head groups (Cooper et al. 1998; Plant 1993; Terrettaz et al. 1993). Before use, the surface of the HPP chip was cleaned by an injection of the nonionic detergent *N*-octyl β-d-glucopyranoside (100 µl, 40 mM) at low flow. The DOPS/DOPC (70:30) 1mM and DOTAP (100) 1mM liposomes were separately injected onto the active surface (flowcell 1) and the control surface (flowcell 2) of the HPP chip, respectively. These injections were applied at low flow for 60mn. Then to remove any putative multilamellar structures or any loosely bound liposomes

from the lipid surface, sodium hydroxide (200 µl, 20 mM) was injected several times until producing a stable baseline with signal ranging from 2500-3200 resonance units (RU). To verify the complete coverage of the sensor chip by the lipids, we injected bovine serum albumin (BSA)-solution. A fully covered sensor, a fully covered sensor chip showed a lack of BSA binding (<100 RU) whereas the uncovered surface showed higher non-specific binding to sensor chip coating (≥800 RU).

2.4 SPR analysis of M1 binding to the lipid monolayer

In this work, we used SPR to evaluate M1 binding to the surface-supported lipid monolayer. First, to further validate the accuracy and precision of the SPR machine for measuring K_D we used a lipid-binding drug as control. The propranolol drug is known to binds to PS and has already established K_D. For that, we monitored the binding of propranolol with determined concentration to PS monolayer. Then the obtained calibration curve was used to determine the concentration.

In our case, the dissociation of M1 from the PS monolayer was very slow (5% after 1 h), indicating a tight M1 binding to the PS lipids. Thus we assumed the dissociation constant K_{off} to be negligible.

In our case the response curves of M1 binding to the lipids were fitted to the Hill-Waud binding model (equation 3) using Sigma plot 12.0 software:

$$R_{eq} = \frac{R_{max}[A]^b}{K_D^b + [A]^b}$$

Equation 3

Whereas [A] is the analyte concentration, R_{eq} is the near-equilibrium resonance unit (RU) value at a given concentration [A] for the protein. K_D is the dissociation constant, R_{max} indicates the maximal R_{eq} value when the binding is saturated, b is the Hill cooperativity coefficient (in case of a 1:1 Langmuir model n=1).

As mentioned earlier on the same sensor chip, the flow cell coated with lipid monolayer DOPC/POPS (70:30) is considered to be the active surface while the negative control (reference surface) is coated with DOTAP serve for estimation of bulk RI shift. Then for analysis, reference sensorgrams were systematically subtracted from reaction sensorgrams and normalized. All solutions were freshly prepared, degassed, and filtered through 0.22 µm pores, and measurements were performed at 24 °C in PBS (pH 7.4). The monolayer regeneration was performed after every injection to wash off the bound protein by a short injection of 2xPBS (pH=10).

In each case, the experiments were repeated at least independently four times (with different protein purification every time).

2.4.1 Testing the effect of PHE on M1 binding to PS lipids

The SPR sensor ship was prepared as previously mentioned. Then the M1 protein (1µM) was injected on flow cell 1, while the M1 protein (1µM) incubated previously with the PHE drug (100µM) was injected on flow cell two.

For estimation of bulk RI shift caused by the PHE drug solvent (3% DMSO), PHE drug (100µM) in PBS was injected on the lipid monolayer surface. Then, the obtained sensorgrams were systematically subtracted from the reaction sensorgrams of flowcell two and normalized.

2.5 Preparation of GUVs

Giant unilamellar vesicles (GUVs) were prepared using the electroformation method (also called electroswelling). For that, an alternating electric current is applied across a hydrated film of lipids deposited between two ITO plates. The vesicles continue to grow until they detach from the surface. Depending on the type of lipid and the used buffer, the produced unilamellar vesicle diameters vary between 1 and 100 µm. In our case, different lipid compositions were used to prepare the vesicles. Typically, DOPC and cholesterol were mixed with various amounts of negatively charged lipids (e.g. DOPS) at molar ratios between 10 and 50 mol%. Rhodamine-DOPE 0.05 or 0.1 mol% was added as a tracer to allow GUVs membrane visualization by confocal microscopy. The GUVs electroformation chamber consisted of two conductive ITO coverslips facing each other and separated by a 3-mm thick Teflon spacer. The total volume of the chamber was ~300 µl. Thirty microliters of 3 mM lipid solution in chloroform and/or ethanol were spread on a preheated ITO coverslip, forming a thin lipid film. The solvent was evaporated using a nitrogen flow for 5 min at room temperature (note that solvent evaporation under vacuum for 1 h did not show a difference in vesicle behavior). After assembly, the chamber was filled with a sucrose solution in deionized water (e.g. 150 mM) and connected to a voltage generator (AC generator FG 250 D, H-Tronic, Hirschau, Germany). For experiments at low pH, the chamber was filled with 150 mM sucrose, 10 mM acetate buffer solution at pH 5. A sinusoidal electric field of 1.4 V at 10 Hz was applied for 1.5 h at room temperature. To facilitate the detachment of GUVs from the slides, the voltage was decreased to 0.5 V for 30 min. The GUVs were used within 12 h of production. For microscopy observation, the vesicle suspension was smoothly transferred to a 35mm borosilicate glass petri dish (CellVis, Mountain View, CA, U.S.A.), which was previously passivated with a 1% bovine serum albumin solution. This imaging chamber allows large sample volumes that

reduce any effect of osmotic imbalances due to buffer evaporation during the extended experimental FCS analysis. The M1 protein added to the chamber was mixed by very smooth pipetting to allow protein binding to GUVs membranes.

Giant unilamellar vesicles formed of L_O phase and L_D phase were prepared using a lipid mixture consisting of 10 mol% cholesterol, 45 mol% DOPC, 15 mol% DPPG, and 30 mol% DSPC. Additionally, 0.05 mol% Rhodamine-DOPE was added to visualize the different lipid domains. Lipids were dissolved in chloroform/methanol 9:1 v:v (5 mM, prepared freshly and kept under a nitrogen atmosphere). The obtained lipid film was subjected to the electroformation procedure (see the previous paragraph) at 55°C for 1.5 h. The temperature increases above the T_m allows all the lipids to mix. After the end of electroformation, the chamber was then cooled down slowly at room temperature before imaging. This slow cooling process allows the phase separation to develop adequately. In fact below its miscibility transition temperature (Tm), the saturated and the unsaturated lipids separate into two liquid phases: The liquid-ordered (L_O) phase rich in high Tm lipids and the liquid disordered (L_D) phase rich in low Tm lipids.

2.6 M1 labeling and fluorescence GUVs imaging

First, the M1 protein present in the elution buffer was diluted with deionized water to reach the target approximate osmolarity. For experiments in which GUVs were prepared in 150 mM sucrose (see experiments shown in figures 21, 25, and 26), the purified M1 solution (with or without Alexa Fluor 488 succinimidyl ester) was diluted approximately five-fold. Typical protein concentrations at this step were ~12 μM. The protein solution was then mixed with the GUVs suspension in the imaging chamber with different volume ratios to obtain the final desired protein concentration (usually between 5 and 10 μM) in a total volume of 300 μl. This procedure ensured that sugar

concentration and osmotic pressure across GUVs membranes were always reproducible, at the expense of slight variations in buffer composition (e.g. NaCl between ~25 and ~70 mM, as mentioned in each figure caption). It is worth mentioning that no significant alteration in M1–lipid interactions were reported in the presence of NaCl between 0 and 150 mM (Baudin et al. 2001).

For the experiments performed in the presence of the M1-multimerization inhibitor PHE, M1 protein present in the elution buffer (~60 µM) was incubated with PHE (100 µM, unless differently stated) for 30 min. Afterward, the mixture was incubated with 4 µM Alexa Fluor 488 succinimidyl ester, for 2 h at 4°C. Finally, the protein solution was diluted with deionized water to approximatively match the osmolarity of the vesicle suspension and mixed with the GUVs, to obtain a final protein concentration of 10 µM (and ~25 µM PHE).

For the experiments performed at pH 5, M1 was purified and labeled at low pH as mentioned above, then the labeled M1 was subsequently diluted using deionized water to equal the osmolarity of the GUVs lumen solution. The solution was then mixed with the GUVs suspension, to obtain a final protein concentration of 10 µM.

We have also confirmed that the presence of imidazole does not affect membrane curvature for at least 2 h and that Alexa Fluor 488 succinimidyl ester does not significantly interact with GUVs. Nevertheless, in the case of samples that required higher protein concentrations (i.e. >10 µM M1) or extensive removal of free dye, the elution buffer was exchanged after protein labeling, using a PD-10 column. In this case, the protein was eluted using two-fold diluted PBS (pH 7.4), to equal the osmolarity of GUVs samples prepared in 150 mM sucrose.

Imaging was performed on a confocal fluorescence laser scanning microscopy (CLSM) Zeiss LSM780 system (Carl Zeiss, Oberkochen, Germany) using a 40× 1.2 NA water-immersion objective. Samples were excited with a 488-nm argon laser (for Alexa Fluor 488 succinimidyl ester) or a 561-nm diode laser (for Rhodamine-

DOPE). For measurements performed using 488 nm excitation, fluorescence was detected between 499 and 695 nm, after passing through a 488-nm dichroic mirror, using GaAsP (gallium arsenide phosphide) detectors. For measurements performed with 561 nm excitation, fluorescence emission was separated using a 488/561 nm dichroic mirror and was detected between 570 and 695 nm.

ImageJ (NIH, Bethesda, MA, U.S.A.) was used to analyze microscopy images and determine the circularity of randomly selected GUVs. Vesicles with a circularity <0.85 were defined as deformed/non-spherical.

2.7 M1-GUVs FCS analysis:

The autocorrelations obtained were corrected for bleaching, then intensity data acquisition and analysis were performed as described by (Dunsing et al. 2017; Dunsing and Chiantia 2018; Ries and Schwille 2006).

Protein brightness and fluorescence intensity were normalized to take into consideration day-to-day variations in laser power, optics alignment, and degree of protein labeling, as described previously (Hilsch et al. 2014).

2.8 Cryogenic transmission electron microscopy (cryo-TEM)

This part was performed in collaboration with Dr. Kai Ludwig. LUVs and protein solution or with buffer (control) were mixed in a total volume of 800 µl so to obtain a 10µM final M1 concentration. Typical final lipid concentrations were ~0.5 to 1 mM. Perforated carbon film-covered microscopical 200 mesh grids (R1/4 batch of Quantifoil, MicroTools GmbH, Jena, Germany) were cleaned with chloroform and hydrophilized by 60 s glow discharging at 8 W in a BAL-TEC MED 020 device (Leica Microsystems, Wetzlar, Germany) before 5 µl aliquots of the liposome/protein solution were applied to the grids. The samples

were vitrified by automatic blotting and plunge freezing with an FEI Vitrobot Mark IV (Thermo Fisher Scientific, Waltham, MA, U.S.A) using liquid ethane as a cryogen.

The vitrified specimens were transferred under liquid nitrogen into the autoloader of an FEI TALOS ARCTICA electron microscope (Thermo Fisher Scientific, Waltham, MA, U.S.A). This microscope is equipped with a high- brightness Schottky field-emission gun (XFEG) operated at an acceleration voltage of 200 kV. Micrographs were acquired on an FEI Falcon 3 4k × 4k direct electron detector (Thermo Fisher Scientific, Waltham, MA, U.S.A) using a 70 µm objective aperture at a primary magnification of 28 or 45 k.

III Results

1 SPR based quantification of M1 protein binding

The characterization of the different M1-based constructs binding to lipids was further conducted using SPR. This technique has been previously used to quantify the interactions between lipid membranes and the matrix proteins of several viruses, including HIV and Ebola (Simons and Sampaio 2011; Soni et al. 2013). The principal advantage of this technique is that protein affinity towards model membranes can be quantitatively determined with high sensitivity without any need for labeling with, for example, a fluorescent marker.

SPR measurement of M1 protein binding to the lipid monolayer was monitored at increasing concentrations in the range between 3 nM and 3 µM (10 µM–130 µM for CM1, due to its low affinity to membranes).

To maximize the binding of the different M1 constructs to the lipids, we used liposomes with 70 mol% DOPS concentration to create the lipid monolayer. However, we have to notice that due to the hydrophobic nature of the interaction between sensor chip and lipids, the final relative amount of DOPS in the

monolayer on the functionalized SPR sensor chip might be lower than 70 mol%. In this context as a comparison, the specific monolayer composition is not expected to play an important role among the different protein constructs, as long as it keeps constant among different experiments.

Figure 18 shows an exemplary sensorgram obtained for 1 µM M1. All sensorgrams were corrected using a reference sample and the time point zero corresponds to the beginning of the protein solution injection.

As SPR sensorgrams were characterized by slow association kinetics and complex (i.e. biphasic) behavior, long association times were used to reach equilibrium responses. For that, the injection/binding phase for each concentration lasted ca. 20 min (see arrows in Figure 18). We considered that R_{eq} was simply estimated as the maximum RU recorded after 20 min. Then the obtained R_{eq} values were then plotted against protein concentrations $[C]_x$ and analyzed. After the end of the injection, the dissociation phase was monitored for 5 minutes. In our case, the dissociation of M1 appeared remarkably slow and was not further analyzed. Lipid monolayer regeneration was performed after each protein injection to wash away bound M1. In parallel under our experimental conditions, no binding of M1 was detected to the DOTAP.
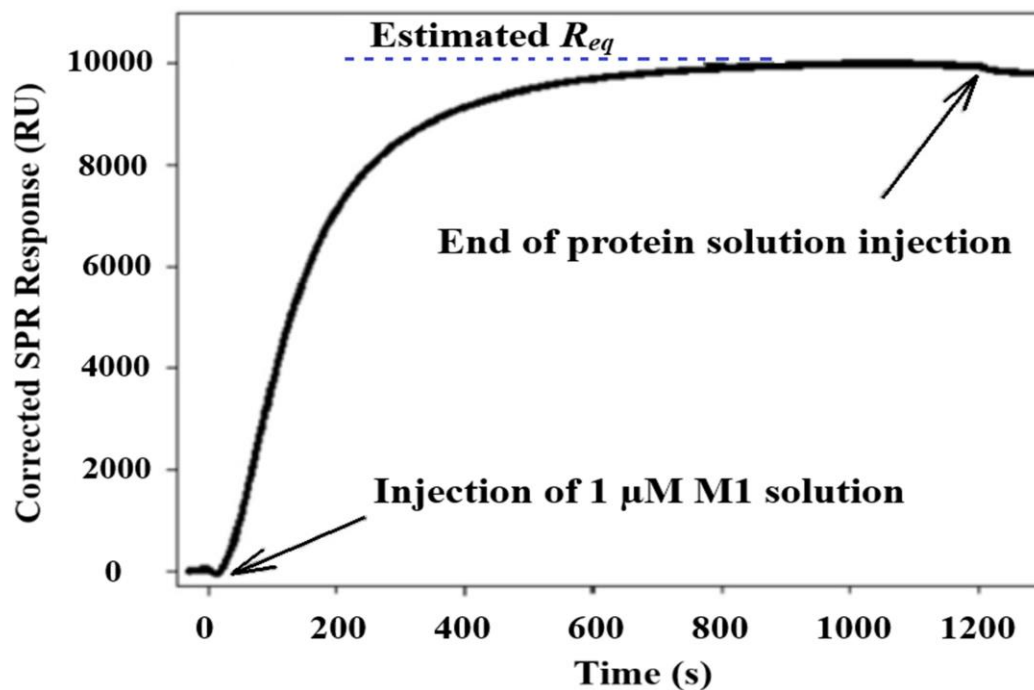
Figure 18 Quantification of M1 binding to DOPC/DOPS membranes via SPR measurements. Representative sensorgrams after reference subtraction were obtained for the binding of M1 (e.g., 1 µM) to a DOPC/DOPS 30:70 monolayer. It can be divided into three phases: association phase (M1 injection), steady-state (equilibrium phase), dissociation phase (after exposure of the chip to the running buffer). The arrows indicate the beginning and the end of protein injection. The experiment was performed at a low flow rate, allowing 1200 s of association and 300 s of dissociation. R_{eq} was estimated as the value of the SPR response reached at the end of the protein (adapted from Dahmani, Ludwig, & Chiantia, 2019).

For SPR data analysis, we focused our attention exclusively on the estimated near-equilibrium value reached after a 20-min binding phase at R_{eq}Similarly to what has been previously reported (Barros et al. 2016), the obtained curves could not be fitted by a simple Langmuir adsorption isotherm, most likely due to collective adsorption, electrostatic surface effects, and protein-protein interaction (i.e. multimerization) that arise simultaneously during membrane binding. For that, fitting with an empirical binding model (Equation 1) was more adapted to the data. As suggested in (Barros et al. 2016), Figure 19 shows typical binding curves for the different M1 constructs obtained by using equation 1.
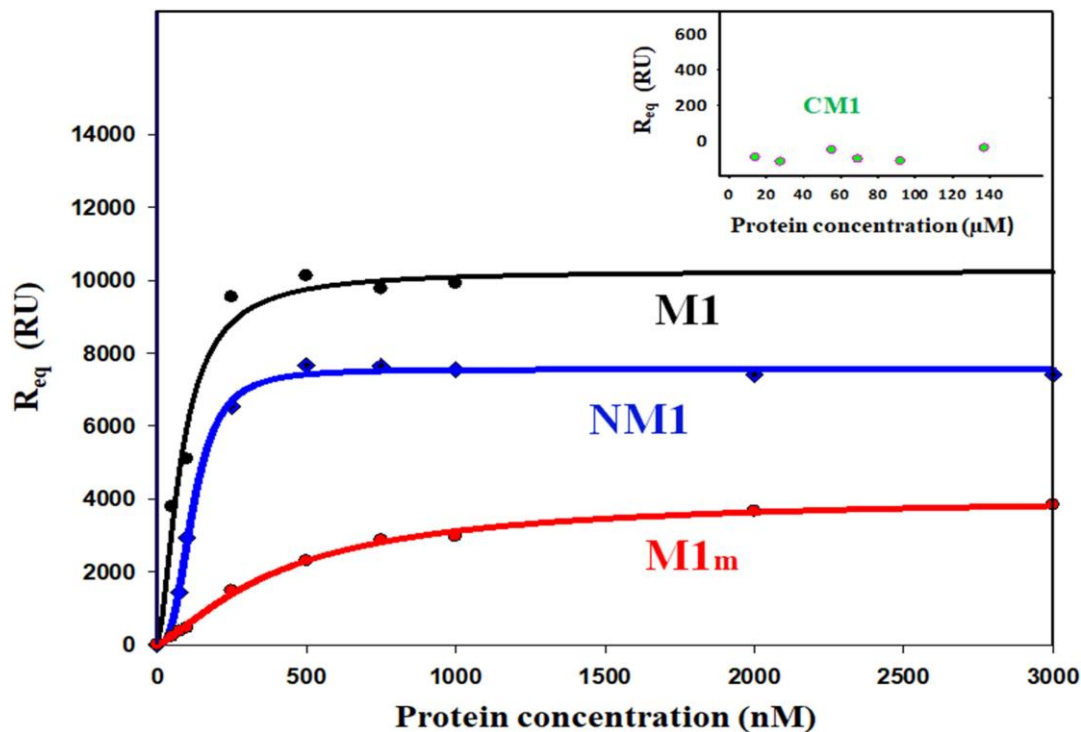
Figure 19 Typical binding curves obtained for the different M1 constructs by monitoring R_{eq} as a function of protein concentration.

M1 (black), NM1 (blue), and M1m (red) were analyzed in the concentration range of 3 nM-3 μM. CM1 concentrations (green) were in the 10 – 130 μM range. The solid lines represent the fitting of the binding curves using an empirical binding model (see text). For each M1 construct, we measured 3-5 independent protein preparations and analyzed a corresponding number of binding curves. The obtained parameters and the standard deviations are reported in Table 1. All measurements were conducted at room temperature (adapted from Dahmani, Ludwig, & Chiantia, 2019).

As represented in Table 1, we were able to obtain the maximum protein binding load (R_∞) and an apparent dissociation constant ($K_d{}^{app}$) of M1, M1m, NM1 and CM1 to DOPC/DOPS monolayers.

Table 1 Parameters obtained from SPR binding curves of the different M1 constructs. R_∞ is the value of RU at the maximum coverage of bound protein, $K_d{}^{app}$ is the apparent dissociation constant of the protein to the lipid monolayer, it corresponds to the protein concentration at which half of the accessible monolayer surface is occupied. n represents the number of independent experiments performed on different protein preparations and analyzed on different days. For each protein, we calculated the average and the standard deviation of each parameter (adapted from Dahmani, Ludwig, & Chiantia, 2019).

Construct	R_∞ (RU)	$K_d{}^{app}$ (nM)	n
M1	8000 ± 300	100 ± 20	5
M1m	2900 ± 900	290 ± 80	4
NM1	7200 ± 400	70 ± 20	4
CM1	-180 ± 80	N/A	3

The measured $K_d{}^{app}$ value for M1 is within the same order of magnitude as previously reported (Batishchev et al. 2016). In parallel, a direct comparison of R_∞ (the total amount of bound protein at excess concentrations) can be applied only between constructs with similar mass, that is, M1 and M1m, as seen indicated in Table 1, M1 showed 3-fold higher binding capacity than M1m. The apparent affinity (i.e. the protein concentration needed to reach half of the maximum protein binding in our experimental setup) is comparable for M1 and NM1, but significantly higher for M1m. Altogether, SPR measurements indicate that the N-terminal domain of M1 has an affinity to DOPS-containing membranes similar to that of the full-length protein, while the substitution of six amino acids on the PBD (as in M1m) markedly decreases protein binding to the membrane.

Finally, no binding could be measured between CM1 and DOPS containing monolayers at protein concentrations up to ca. 130μM. More specifically, the binding of CM1 to DOPC/DOPS monolayers was in general very low (< 500 RU at 30 μM, compared to ca. 10,000 RU for M1 at 1 μM) and comparable to that of the reference surface control containing the positively charged DOTAP lipid.

As shown in figure 20, we can see that the binding is faster in the presence of the drug. This could be due to the bulk RI shift caused by the PHE drug bound to M1, then when the steady-state plateau is reached the amount of M1 binding to lipids in both cases is quite similar. This indicates that PHE has not affected M1 binding to the DOPC: DOPS 80:20 membrane.
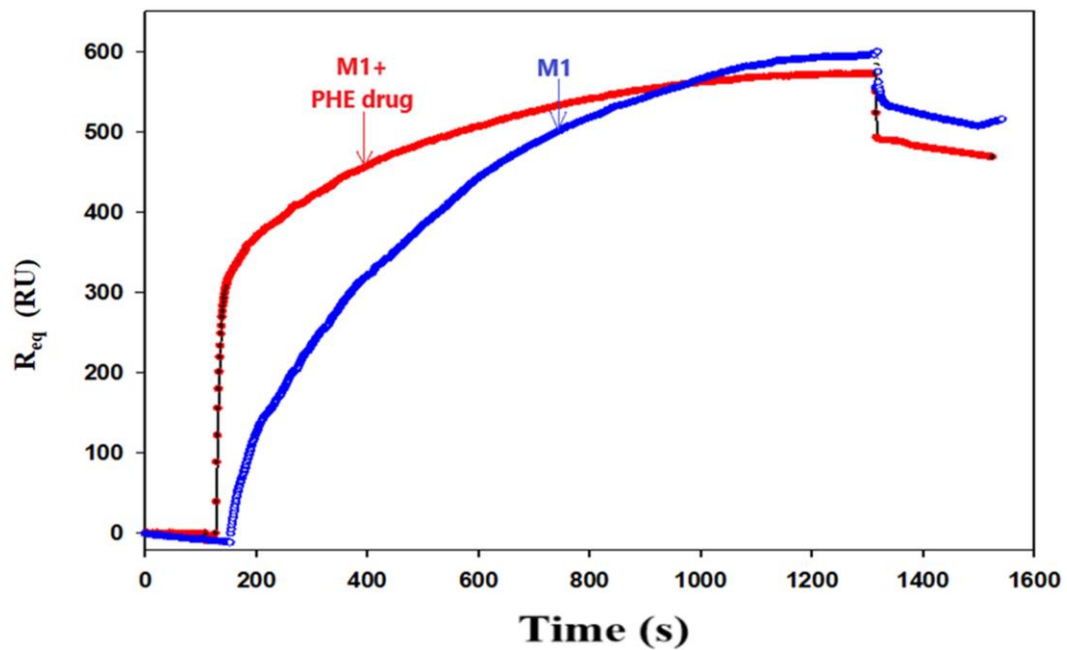
Figure 20 Quantification of the PHE drug effect on M1 binding to lipids in SPR measurements. M1 (1µM) binding to DOPC: DOPS 80:20 membranes in the presence (red) or absence (blue) of the PHE drug (100µM).

2 M1 protein-mediated membrane deformations on GUVs

To confirm whether M1 on its own is sufficient to induce membrane deformation in protein-free lipid bilayers, we incubated GUVs of different compositions in the

presence of 5 µM M1-Alexa 448 (Figure 21). The freshly prepared lipid vesicles included increasing amounts of DOPS (from 0 to 50 mol%) were labeled with small amounts of a fluorescent lipid (Rhodamine-DOPE) and observed *via* CLSM, as it was shown that this lipid promotes M1 binding via electrostatic interactions (Baudin et al. 2001; Das et al. 2012; Höfer et al. 2019a). It is worth noting that the ratio of M1 protein labeling is approximately one in ten. Nevertheless, there was a clear signal of M1 on the lipid layer with a homogenous distribution (Figure 21 insert in panel D and F). Moreover, considerable membrane deformation was observed for GUVs containing high amounts of DOPS (i.e. ≥30 mol %) (Figure 21 C, D, G, H). GUVs containing low amounts of DOPS (e.g. 10 mol%, Figure 21 B) remained mostly spherical. We have to notice that the deformed GUVs remained stable during the measurement time. Although alterations in membrane shape could be obtained also by using not labeled M1, the use of fluorescent M1 was necessary to directly visualize protein binding and organization. As expected, in the absence of DOPS, we can see very little binding of M1 to the membrane and most of the protein remains in the solution outside the GUVs (Figure 21E). In the case of GUVs containing 10mol% DOPS, M1 bound homogeneously to the lipid membrane (Figure 21F). In parallel, the intensity of Alexa 488 fluorescence inside and outside of deformed GUVs was not differentiable (e.g. Figure 21 inset panel D). This may signify that the labeled M1 or the free dye might have crossed the membrane into the lumen of the vesicles in many cases. However, we observed that the shape of deformed GUVs was qualitatively reproducible also whenever M1 was more clearly excluded from the lumen of the vesicles (Figure 25 A, B). Additionally, an increase in membrane acyl-chain order (by increasing cholesterol concentration to 40 mol%, Figure 21 H) did not seem to affect membrane deformation. Similarly, as in the presence of DOPS, GUVs shape alterations by M1 could also be reproduced if DOPS was substituted by other negatively charged lipids, e.g. PIP2 or PG (data not shown).
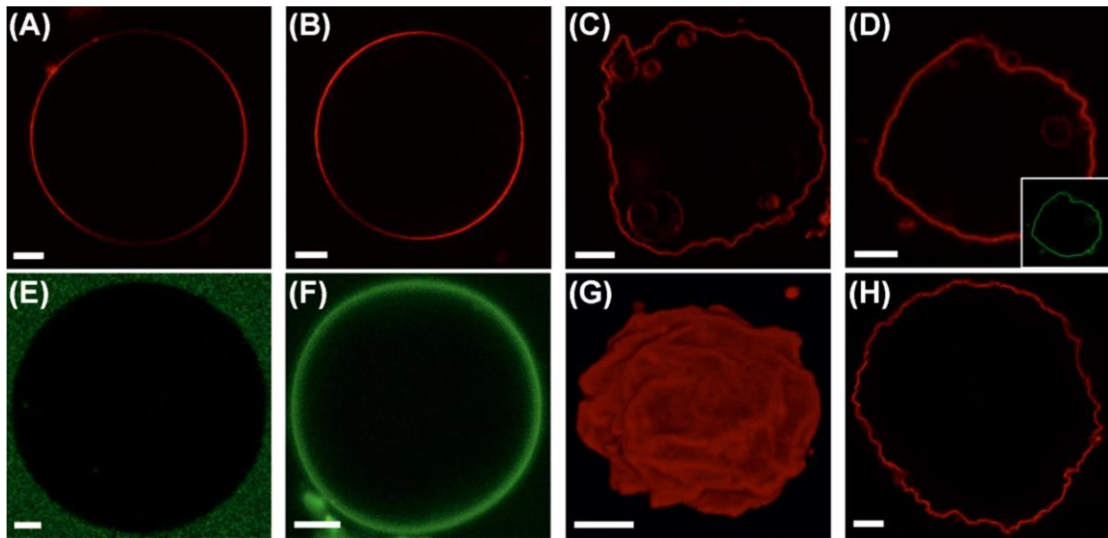
Figure 21 Shape alterations induced by M1 in DOPS-containing GUVs. (**A–D**) Typical GUVs composed of 20 mol% Cholesterol, 20 mol% DOPC and increasing amounts of DOPS ((**A**) 0 mol%, (B) 10 mol%, (**C**) 30 mol%, (**D**) 50 mol%) observed *via* confocal laser scanning microscopy (CLSM) after 30-min incubation with 5 µM M1-Alexa488. Rhodamine-DOPE (0.01 mol%, red channel) was added to allow the visualization of the lipid bilayer *via* CLSM. Inset in (**D–F**): Fluorescence signal originating from M1-Alexa488 (green channel) for typical GUVs containing 0 mol% DOPS ((**E**) corresponding to the sample represented in (A)), 10 mol% DOPS ((F) corresponding to the sample represented in (**B**)) and 50 mol% DOPS (inset in (**D**)). (**G**) Three-dimensional reconstruction of a typical GUV containing 30 mol% DOPS in the presence of 5 µM M1-Alexa488 (corresponding to the sample represented in (**C**)). The fluorescence signal originates from Rhodamine-DOPE (0.01 mol%, red channel). (**H**) CLSM image of a typical GUV composed of 30 mol% DOPC, 30 mol% DOPS, and 40 mol% cholesterol, in the presence of 5 µM M1-Alexa488. The fluorescence signal originates from Rhodamine- DOPE (0.01 mol%, red channel). All GUVs contained 150 mM sucrose in their lumen and were suspended in a phosphate-buffered protein solution (NaCl ~25 mM, pH 7.4) with similar osmolarity (see 'Materials and methods' section). Scale bars are 5 µm. Images were acquired at 23°C.

Finally, we also showed that the N-terminal domain of M1 (NM1 aa. 1–164) is sufficient to induce membrane deformation (Figure 22 A). The C-terminal domain (CM1 aa. 165–252) shows no effect on GUVs shape (Figure 22 B). As shown above, CM1 has a low degree of membrane binding (Figure 19).
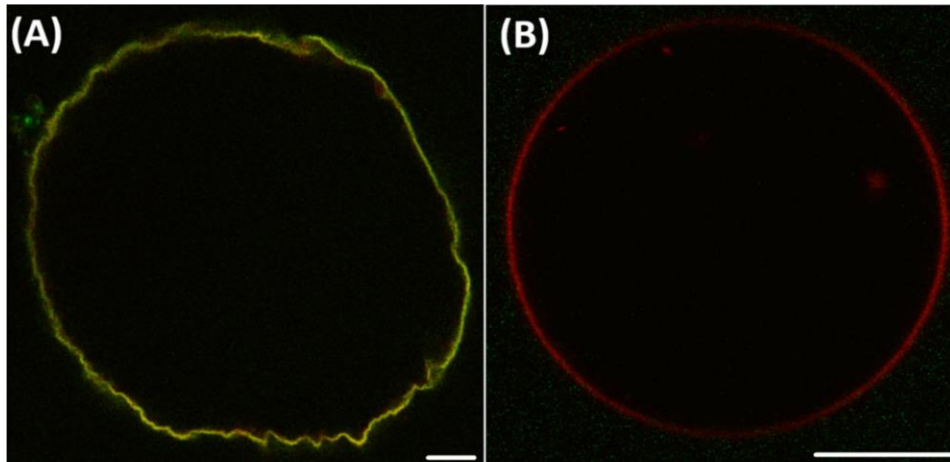
Figure 22 The N-terminal domain of M1 is sufficient to induce membrane deformation. (A) CLSM image of a typical GUV with the following composition: DOPC: cholesterol: DOPS 20:0:20 molar ratios, in the presence of 10 µM NM1-Alexa488 (green channel). The lipid bilayer was labeled with 0.01 mol% Rhodamine-DOPE (red channel). (**B**) CLSM image of a typical GUV composed of DOPC: cholesterol: DOPS 50:20:30 molar ratios, in the presence of 10 µM CM1-Alexa488 (green channel). The lipid bilayer was labeled with 0.01 mol% Rhodamine-DOPE (red channel). All GUVs contained 150 mM sucrose in their lumen and were suspended in a phosphate-buffered protein solution (pH 7.4, NaCl ~45 mM) with similar osmolarity (see Materials and Methods). Scale bars are 5 µm. Images were acquired at 23°C.

Table 2 (row 'M1 pH 7.4') gives a quantitative analysis connected to the percentage of deformed GUVs observed for different lipids compositions, in conditions identical to those relative to the samples shown in Figure 21. To detect protein binding and, thus, involve the quantification of only larger GUVs (>10 µm diameter) that show a significant amount of M1 binding, we increased the protein concentration to 10 µM (18 µM for GUVs with only 10 mol% DOPS). General visual inspection of various vesicles confirmed that membrane deformation is related to higher DOPS concentrations.

Table 2 Quantitative characterization of the amounts of non-spherical GUVs for different membrane compositions and experimental conditions.

GUVs lipid composition DOPC+DOPS mol%	Relative amounts of deformed GUVs				
	DOPS 10%	DOPS 20%	DOPS 30%	DOPS 40%	DOPS 50%
M1 at pH 7.4	0%	24%	49%	83%	89%
	n=29	n=33	n=81	n=84	n=26
M1 at pH 7.4 +PHE			8%	13%	20%
			n=26	n=23	n=15
M1 at pH 5	0%		12%	17%	
	n=46		n=25	n=23	

Percentages of deformed GUVs are reported for the different lipid compositions and experimental conditions. The row 'M1 pH 7.4' refers to the conditions described for the experiments shown in Figure 21. The row 'M1 + PHE pH 7.4' refers to the experiments described in the context of Figure 27 A. The experiment reported in table 2 was performed by treating M1-Alexa488 with PHE concentrations ranging between 75 and 150 µM. The row 'M1 pH 5' refers to the experiments described in the context of Figure 27 B. The total numbers (n) refer in all cases to GUVs that were clearly labeled with fluorescent M1 and had a diameter > 10 µm. The concentration of M1-Alexa488 was 10 µM, with the exceptions of the DOPS 10 mol% (18 µM) and DOPS 50 mol% (6 µM) samples. The percentages summarize the results of at least two independent experiments.

3 M1-mediated deformation on LUVs observed at high resolution

Characterization of M1 mediated bilayer deformation in GUVs investigated by CLSM is limited by optical resolution. In order to get observation with high-resolution and better information regarding the interplay between M1 binding

and membrane curvature, we used cryo-TEM to observe LUVs (diameter ~100 nm) in the presence of M1. For that, lipid vesicles containing DOPC and 40 mol% DOPS were incubated with 10 µM M1 (unlabeled). As shown in Figure 23 (A, B), M1 binds to a large area of the LUVs. Thanks to the high spatial resolution of cryo-TEM, on a nanometer-scale, we can see by observing the apparent bilayer thickness that M1 binding to the vesicles appears not homogeneous. We can distinguish regions of the bilayer with bound M1 (red and yellow arrows) from those devoid of protein (green arrows). Furthermore, we have performed cryo-ET for a better insight into the conditions at the membrane. Slices of the final 3D reconstruction, calculated from tilting series of images of the LUV embedded in vitreous ice, supply a more detailed representation of membrane spatial features, compared with individual cryo-TEM projection images. Figure 23 C shows such a 15-nm thick section through the three-dimensional volume just in the middle of a LUV partially covered by M1. The protein-free bilayer has a thickness of approximately 4 nm. The thickness of regions in which a layer of M1 appears to be bound to the lipid bilayer is between 8 and 9 nm. Interestingly, the presence of M1 on vesicles is correlated to changes in vesicle shape. In fact, protein-free LUV surface regions display a positive mean curvature (referred to as the membrane monolayer exposed to the protein solution) similar to that observed for control samples (Figure 23 D).

Membrane regions to which M1 has bound display various spatial features with tubular structures (e.g. approximately 20 nm radius), As shown by the red arrows in (Figure 23 A-B), we can see very often outward tubulation (i.e. membrane surfaces with zero Gaussian curvature). In parallel, we also observed inward vesiculation or membrane regions with negative Gaussian curvature as shown by the yellow arrows in (Figure 23 A-B).
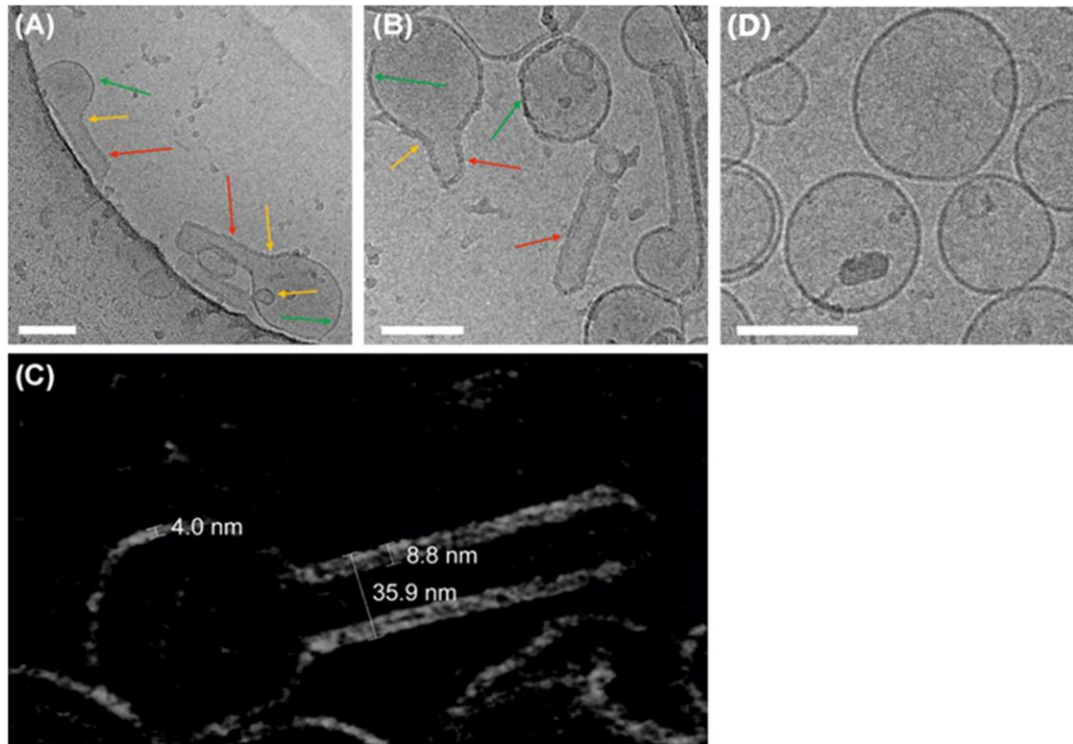
Figure 23 M1 mediate membranes curvature on LUV

(**A, B**) Typical cryo-TEM images of liposomes composed of 40 mol% DOPS in the presence of 10 µM M1 (phosphate buffer pH 7.4, NaCl ~120 mM, see 'Materials and methods' section). The arrows in panels (**A, B**) indicate protein-free membrane portions of vesicles (green arrows) or M1-bound portions of the bilayer which appear thicker (red arrows: tubules, yellow arrows tubule necks, and inward vesiculation), due to the presence of bound M1. Scale bars are 100 nm. (**C**) Cryo-ET of a typical M1-bound liposome (tomography series ±60° at 2° angular increment): the image shows a 15-nm thick section through the three-dimensional volume just in the middle of a LUV incompletely bound to M1 (note the inverted contrast of the so-called Voltex representation, i.e. lipid- and protein densities appear light). The numbers indicate the thickness of the bare lipid bilayer (~4 nm), lipid bilayer with bound M1 (~8–9 nm), and the diameter of a tubule originating from a vesicle (~36 nm). (**D**) cryo- TEM image of liposomes without M1 (protein-free controls). Few multilamellar vesicles can be observed but the shape of the liposomes is generally spherical. The scale bar is 100 nm.

4 M1 binding to lipid domains induced localized membrane bending

Previous experiments reported that IAV assembly and budding occur specifically in an area corresponding to raft confinement PM domains (Veit and Thaa 2011). Furthermore, it is known that M1 binds to negatively charged lipids (Baudin et al. 2001; Kerviel et al. 2016). To demonstrate whether the spatial confinement of acidic lipids within membrane domains can allow reproducing M1-mediated localized budding, we produced GUVs displaying phase separation in ordered domains (i.e. bilayer regions characterized by highly ordered lipid acyl chains, enriched in saturated PC and saturated PG) and disordered domains (enriched in unsaturated PC). In the past, similar (supported) lipid bilayers with phase separation were produced using a mixture of DOPC, DSPS, DSPC, and cholesterol (Bobone et al. 2017). When producing GUVs, we have noticed that exchanging the saturated PS (i.e. DSPS) with saturated PG (i.e., dipalmitoylphosphatidylglycerol, DPPG) improved the yield of phase-separated GUVs. Figure 24A-B shows an example of such GUVs observed *via* CLSM (cholesterol:DPPG:DSPC: DOPC, 10:15:30:45 molar ratios). The red channel refers to the lateral distribution of a fluorescent unsaturated lipid analog (i.e. Rhodamine-DOPE), which strongly partitions into the disordered bilayer phase (mainly, rich in DOPC). The green channel refers to the distribution of a water-soluble fluorescent dye (Alexa Fluor 488 succinimidyl ester). The presence of the dye in the outer milieu allowed the visualization of the whole GUV shape. Ordered lipid domains (plausibly, rich in DPPG and DSPC) can be thus simply identified by the low-partition of Rhodamine-DOPE and appear as dark membrane regions. We also verified that Alexa-free dye does not show unspecific binding to the saturated and unsaturated lipids. Finally, in the vast majority of cases, Alexa488 appeared to be excluded from the lumen of the vesicles (e.g. Figure 24A-B). In agreement with previous observations (Bacia et al. 2005; Chen et al. 2016), we noticed that ordered domains sometimes protruded outward

budding (e.g. Figure 24B), independently of the presence of the protein. This membrane bending is mainly resulting from the line energy that tends to reduce the contour length of the raft domains at the boundary and the lateral tension due to the difference in the packing density. The L_O phase separation is caused by the hydrophobic mismatch and the lateral line tension at the boundaries (Figure 24D to G). After the addition of 10 µM M1-Alexa488, all the vesicles show localized binding of M1. Approximately half of this the vesicles showed deviations from spherical (shape Figure 24F-G). More in detail, we observed in certain cases M1-Alexa488 (green channel) irregularly shaped ordered domains with inward and outward budding (approximately 75% of the cases, typical domain size was approximately 20±10 µm), as shown, e.g. in Figure 24F. In other instances, we observed M1-Alexa488 bound to smaller ordered domains which showed only inward budding (approximately 25% of the cases, typical domain size approximately 4+−1 µm), as shown, for example in Figure 24G.
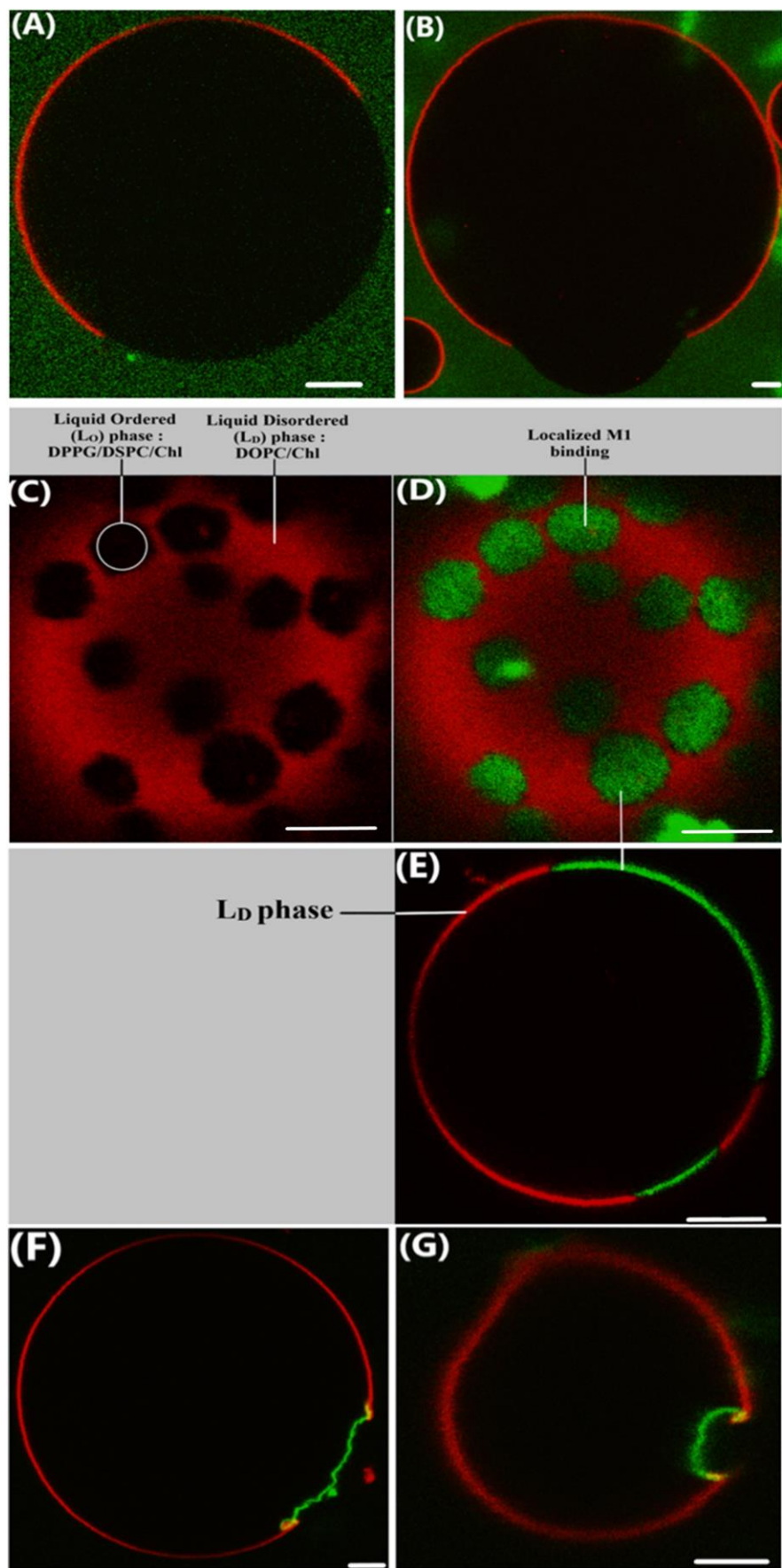
Figure 24 M1 binding to acidic lipid micro-domains causes localized inward membrane deformation. (**A-D**). Typical GUV composed of cholesterol: DPPG:DSPC: DOPC, 10:15:30:45 molar ratios, imaged *via* CLSM. (**A-B**) Saturated lipids (DPPG: DSPC) below its miscibility transition temperature (Tm) form the L_O) phase. The lipid fluorescent dye (Rhodamine-DOPE 0.01 mol% (red channel, strongly enriched in the disordered phase)) partitions more into the L_D phase making it brighter while L_O remains dark. The water-soluble Alexa Fluor 488 succinimidyl ester in the outer milieu of the vesicles (green channel). (**B**) Lateral tension on GUVs microdomains causes outward budding. (**C-D**) The top view of GUVs shows that microdomains form circular shapes (**E-F-G**) Typical GUVs with the same compositions as in (**A-B**), in the presence of 10 μM M1-Alexa488. The protein is visualized in the green channel and the lateral distribution of Rhodamine-DOPE is represented in the red channel. GUVs similar to that shown in (**E**) were observed approximately in 25% of the cases and thus shown in (**F**) represent of the cases 55 %. GUVs similar to that shown in (**G**) (inward budding of the whole ordered domain) were observed in approximately 20% of the cases**.** All GUVs contained 150 mM sucrose in their lumen and were suspended in a phosphate-buffered protein solution (NaCl ~45 mM, pH 7.4) with similar osmolarity (see 'Materials and methods' section). Scale bars are 5 μm. Images were acquired at 23°C. The protein is visualized in the green channel and the lateral distribution of Rhodamine-DOPE is represented in the red channel.

In the aim to verify if the M1 was bound to the inner leaflet of the deformed GUVs. The presence of the free dye or the labeled M1 in the lumen of the vesicles was verified by the offline increase of the green signal.

Figure 25 shows that the high contrast visualization of the green signal increased offline. M1 is more clearly excluded from the lumen of the vesicles.
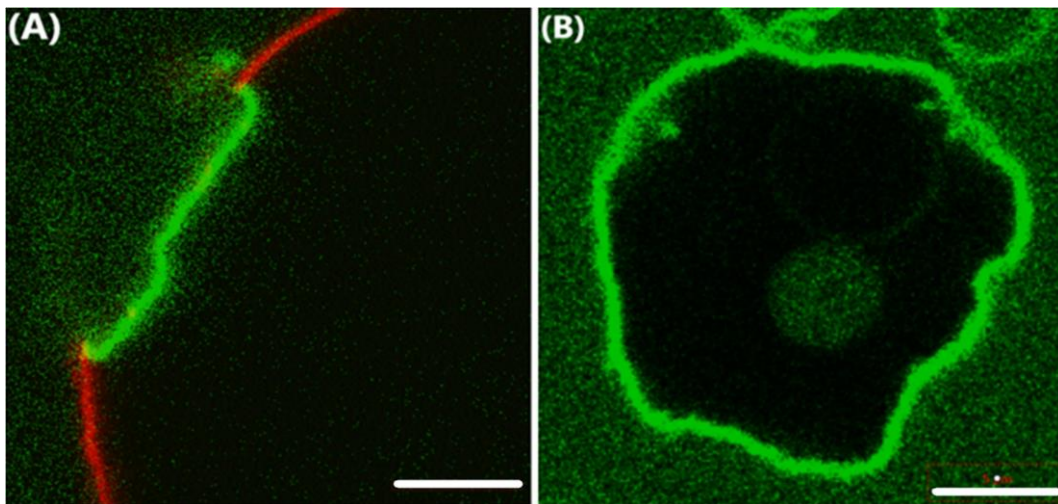
Figure 25 Control experiments showing the effect of labeling and buffer conditions. Typical GUVs with deformed micro-domain in the presence of 10 μM M1-Alexa488. High contrast visualization of the green signal increased offline demonstrates the presence of unbound M1-Alexa488 (green channel) in the outer milieu of the GUVs and its absence in the lumen. (**B**) CLSM image of a GUV composed of DOPC: DOPS 70:30 molar ratios, in the presence of 2 μM M1-Alexa488 (green channel). GUVs contained 150 mM sucrose in their lumen and were suspended in a phosphate-buffered protein solution (pH 7.4, NaCl ~45 mM) with similar osmolarity (see Materials and Methods). In this specific case (representative of ca. 10% of the observed GUVs), it is possible to observe that the concentration of M1-Alexa488 is very low in the lumen. In other words, the protein is probably bound only to the outer leaflet of the GUV. Nevertheless, the general shape of the deformed vesicle is comparable to other cases (e.g. Figure 22) for which the presence of M1 in the GUV lumen cannot be excluded. Scale bars are 5 μm.

5 Detergent assisted M1 layer isolation from GUVs

So far, we have demonstrated that M1 binding to the lipids causes alterations in the 3D spatial organization of the vesicles. Next, we investigated whether M1–M1 interactions over the membrane vesicle could be also involved in the membrane deformation process. Figure 26 A-B shows a typical GUV containing 30 mol% DOPS in the presence of 5 μM M1-Alexa488. As expected, after 30 min of incubation, deformed vesicles could be observed by monitoring the spatial distribution of a fluorescent lipid analog (Figure 26 B) or the labeled protein itself (Figure 26 A). It is worth noting that the observed alterations in membrane shape are specific to M1. We have confirmed that extensive binding of a control protein that has a high affinity to PS (i.e. Annexin V) does not cause significant membrane deformation (Figure 28).

We then proceeded to dissolve the GUVs, by adding 1.7 mM Triton X-100. Most of the lipids were effectively dissolved by the treatment, as demonstrated by the strong decrease in the fluorescence signal of the lipid analog (Figure 26D, for an exemplary GUV). Interestingly, we observed that the M1 protein layer around the GUVs remained intact and was not affected by the detergent treatment, as it formed a stable lipid-free three-dimensional structure (Figure 26C). We obtained similar results if lipids were dissolved using a mixture of different detergents (Triton X-100 1.7 mM, n-Dodecylphosphocholine 1mM, CHAPS 10 mM, and n-Dodecyl-β-Maltoside 1 mM).
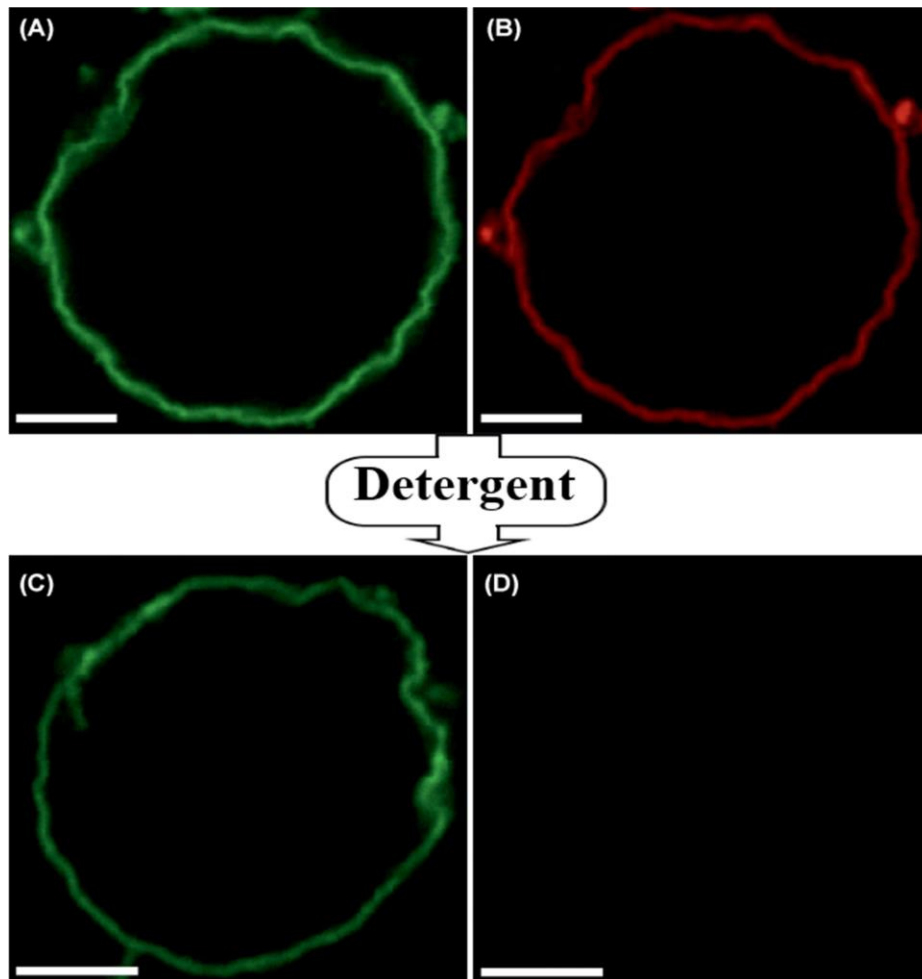
Figure 25 M1 layer interacting with the membrane is stable even after lipid removal.
(A, B) CLSM image of a typical GUV composed of DOPC:cholesterol: DOPS 50:20:30, after incubation with 5 μM M1-Alexa488 (green channel, (**A**)). The lipid bilayer is visualized via the addition of 0.05 mol% Rhodamine-DOPE (red channel, (**B**)). (**C, D**) CLSM image of a (different) typical GUV after treatment for 5 min with detergent (e.g. 1.7 mM Triton X- 100). with M1-Alexa488 (green channel, (C)), and. Rhodamine-DOPE (red channel, (**D**)). The excitation laser power used to acquire the image shown in (D) was approximately seven times higher than the power used to acquire the image shown in (B). All GUVs contained 150 mM sucrose in their lumen and were suspended in a phosphate-buffered protein solution (NaCl ~25 mM, pH 7.4) with similar osmolarity (see 'Materials and method' section). Scale bars are 5 μm. Images were acquired at 23°C.

6 Effect of M1–M1 interactions inhibition on membrane deformation

The results above suggest that M1 forms a stable protein stable network around GUVs that remains intact even after lipid removal. This observation means that the bound M1 form significant inter-protein interactions. To confirm whether M1–M1 interactions play a specific role in altering membrane curvature, we investigated conditions that inhibited protein multimerization, while not completely affecting membrane binding. First, GUVs containing 40mol% DOPS were incubated in the presence of 10 µM M1-Alexa488 pre-treated with 100 µM PHE. PHE is a small molecule that disrupts M1–M1 interactions *via* direct interaction with the protein (Mosier et al. 2016). The above-mentioned DOPS and M1 concentrations were selected so that a strong deformation of the GUV bilayer would have been expected (compare with e.g. Figure 21). Strikingly, results show that in the presence of PHE drug most of the GUVs appeared spherical, as shown in Figure 27A. The same effect was also observed under slightly different conditions (i.e. DOPS concentrations between 30 and 50 mol% and M1-Alexa488 incubated with 75–150 µM PHE, see Table 2).

 In a second experiment, GUVs containing 40 mol% DOPS were incubated in the presence of 10 µM M1-Alexa488 at pH 5. Previous works already suggested that low pH interferes with M1 multimerization without affecting M1 binding (Hilsch et al. 2014; Zhang et al. 2012; Zhirnov 1992; Shtykova et al. 2017). Similarly, we observed here that the GUVs remained spherical (e.g. Figure 27 B). Similar results were obtained for GUVs containing 30 mol% DOPS (Table 2 for a quantitative summary).
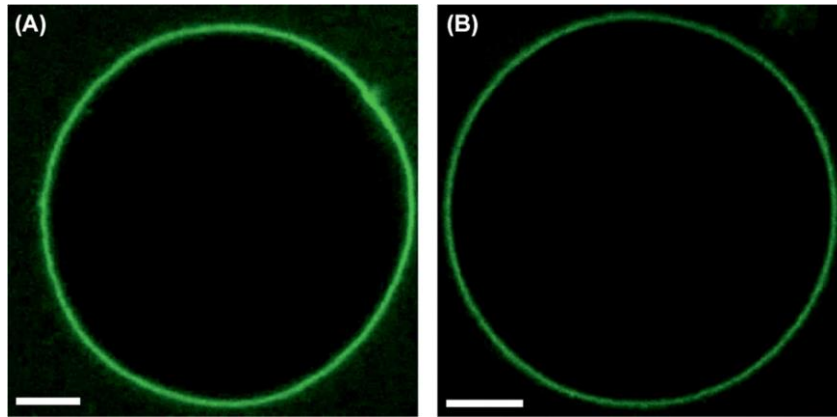
Figure 26 M1 induced membrane deformation requires M1 multimerization.
(**A**) CLSM image of a typical GUV composed of 40 mol% DOPS and 60 mol% DOPC, in the presence of 10 µM fluorescent M1-Alexa488, which was pre-incubated with 100 µM PHE for 30 min. GUVs contained 150 mM sucrose in their lumen and were suspended in a phosphate-buffered protein solution (NaCl ~45 mM, pH 7.4) with similar osmolarity (see 'Materials and methods' section). (**B**) CLSM image of a typical GUV with the same composition as in (A), at pH 5, in the presence of 10 µM M1-Alexa488. These GUVs contained 150 mM sucrose, 10 mM sodium acetate buffer solution at pH 5 in their lumen. The external solution consisted of 10 µM M1-Alexa488 in ~15 mM sodium acetate buffer (pH 5) with ~70 mM NaCl and ~30 mM sucrose (i.e. slightly hyperosmotic conditions, see 'Materials and methods' section). Scale bars are 5 µm. Images were acquired at 23°C.

7 M1 and Annexin-V lateral mobility on GUVs membrane characterized by qualitative fluorescence recovery after photobleaching

To investigate the lateral mobility of the M1-Alexa488 on the GUVs, a qualitative analysis of fluorescence recovery after photobleaching was performed. For that, a selected area representing a section with fluorescent M1 proteins bound to the GUVs membrane was irreversibly bleached by a short and powerful laser pulse (Figure 28 C). The sample was then checked 5 min postbleaching. The bleached area did not show any membrane recovery by the unbleached fluorescent M1 surrounding it (Figure 28 D). Inversely in other experiments, the Annexin V-FITC dye (control) showed fast recovery (within few seconds) after bleaching (Figure 28 A-B).
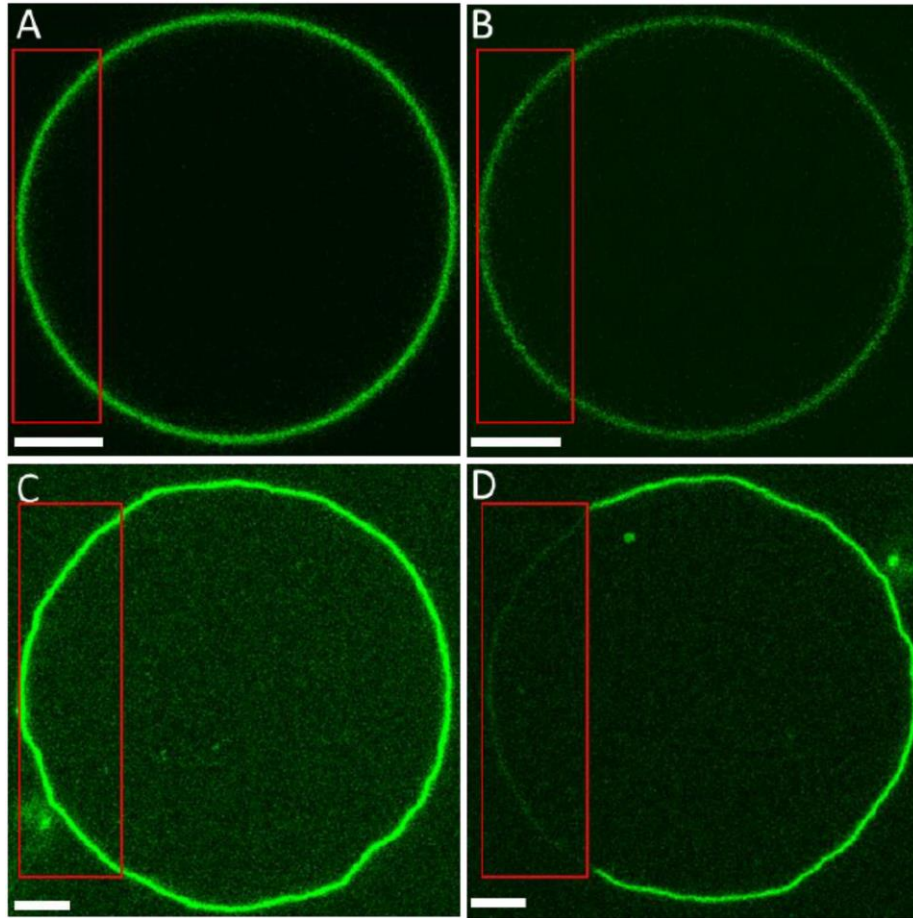
Figure 27 Comparison of M1 and Annexin binding. Annexin V is characterized by faster dynamics and does not induce significant membrane deformation (**A-B**): Representative bleaching/recovery experiment for GUVs composed of DOPC: DOPS 70:30 molar ratio, in the presence of 20 μM FITC-Annexin V. It is worth noting that the affinity of Annexin V for PS-containing membrane (Rosenbaum et al. 2011; Kim et al. 2015) is similar or even higher than that of M1 (Brevnov et al. 2016; Höfer et al. 2019a). Panel A shows a typical vesicle before bleaching the fluorescent protein in the region enclosed in the red rectangle. The vast majority of the examined GUVs do not show visible membrane deformation, although these samples were observed in slightly hyperosmotic buffer conditions (i.e. 150 mM sucrose in the lumen of the GUVs; 180 mM glucose, 3 mM CaCl2, 20 mM NaCl in the external milieu). Panel B shows the same vesicle 5 s after a 10 s bleaching cycle at high laser power. Complete fluorescence signal recovery within few seconds suggests significantly fast protein lateral diffusion. (**C-D**): Bleaching experiment for GUVs with the same composition as in panels A-B, in the presence of 10 μM Alexa488-M1. Panel C shows a typical vesicle before bleaching the region enclosed in the red rectangle. Circa 50% of the examined GUVs displayed a deviation from the spherical shape. To exclude that low membrane tension might play a role in membrane deformation, these GUVs were prepared in slight hypoosmotic conditions (i.e. 180 mM sucrose in the lumen of the GUVs and 2-fold diluted PBS buffer in the external milieu, NaCl ~70 mM). Panel D shows the same vesicle 5 minutes after a 10 s bleaching cycle at high laser power. The absence of fluorescence signal recovery suggests the protein lateral diffusion is much slower compared to the case of Annexin V (Panels A-B). On the other hand, fast fluorescence signal recovery was observed for a fluorescent lipid probe. Imaging was performed at 25 °C. Scale bars are 5 μm.

8 FCS measurements of lateral dynamics and multimerization for M1 bound to GUVs

To further demonstrate if M1 multimerization has a determinant role in causing bilayer deformation, we used sFCS as an alternative method to study protein-protein interactions. Previous fluctuation analysis for M1 on supported lipid bilayers (Hilsch et al. 2014) showed that M1 multimerize upon binding to lipids. In this work, we used sFCS directly to quantify M1 protein binding, diffusional dynamics, and multimerization in spherical or deformed GUVs. The scanning FCS approach (compared with e.g. point-FCS) is particularly adapted to investigate non-supported membranes such as GUVs or the cellular PM.

For that, GUVs containing 30 mol% DOPS were incubated with 10 µM M1-Alexa488 in different conditions. First, we compared the properties of M1 bound to spherical or deformed GUV within a sample prepared at pH 7.4. The deformed GUVs represent on average ~50% of the samples. Additionally, we have performed sFCS analysis on spherical GUVs in samples that were prepared at pH 5 or that were treated with the M1 multimerization inhibitor PHE (Mosier et al. 2016). These measurements are referred to as 'pH 5' and 'PHE', respectively. Both cases are supposed to show low M1 multimerization and decreased membrane deformation, as mentioned in the previous paragraph.

Figure 29 B shows the measured molecular brightness analysis for the above-cited experimental conditions. The molecular brightness is defined as the fluorescence signal detected for each diffusing object per unit of time. In a very simple approximation, we consider that a fluorescent n-mer contains n-times more fluorescent labels than a monomer. The molecular brightness correlates linearly with the size of the fluorescence multimers (e.g. the molecular brightness for a dimer is two times larger than the one of a monomer). In other words, the molecular brightness can be used here to determine the clustering degree of membrane-bound proteins (Hilsch et al. 2014; Höfer et al. 2019a).

In our case, the low degree of the M1 protein labeling (~0.1 label/protein ratio) indicates that the real number of fluorescent molecules in multimers of different sizes can be very similar. In this case, fluorescent monomers and other very small oligomers can contain both exactly one fluorescent label. This effect can be accounted for, as previously described (Dunsing et al. 2018). M1 is also probably present as an undefined mixture of different multimeric species, however, due to its limitation, FCS calculation would allow us to determine only the weighted average of different multimeric species.

Finally, in order to convert molecular brightness values into the multimerization degree of the proteins, a monomeric reference is needed. The same fluorophore (that we used for protein labeling) diffusing in the solution or bound to the M1 protein on the membrane would not be a precise reference in general (due to differences in the geometrical properties and changes in quantum yield of the probe). For that reason, some simplifications are performed in order to estimate the multimerization variations among the different samples (Macdonald et al. 2010). Here we assume for the account of simplicity that the lowest measured average brightness value (~0.025 a.u., sample 'pH 5') corresponds to M1 dimers (Zhang et al. 2012) using the formula as described by (Dunsing et al. 2018).

From our results, we could estimate that M1 forms approximatively decamers in spherical vesicles, 25-mers (and up to 100-mers) in deformed vesicles, and 15-mers in samples treated with PHE. These estimations take the degree of protein labeling into account.

In summary, our brightness measurements show that M1 bound to deformed vesicles (at pH 7.4, in the absence of PHE) is characterized by a significantly higher degree of multimerization, in comparison to the protein-bound to spherical GUVs within the same samples. Also, both the presence of the multimerization inhibitor PHE and lower pH resulted in significantly decreased M1 multimerization.

M1 diffusional dynamics is related to both protein-membrane interactions and the size of the formed protein multimers. M1 lateral diffusional in deformed vesicles is slower in comparison to spherical vesicles. In conclusion, these data indicate that M1-induced membrane deformation is correlated to a significant increase in protein multimerization and a decrease in protein lateral dynamics.
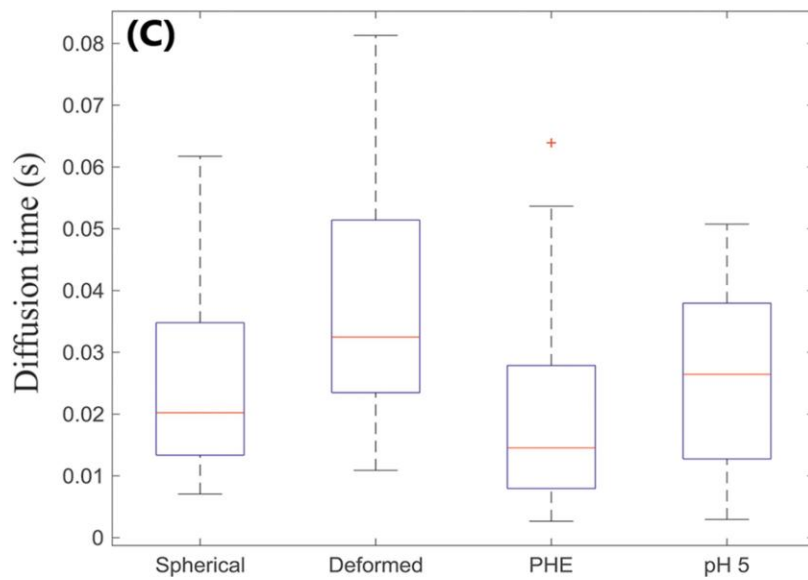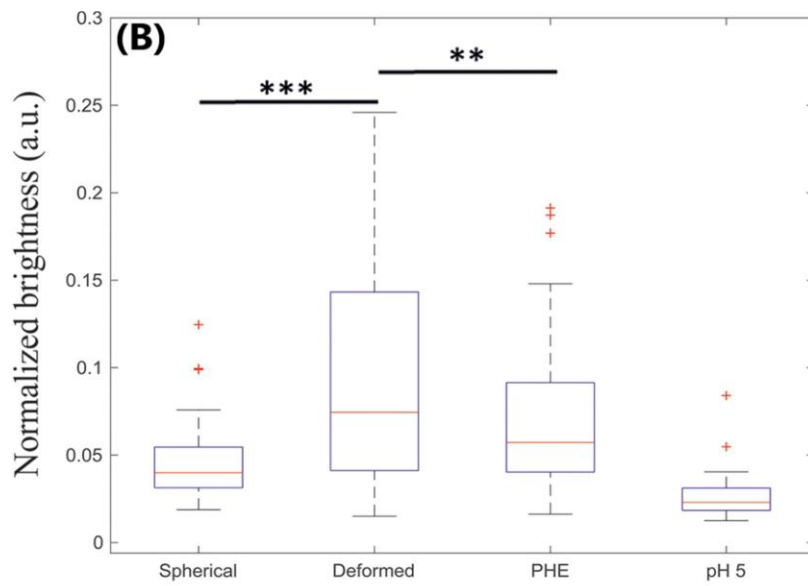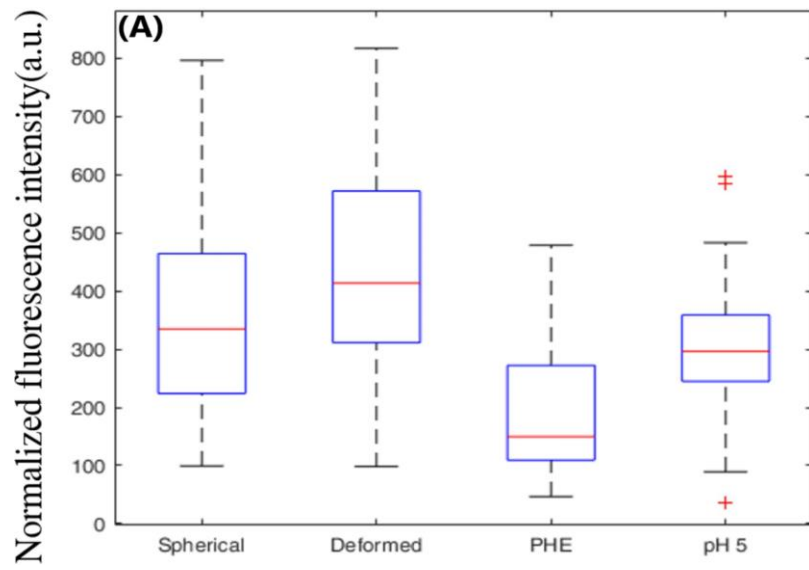
Figure 28 sFCS analysis of M1 binding, brightness, and diffusional dynamics in spherical and deformed GUVs. GUVs composed of 30 mol% DOPS and 70 mol% DOPC were incubated with 10 µM M1-Alexa488. The categories 'Spherical' and 'Deformed' refer to measurements in GUVs from samples at pH 7.4 (NaCl ~45 mM), in the absence of PHE. In these conditions, ~50% of the GUVs are clearly non-spherical (see Table 2). The category 'PHE' refers to spherical GUVs in samples prepared at pH 7.4 (NaCl ~45 mM), using 100 µM PHE. In these conditions, ~90% of the GUVs are clearly spherical (see Table 2). The category 'pH 5' refers to spherical GUVs in samples prepared at pH 5 (NaCl ~70 mM), in the absence of PHE. In these conditions, ~90% of the GUVs are clearly spherical (see Table 2). Details of sample preparation are described in the 'Materials and methods' section. sFCS measurements were performed on 16–34 GUVs from two independent sample preparations and the results were pooled together. Each measurement provided M1-Alexa488 normalized fluorescence intensities (shown as box plot in (A)), normalized brightness values (shown as box plot in (B)), diffusion times (shown as box plot in (C)). Upper outliers from the 'Deformed' category are not included in the plot. '***' indicates a statistically significant difference between categories, with a two-sided t-test probability outcome $P<0.01$. '**' indicates a statistically significant difference between categories, with a two-sided t-test probability outcome $P<0.05$. In the case of diffusion time measurements (C), the category 'Deformed' is significantly different from all the other categories, with a two-sided t-test probability outcome $P<0.01$, in all cases.

IV Discussion

The IAV assembly on the PM of infected cells is a complex process governed by multiple and interdependent protein-protein and protein-lipid interactions. During the budding step, M1 is supposed to orchestrate this process by concurrent interactions with viral proteins, vRNPs, and lipids at the assembly site. Before the new virion release from the PM of an infected cell, the lipid bilayer has to undergo a local shape change. Thus, the viral constituents combined with cellular components must induce a negative curvature on the inner leaflet of the PM so that a virion can bud out from the host cell. Earlier studies have proposed that different viral proteins might be responsible for the PM bending, but no clear confirmation has been presented yet, while the analysis *in cellulo* brings only minor information due to the limited resolution. In fact, the coexistence of different viral and cellular proteins does not permit the isolation and determination of specific protein-lipid or protein-protein interactions (Latham and Galarza 2001; Wang et al. 2010).

In this work, we modeled both M1-lipid and M1-M1 interactions in a controlled environment by using physical models of the PM (i.e. planar lipid monolayer, GUVs, or LUVs) analyzed by SPR and several microscopy methods. Since only the total amount of bound protein is determined by SPR, this technique cannot correctly distinguish between the binding of monomers or small oligomers and the creation of bigger multimers at the membrane interface. At the same time, fluorescence-based analysis of M1 bound to SLBs or GUVs can bring distinct details concerning protein-lipid and protein-protein interactions. Previous studies for qualitative characterization of M1 interaction with model membrane have suggested that the N-terminal domain plays a fundamental role in binding to anionic lipids (Noton et al. 2007), however, until now no consensus was reached concerning the specific regions mediating M1 membrane binding (Kretzschmar et al. 1996; Ye et al. 1987; Gregoriades and Frangione 1981).

The use of the three different constructs derived from M1 allowed us to determine the regions that mediate protein-lipid interaction and protein- multimerization in the membrane-bound state. SPR and microscopy (confocal, electron) experiments confirmed the strong interactions between M1 and negatively charged membranes. M1 showed more affinity with inositol lipids in comparison to PS (data not shown).

The M1 polybasic domain has been widely studied in the last two decades and its role for IAV replication was established in many studies (Burleigh et al. 2005; Liu and Ye 2002; Arzt et al. 2004). The importance of the six basic amino acids present in the polybasic domain (PBD, aa 95–105) for interaction with negatively charged lipid membranes was proposed based on liposome-binding experiments (Noton et al. 2007). Although analysis performed in a cellular context showed no vital role of this domain in mediating the binding to PM (Thaa et al. 2009), in our case, both confocal microscopy and SPR analysis showed a weak interaction between M1m (PBD substituted by neutral amino acids) and PS-containing lipid membranes in comparison to M1. In fact, SPR data indicates a 65% decrease of M1m protein binding compared to M1 and the apparent K_d of M1m is ca. 3-4 times higher than that of M1 (Figure 19 and Table 1). This observed decrease in binding could be related to a less stable interaction between M1m and PS-rich membranes. In parallel, SPR analysis of NM1 binding to PS-containing lipids showed similar K_d values (i.e., ~80-90 nM) as for M1. All these results indicate that M1 may associate with membranes via multiple binding sites present on the N-terminal side. However, other studies showed that the middle region 91-158 aa, which includes the PBD domain and the neighboring patch of positively charged residues is important for M1 oligomerization (Noton et al. 2007).
A recent analysis performed on solid-supported bilayers has shown that M1 bound to negatively charged lipids undergoes also extensive protein multimerization that could arise possibly via M1-M1 electrostatic and hydrophobic interactions (Hilsch et al. 2014).

4.1 M1 interactions with GUVs

Surprisingly, M1 binding to GUVs enriched with PS caused a considerable alteration in the shape of the vesicles. Observation with confocal microscopy indicated homogeneous M1 binding followed by irregular membrane deformation. In general, deformed GUVs have both regions with negative and positive curvatures. Logically, the first assumption is to believe that M1 has probably no preferred curvature orientation. However, we hypothesize that the membrane curvature irregularities are due to the heterogeneous multimerization of M1 over the vesicle surface. In fact, we suppose that the high multimerization of M1 in some areas can cause negative curvature which leads to vesicle internal volume compression, then to compensate for the lost volume, it is possible that the pressure applied by the lumen solution lead to outward budding (positive curvature) in areas where M1 multimerization is weaker.

Another exploration to explain the presence of negative and positive curvatures is to believe that GUVs might become (temporarily) unstable, due to the important and extensive deformation and volume decrease, thus leading to the leak out of the internal solution. Accordingly, we have considered that M1 might indeed penetrate into the lumen of vesicles and thus bind to the membrane inner leaflet.

Nevertheless, membrane deformation with both positive and negative curvature on vesicles is also observed for the cases in which the protein is mainly bound to the outer leaflet (Figure 25 A-B).

Since it is known that PS does not decrease the bending stiffness of a lipid bilayer (Song and Waugh 1990; Dimova 2014) The shape alteration observed for vesicles containing higher amounts of DOPS is not due to its effect on the physical properties of the membrane. In our case, M1 caused also membrane deformation on vesicles enriched with cholesterol or other lipids replacing PS (such as PG, PIP2, or metal-ion-chelating lipids binding the His-tag of M1). This fact shows that M1 mediated deformation does not rely on the different characteristics

(degree of saturation, shape, charge) of the lipids or the membrane rigidity. We further noticed that M1-induced deformation does not require flaccid vesicles since it can arise even in slightly hypoosmotic conditions.

The N-terminal domain of M1 is also able to induce membrane deformation. This is in line with previous observations demonstrating that NM1 can mediate M1–lipid and M1–M1 interactions and thus it can be considered as the main determinant of M1 multimerization (Baudin et al. 2001; Höfer et al. 2019a). This confirms that the C-terminal domain is either not implicated directly in binding to lipids or M1-M1 interaction and maybe its role is to be exposed to the cytosol for further interaction with the viral RNA during virus assembly.

Our purpose in performing sFCS analysis was to investigate the positive correlation between PS enrichment and M1 binding to the GUVs quantitatively (i.e., by normalized fluorescence intensity, figure 29A). FCS also allowed us to measure the formation of multimers (i.e., by an increase in normalized molecular brightness, Figure 29B) and decrease of protein dynamics (lateral diffusion properties of M1 multimers, figure 29C). We were able to quantitatively verify that M1 bound to deformed vesicles shows slower lateral mobility over the lipids and forms in general larger multimers (up to approximately ten-fold). In spherical vesicles, M1 showed faster mobility and lower oligomeric status. All these results support the hypothesis that M1 undergoes multimerization upon binding to lipids and confirm the existence of a positive correlation between the intrinsic property of M1 to self-assemble upon binding M1 multimerization and vesicle deformation.

In this context, the limitations of the sFCS approach should be mentioned: First, the reported brightness and diffusion values refer to an average of different multimeric species that might be present in the sample. Second, the presence of an immobile protein fraction would not be detected by fluorescence fluctuations techniques which, in general, report only the properties of diffusing molecules.

Third, membrane geometry and the detection area are not well-defined in the case of deformed membranes with large curvature (compared with the typical size of the detection volume of $\sim$160 nm). In other words, a larger than expected bilayer surface (due to ruffling within the detection volume) might be observed during our experiments. As a consequence, protein diffusion times and total fluorescence intensity might be overestimated in deformed vesicles. On the other hand, protein brightness and multimerization would be underestimated. Fourthly, a limitation for the brightness resolution could also be expected due to the low degree of M1 labeling (molar ratio ranged between 0.1- 0.15 of dye molecules per protein). In this case, the real number of fluorescent molecules in multimers of different sizes can be very similar. In other words, the signal fluctuations values will be close between multimers composed of an (n) number of M1 protein and multimers composed of ($\sim$10.n) number of M1 protein. In this case, we will not be able to discriminate between different multimers that have a difference of size with a factor less than $\sim$10. However, these limitations do not affect our main findings: that M1 binding depends on the amount of PS and M1 lateral mobility variation is related to the degree of the protein multimerization.

4.2 Characterization of M1 mediated bilayer deformation with LUVs

Membrane regions on LUVs to which M1 has bound display tubular structures (e.g. approximately 20 nm radius) showing outward tubulations (i.e. membrane surfaces with zero Gaussian curvature). The protein is also found concentrated in membrane regions within the neck of tubes (negative Gaussian curvature).

It is also possible, that similarly as for the GUVs, M1 caused irregular membrane deformations (with inward and outward curvature). We also established two hypotheses to explain the appearance of such outward tubulations on the LUVs. First, while comparing these results with the possible membrane-bending properties of M1 in a physiological context, it must be kept in mind that due to their small diameter, LUVs are more positively curved in comparison to the

GUVs or the cell PM. In fact, for liposomes the lipids tails in the inner monolayer tend to be more disordered while the lipid head groups are more closely packed and dehydrated. The opposite is observed in the out layer since they are much less confined. In this case, we hypothesize that the bound M1 follows the contour of the positively curved membrane and is disposed of in a specific way that leads to outward tubulation instead of inward deformation. This observation could imply that the M1-formed coating above the lipid bilayer can adapt to the initial positive membrane curvature of the liposomes.

Secondly, it is also possible that due to their small diameter and their high positive curvature. The LUVs favor M1 multimerization into spirals (helical oligomers) that promote membrane outward tubulovesicular extensions.

Furthermore, we have to notice that the protein-lipid ratio in the case of the LUVs was at least ten times higher than the one used for GUVs samples and this difference might play a role in the formation of protein-lipid structures. Nevertheless, taken together, the experiments performed in GUVs and LUVs suggest that M1 is sufficient to induce membrane deformation alone.

Figure 30 shows the representative hypothesis of M1 mediated membrane bending
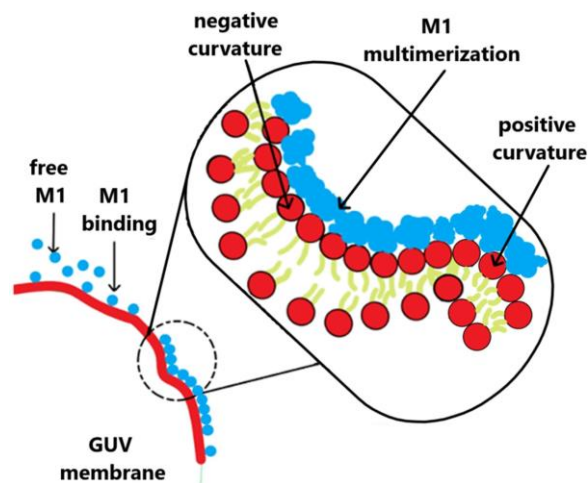
Figure 30 Schematic representation of M1 multimerization mediated deformation on GUVs membrane. M1 protein (blue) binding to anionic lipids (red) leads to membrane curvature in areas where M1 undergoes multimerization.

4.3 Hypothesis on M1 mediated budding

Another element that was studied in these experiments concerned the lateral organization of lipids in the bilayer. Earlier investigations suggested that in infected cells, M1 binding and multimerization on the PM are modulated by the presence of lipid domains enriched with negatively charged lipids (Bobone et al. 2017). These domains are composed of saturated lipids which are characterized by relatively high values of membrane bending rigidity (cfr., for example, approximately 65 kT for a DPPC: cholesterol 80:20 bilayer) (Doktorova et al. 2017). In our case, the ordered domains present on GUVs allowed localized clustering of M1 and variations from the original spherical shape (Figure 24 C-G). The observation of ordered domains bending in the presence of M1 suggests that the membrane rigidity(stiffness) does not play a role.

We can see that with smaller domains, M1 caused only inward budding (Figure 24 G), while for bigger domains, M1 caused irregular membrane deformations (with positive and negative curvature) (Figure 24 F). However, in this case, we can see that the whole deformed domain section is closer to the inner compartment (or lumen) of the vesicle. These observations led us to conclude that the resultant forces go mainly toward an inward budding which favors negative curvature.

We have to notice that this phenomenon might be relevant *in vivo* since M1 is supposed to be confined in small domains on the PM of infected cells (Schmitt and Lamb 2005; Leser and Lamb 2017) and therefore, rise to a high local concentration (McLaughlin and Murray 2005) that probably favors M1 multimerization and budding initiation. In parallel, the possibility that e.g. other viral proteins might modulate this effect (by e.g. making negative curvature of the leaflet interacting with M1 energetically favorable over positive curvature) is currently under investigation.

Spherical viruses budding is a membrane bending process that leads in most cases to the formation of bud with a Ω-shape. Besides the demonstrated role of M1 in causing inward budding on vesicles with small domains, The positive curvature that arises at the edge of the bud could correspond to the M1 protein-free surface. We believe that this positive curvature at the periphery of the budding site could support the hydrophobic insertion of M2 during virus assembly. This step is important since M2 can further amplify membrane positive curvature leading to subsequent neck narrowing (radius decreases/diameter restriction) and virion scission. For that, further work is needed to understand how M2 protein interaction with M1 at the boundary of the raft-like lipid microdomains and the adjacent plasma membrane could allow vesiculation in GUVs.

Furthermore, it is worth mentioning that M1 was reported to form various multimeric arrangements (e.g. helical (Shtykova et al. 2013)) that, in vivo, might result in a different remodeling of lipid membranes, compared with the one presented in the current work. A previous study showed that the influenza C virus matrix protein forms elongated inward lipid tubules (by inducing negative membrane curvature) on GUVs. Inversely the N-terminal domain was not sufficient to cause membrane curvature (Saletti et al. 2017). Despite significant similarities in tertiary structure, the low sequence similarity between the two proteins and the morphologically different membrane formations observed in cells infected by the two viruses (Nishimura et al. 1990; Muraki et al. 2004) does not allow extending the conclusions regarding the matrix protein of influenza C virus directly to IAV M1.

All these observations with the GUVs (with and without domains) and with LUVs show that the spatial localization and membrane geometry play role in the direction of M1-induced deformation.

4.4 Mechanism of membrane curvature mediated by M1

Since at least four different mechanisms are reported to explain the protein-mediated curvature on lipid bilayer, we wanted to further clarify the molecular mechanism used by M1 to drive membrane deformation. We observed that M1 protein loses its ability to induce GUVs membrane curvature in conditions in which M1 multimerization was hindered (i.e. low pH or in the presence of a multimerization inhibitor drug). The use of Annexin V (in comparable amounts with M1) as control confirms that the binding to GUVs did not affect membrane shape. Taken together, these observations suggest that membrane insertion (assuming that protein insertion is indeed not altered by low pH or PHE treatment) or protein crowding might not be the main factor driving M1-induced curvature.

Both M1-GUVs treatments with a detergent for lipid solubilization and qualitative fluorescence recovery after photobleaching experiments demonstrated that the strength of M1–M1 interactions allow the formation of a stable coating over the vesicles. The shell formed by the multimerized M1 created a kind of stable and rigid 3D cage or capsid. Furthermore, the structure is stable over time and seems to impose its irregular (corrugated) shape on the underlying bilayer.

V Conclusions

The IAV assembly and budding involve generally the interaction of the viral proteins with the host cell lipid rafts. It is thought that this process is initiated by the binding and clustering of the surface viral glycoproteins together with the M1 protein. Until now, it is not clear which driving force is behind the localized clustering and membrane bending at the budding site. As shown in our work, M1 binding and multimerization caused membrane curvature on its own with sufficient tension to create inward vesiculation on rigid lipid bilayers. This demonstrates that M1 might drive the IAV budding through the PM (likely in concert with other membrane and/or viral components that help to determine a specific curvature). These results could explain the capacity of M1 to drive the assembly and production of immature virus-like particles (VLPs) by itself when overexpressed alone in cell models. Our results further confirm the natural tendency and biologically determined function of M1 to form the capsid that provides mechanical stability to the virus.

Since it is believed that M1 is the major genetic determinant for the virus morphology phenotypes, further work on model membranes is needed to further establish the role of lipids (asymmetry) and M1 mutations in varying the virus shape. It would also be very relevant to analyze M1 interactions with HA clustered on raft-like lipids, its effect on M1 multimerization, and bud initiation.

VI References

1,2-Dioleoyl-sn-glycero-3-phospho-L-serine, sodium salt - PubChem: 1,2-Dioleoyl-sn-glycero-3-phospho-L-serine, sodium salt. CID=44251426. Hg. v. National Center for Biotechnology Information. Online verfügbar unter https://pubchem.ncbi.nlm.nih.gov/compound/44251426, zuletzt geprüft am 26.04.2020.

Acharya, Rudresh; Carnevale, Vincenzo; Fiorin, Giacomo; Levine, Benjamin G.; Polishchuk, Alexei L.; Balannik, Victoria et al. (2010): Structure and mechanism of proton transport through the transmembrane tetrameric M2 protein bundle of the influenza A virus. In: *Proceedings of the National Academy of Sciences of the United States of America* 107 (34), S. 15075–15080. DOI: 10.1073/pnas.1007071107.

Adu-Gyamfi, Emmanuel; Soni, Smita P.; Xue, Yi; Digman, Michelle A.; Gratton, Enrico; Stahelin, Robert V. (2013): The Ebola virus matrix protein penetrates into the plasma membrane: a key step in viral protein 40 (VP40) oligomerization and viral egress. In: *The Journal of biological chemistry* 288 (8), S. 5779–5789. DOI: 10.1074/jbc.M112.443960.

Air, Gillian M. (2012): Influenza neuraminidase. In: *Influenza and other respiratory viruses* 6 (4), S. 245–256. DOI: 10.1111/j.1750-2659.2011.00304.x.

Ali, A.; Avalos, R. T.; Ponimaskin, E.; Nayak, D. P. (2000): Influenza virus assembly: effect of influenza virus glycoproteins on the membrane association of M1 protein. In: *Journal of virology* 74 (18), S. 8709–8719. DOI: 10.1128/jvi.74.18.8709-8719.2000.

Alimohamadi, Haleh; Rangamani, Padmini (2018): Modeling Membrane Curvature Generation due to Membrane⁻Protein Interactions. In: *Biomolecules* 8 (4). DOI: 10.3390/biom8040120.

Allender, D. W.; Schick, M. (2006): Phase separation in bilayer lipid membranes: effects on the inner leaf due to coupling to the outer leaf. In: *Biophysical journal* 91 (8), S. 2928–2935. DOI: 10.1529/biophysj.106.086868.

Aloia, R. C.; Tian, H.; Jensen, F. C. (1993): Lipid composition and fluidity of the human immunodeficiency virus envelope and host cell plasma membranes. In: *Proceedings of the National Academy of Sciences of the United States of America* 90 (11), S. 5181–5185. DOI: 10.1073/pnas.90.11.5181.

Alonso, M. A.; Millán, J. (2001): The role of lipid rafts in signalling and membrane trafficking in T lymphocytes. In: *Journal of cell science* 114 (Pt 22), S. 3957–3965.

Antonny, B.; Bigay, J.; Casella, J-F; Drin, G.; Mesmin, B.; Gounon, P. (2005): Membrane curvature and the control of GTP hydrolysis in Arf1 during COPI vesicle formation. In: *Biochemical Society transactions* 33 (Pt 4), S. 619–622. DOI: 10.1042/BST0330619.

Antonny, Bruno (2011): Mechanisms of membrane curvature sensing. In: *Annual review of biochemistry* 80, S. 101–123. DOI: 10.1146/annurev-biochem-052809-155121.

Archetti, I. (1955): Appearances associated with filamentous forms of influenza viruses. In: *Archiv fur die gesamte Virusforschung* 6 (1), S. 29–35. DOI: 10.1007/bf01242050.

Arzt, S.; Baudin, F.; Barge, A.; Timmins, P.; Burmeister, W. P.; Ruigrok, R. W. (2001): Combined results from solution studies on intact influenza virus M1 protein and from a new crystal form of its N-terminal domain show that M1 is an elongated monomer. In: *Virology* 279 (2), S. 439–446. DOI: 10.1006/viro.2000.0727.

Arzt, Steffi; Petit, Isabelle; Burmeister, Wilhelm P.; Ruigrok, Rob W. H.; Baudin, Florence (2004): Structure of a knockout mutant of influenza virus M1 protein that has altered activities in membrane binding, oligomerisation and binding to NEP (NS2). In: *Virus research* 99 (2), S. 115–119. DOI: 10.1016/j.virusres.2003.10.010.

Bacia, Kirsten; Schwille, Petra; Kurzchalia, Teymuras (2005): Sterol structure determines the separation of phases and the curvature of the liquid-ordered phase in model membranes. In: *Proceedings of the National Academy of Sciences of the United States of America* 102 (9), S. 3272–3277. DOI: 10.1073/pnas.0408215102.

Badham, Matthew D; Rossman, Jeremy S. (2016): Filamentous Influenza Viruses. In: *Current clinical microbiology reports* 3 (3), S. 155–161. DOI: 10.1007/s40588-016-0041-7.

Balla, Tamas (2013): Phosphoinositides: tiny lipids with giant impact on cell regulation. In: *Physiological reviews* 93 (3), S. 1019–1137. DOI: 10.1152/physrev.00028.2012.

Balleza, Daniel (2012): Mechanical properties of lipid bilayers and regulation of mechanosensitive function: From biological to biomimetic channels. In: *Channels* 6 (4), S. 220–233. DOI: 10.4161/chan.21085.

Barman, Subrata; Ali, Ayub; Hui, Eric K.-W.; Adhikary, Lopa; Nayak, Debi P. (2001): Transport of viral proteins to the apical membranes and interaction of matrix protein with glycoproteins in the assembly of influenza viruses. In: *Virus research* 77 (1), S. 61–69. DOI: 10.1016/S0168-1702(01)00266-0.

Barman, Subrata; Nayak, Debi P. (2007): Lipid raft disruption by cholesterol depletion enhances influenza A virus budding from MDCK cells. In: *Journal of virology* 81 (22), S. 12169–12178. DOI: 10.1128/JVI.00835-07.

Baron, Joanna; Tarnow, Carolin; Mayoli-Nüssle, Deborah; Schilling, Eva; Meyer, Daniela; Hammami, Maya et al. (2013): Matriptase, HAT, and TMPRSS2 activate the hemagglutinin of H9N2 influenza A viruses. In: *Journal of virology* 87 (3), S. 1811–1820. DOI: 10.1128/JVI.02320-12.

Barros, Marilia; Heinrich, Frank; Datta, Siddhartha A. K.; Rein, Alan; Karageorgos, Ioannis; Nanda, Hirsh; Lösche, Mathias (2016): Membrane Binding of HIV-1 Matrix Protein: Dependence on Bilayer Composition and Protein Lipidation. In: *Journal of virology* 90 (9), S. 4544–4555. DOI: 10.1128/JVI.02820-15.

Batishchev, O. V.; Shilova, L. A.; Kachala, M. V.; Tashkin, V. Y.; Sokolov, V. S.; Fedorova, N. V. et al. (2016): pH-Dependent Formation and Disintegration of the Influenza A Virus Protein Scaffold To Provide Tension for Membrane Fusion. In: *Journal of virology* 90 (1), S. 575–585. DOI: 10.1128/JVI.01539-15.

Baudin, F.; Petit, I.; Weissenhorn, W.; Ruigrok, R. W. (2001): In vitro dissection of the membrane and RNP binding activities of influenza virus M1 protein. In: *Virology* 281 (1), S. 102–108. DOI: 10.1006/viro.2000.0804.

Baumgart, Tobias; Hess, Samuel T.; Webb, Watt W. (2003): Imaging coexisting fluid domains in biomembrane models coupling curvature and line tension. In: *Nature* 425 (6960), S. 821–824. DOI: 10.1038/nature02013.

Bavari, Sina; Bosio, Catharine M.; Wiegand, Elizabeth; Ruthel, Gordon; Will, Amy B.; Geisbert, Thomas W. et al. (2002): Lipid raft microdomains: a gateway for compartmentalized trafficking of Ebola and Marburg viruses. In: *The Journal of experimental medicine* 195 (5), S. 593–602. DOI: 10.1084/jem.20011500.

Beber, Alexandre; Taveneau, Cyntia; Nania, Manuela; Tsai, Feng-Ching; Di Cicco, Aurelie; Bassereau, Patricia et al. (2019): Membrane reshaping by micrometric curvature sensitive septin filaments. In: *Nature communications* 10 (1), S. 420. DOI: 10.1038/s41467-019-08344-5.

Berland, K. M.; So, P. T.; Chen, Y.; Mantulin, W. W.; Gratton, E. (1996): Scanning two-photon fluctuation correlation spectroscopy: particle counting measurements for detection of molecular aggregation. In: *Biophysical journal* 71 (1), S. 410–420. DOI: 10.1016/S0006-3495(96)79242-1.

Bertin, A.; McMurray, M. A.; Thai, L.; Garcia, G.; Votin, V.; Grob, P. et al. (2010): Phosphatidylinositol-4,5-bisphosphate Promotes Budding Yeast Septin Filament Assembly and Organization. In: *Journal of molecular biology* 404 (4). DOI: 10.1016/j.jmb.2010.10.002.

Bertin, Aurelie; McMurray, Michael A.; Grob, Patricia; Park, Sang-Shin; Garcia, Galo; Patanwala, Insiyyah et al. (2008): Saccharomyces cerevisiae septins: supramolecular organization of heterooligomers and the mechanism of filament assembly. In: *Proceedings of the National Academy of Sciences of the United States of America* 105 (24), S. 8274–8279. DOI: 10.1073/pnas.0803330105.

Bialas, Kristy M.; Bussey, Kendra A.; Stone, Raychel L.; Takimoto, Toru (2014): Specific nucleoprotein residues affect influenza virus morphology. In: *Journal of virology* 88 (4), S. 2227–2234. DOI: 10.1128/JVI.03354-13.

Bigay, Joëlle; Antonny, Bruno (2012): Curvature, lipid packing, and electrostatics of membrane organelles: defining cellular territories in determining specificity. In: *Developmental cell* 23 (5), S. 886–895. DOI: 10.1016/j.devcel.2012.10.009.

Blijleven, Jelle S.; Boonstra, Sander; Onck, Patrick R.; van der Giessen, Erik; van Oijen, Antoine M. (2016): Mechanisms of influenza viral membrane fusion. In: *Seminars in cell & developmental biology* 60, S. 78–88. DOI: 10.1016/j.semcdb.2016.07.007.

Boal, David H. (2012): Mechanics of the cell. 2nd ed. Cambridge, New York: Cambridge University Press.

Bobone, Sara; Hilsch, Malte; Storm, Julian; Dunsing, Valentin; Herrmann, Andreas; Chiantia, Salvatore (2017): Phosphatidylserine Lateral Organization Influences the Interaction of Influenza Virus Matrix Protein 1 with Lipid Membranes. In: *Journal of virology* 91 (12). DOI: 10.1128/JVI.00267-17.

Böttcher, Eva; Matrosovich, Tatyana; Beyerle, Michaela; Klenk, Hans-Dieter; Garten, Wolfgang; Matrosovich, Mikhail (2006): Proteolytic activation of influenza viruses by serine proteases TMPRSS2 and HAT from human airway epithelium. In: *Journal of virology* 80 (19), S. 9896–9898. DOI: 10.1128/JVI.01118-06.

Böttcher-Friebertshäuser, Eva; Freuer, Catharina; Sielaff, Frank; Schmidt, Sarah; Eickmann, Markus; Uhlendorff, Jennifer et al. (2010): Cleavage of influenza virus hemagglutinin by airway proteases TMPRSS2 and HAT differs in subcellular localization and susceptibility to protease inhibitors. In: *Journal of virology* 84 (11), S. 5605–5614. DOI: 10.1128/JVI.00140-10.

Bourmakina, Svetlana V.; García-Sastre, Adolfo (2003): Reverse genetics studies on the filamentous morphology of influenza A virus. In: *The Journal of general virology* 84 (Pt 3), S. 517–527. DOI: 10.1099/vir.0.18803-0.

Bourmakina, Svetlana V.; García-Sastre, Adolfo (2005): The morphology and composition of influenza A virus particles are not affected by low levels of M1 and M2 proteins in infected cells. In: *Journal of virology* 79 (12), S. 7926–7932. DOI: 10.1128/JVI.79.12.7926-7932.2005.

Bouvier, Nicole M.; Palese, Peter (2008): The biology of influenza viruses. In: *Vaccine* 26 Suppl 4, D49-53. DOI: 10.1016/j.vaccine.2008.07.039.

Bradley, Konrad C.; Jones, Cheryl A.; Tompkins, S. Mark; Tripp, Ralph A.; Russell, Rupert J.; Gramer, Marie R. et al. (2011): Comparison of the receptor binding properties of contemporary swine isolates and early human pandemic H1N1 isolates (Novel 2009 H1N1). In: *Virology* 413 (2), S. 169–182. DOI: 10.1016/j.virol.2011.01.027.

Breidigan, Jeffrey Michael; Krzyzanowski, Natalie; Liu, Yangmingyue; Porcar, Lionel; Perez-Salas, Ursula (2017): Influence of the membrane environment on cholesterol transfer. In: *Journal of lipid research* 58 (12), S. 2255–2263. DOI: 10.1194/jlr.M077909.

Brevnov, V. V.; Fedorova, N. V.; Indenbom, A. V. (2015): Effects of pH on the adsorption of the viral matrix protein M1. In: *Biochem. Moscow Suppl. Ser. A* 9 (2), S. 84–91. DOI: 10.1134/S199074781502004X.

Brown, D. A.; London, E. (1998): Functions of lipid rafts in biological membranes. In: *Annual review of cell and developmental biology* 14, S. 111–136. DOI: 10.1146/annurev.cellbio.14.1.111.

Brown, Deborah A. (2006): Lipid rafts, detergent-resistant membranes, and raft targeting signals. In: *Physiology (Bethesda, Md.)* 21, S. 430–439. DOI: 10.1152/physiol.00032.2006.

Brown, Michael F. (2012): Curvature forces in membrane lipid-protein interactions. In: *Biochemistry* 51 (49), S. 9782–9795. DOI: 10.1021/bi301332v.

Buchkovich, Nicholas J.; Henne, William Mike; Tang, Shaogeng; Emr, Scott D. (2013): Essential N-terminal insertion motif anchors the ESCRT-III filament during MVB vesicle formation. In: *Developmental cell* 27 (2), S. 201–214. DOI: 10.1016/j.devcel.2013.09.009.

Bui, M.; Whittaker, G.; Helenius, A. (1996): Effect of M1 protein and low pH on nuclear transport of influenza virus ribonucleoproteins. In: *Journal of virology* 70 (12), S. 8391–8401.

Bullough, P. A.; Hughson, F. M.; Skehel, J. J.; Wiley, D. C. (1994): Structure of influenza haemagglutinin at the pH of membrane fusion. In: *Nature* 371 (6492), S. 37–43. DOI: 10.1038/371037a0.

Burleigh, Laura M.; Calder, Lesley J.; Skehel, John J.; Steinhauer, David A. (2005): Influenza a viruses with mutations in the m1 helix six domain display a wide variety of morphological phenotypes. In: *Journal of virology* 79 (2), S. 1262–1270. DOI: 10.1128/JVI.79.2.1262-1270.2005.

Busch, David J.; Houser, Justin R.; Hayden, Carl C.; Sherman, Michael B.; Lafer, Eileen M.; Stachowiak, Jeanne C. (2015): Intrinsically disordered proteins drive membrane curvature. In: *Nature communications* 6, S. 7875. DOI: 10.1038/ncomms8875.

Byfield, Fitzroy J.; Aranda-Espinoza, Helim; Romanenko, Victor G.; Rothblat, George H.; Levitan, Irena (2004): Cholesterol depletion increases membrane stiffness of aortic endothelial cells. In: *Biophysical journal* 87 (5), S. 3336–3343. DOI: 10.1529/biophysj.104.040634.

Calder, Lesley J.; Wasilewski, Sebastian; Berriman, John A.; Rosenthal, Peter B. (2010): Structural organization of a filamentous influenza A virus. In: *Proceedings of the National Academy of Sciences of the United States of America* 107 (23), S. 10685–10690. DOI: 10.1073/pnas.1002123107.

Campbell, Patricia J.; Danzy, Shamika; Kyriakis, Constantinos S.; Deymier, Martin J.; Lowen, Anice C.; Steel, John (2014a): The M segment of the 2009 pandemic influenza virus confers increased neuraminidase activity, filamentous morphology, and efficient contact transmissibility to A/Puerto Rico/8/1934-based reassortant viruses. In: *Journal of virology* 88 (7), S. 3802–3814. DOI: 10.1128/JVI.03607-13.

Campbell, Patricia J.; Kyriakis, Constantinos S.; Marshall, Nicolle; Suppiah, Suganthi; Seladi-Schulman, Jill; Danzy, Shamika et al. (2014b): Residue 41 of the Eurasian avian-like swine influenza a virus matrix protein modulates virion filament length and efficiency of contact transmission. In: *Journal of virology* 88 (13), S. 7569–7577. DOI: 10.1128/JVI.00119-14.

Campelo, Felix; McMahon, Harvey T.; Kozlov, Michael M. (2008): The hydrophobic insertion mechanism of membrane curvature generation by proteins. In: *Biophysical journal* 95 (5), S. 2325–2339. DOI: 10.1529/biophysj.108.133173.

Casares, Doralicia; Escribá, Pablo V.; Rosselló, Catalina Ana (2019): Membrane Lipid Composition: Effect on Membrane and Organelle Structure, Function and Compartmentalization and Therapeutic Avenues. In: *International journal of molecular sciences* 20 (9). DOI: 10.3390/ijms20092167.

Castillo, Rolando I.; Rojo, Leonel E.; Henriquez-Henriquez, Marcela; Silva, Hernán; Maturana, Alejandro; Villar, María J. et al. (2016): From Molecules to the Clinic: Linking Schizophrenia and Metabolic Syndrome through Sphingolipids Metabolism. In: *Frontiers in Neuroscience* 10. DOI: 10.3389/fnins.2016.00488.

Chabanon, Morgan; Rangamani, Padmini (2018): Gaussian curvature directs the distribution of spontaneous curvature on bilayer membrane necks. In: *Soft matter* 14 (12), S. 2281–2294. DOI: 10.1039/c8sm00035b.

Chan, Robin; Uchil, Pradeep D.; Jin, Jing; Shui, Guanghou; Ott, David E.; Mothes, Walther; Wenk, Markus R. (2008): Retroviruses human immunodeficiency virus and murine leukemia virus are enriched in phosphoinositides. In: *Journal of virology* 82 (22), S. 11228–11238. DOI: 10.1128/JVI.00981-08.

Chen, Benjamin J.; Leser, George P.; Jackson, David; Lamb, Robert A. (2008): The influenza virus M2 protein cytoplasmic tail interacts with the M1 protein and influences virus assembly at the site of virus budding. In: *Journal of virology* 82 (20), S. 10059–10070. DOI: 10.1128/JVI.01184-08.

Chen, Benjamin J.; Leser, George P.; Morita, Eiji; Lamb, Robert A. (2007): Influenza virus hemagglutinin and neuraminidase, but not the matrix protein, are required for assembly and budding of plasmid-derived virus-like particles. In: *Journal of virology* 81 (13), S. 7111–7123. DOI: 10.1128/JVI.00361-07.

Chen, Benjamin J.; Takeda, Makoto; Lamb, Robert A. (2005): Influenza virus hemagglutinin (H3 subtype) requires palmitoylation of its cytoplasmic tail for assembly: M1 proteins of two subtypes differ in their ability to support assembly. In: *Journal of virology* 79 (21), S. 13673–13684. DOI: 10.1128/JVI.79.21.13673-13684.2005.

Chen, J.; Skehel, J. J.; Wiley, D. C. (1999a): N- and C-terminal residues combine in the fusion-pH influenza hemagglutinin HA(2) subunit to form an N cap that terminates the triple-stranded coiled coil. In: *Proceedings of the National Academy of Sciences of the United States of America* 96 (16), S. 8967–8972. DOI: 10.1073/pnas.96.16.8967.

Chen, Yan; Müller, Joachim D.; So, Peter T.C.; Gratton, Enrico (1999b): The Photon Counting Histogram in Fluorescence Fluctuation Spectroscopy. In: *Biophysical journal* 77 (1), S. 553–567. DOI: 10.1016/S0006-3495(99)76912-2.

Chen, Zhiming; Atefi, Ehsan; Baumgart, Tobias (2016): Membrane Shape Instability Induced by Protein Crowding. In: *Biophysical journal* 111 (9), S. 1823–1826. DOI: 10.1016/j.bpj.2016.09.039.

Chenavas, Sylvie; Estrozi, Leandro F.; Slama-Schwok, Anny; Delmas, Bernard; Di Primo, Carmelo; Baudin, Florence et al. (2013): Monomeric nucleoprotein of influenza A virus. In: *PLoS pathogens* 9 (3), e1003275. DOI: 10.1371/journal.ppat.1003275.

Chernomordik, Leonid V.; Kozlov, Michael M. (2008): Mechanics of membrane fusion. In: *Nature structural & molecular biology* 15 (7), S. 675–683. DOI: 10.1038/nsmb.1455.

Cheung, Timothy K. W.; Poon, Leo L. M. (2007): Biology of influenza a virus. In: *Annals of the New York Academy of Sciences* 1102, S. 1–25. DOI: 10.1196/annals.1408.001.

Childs, Robert A.; Palma, Angelina S.; Wharton, Steve; Matrosovich, Tatyana; Liu, Yan; Chai, Wengang et al. (2009): Receptor-binding specificity of pandemic influenza A (H1N1) 2009 virus determined by carbohydrate microarray. In: *Nature biotechnology* 27 (9), S. 797–799. DOI: 10.1038/nbt0909-797.

Chizhmakov, I. V.; Geraghty, F. M.; Ogden, D. C.; Hayhurst, A.; Antoniou, M.; Hay, A. J. (1996): Selective proton permeability and pH regulation of the influenza virus M2 channel expressed in mouse erythroleukaemia cells. In: *The Journal of physiology* 494 (Pt 2), S. 329–336. DOI: 10.1113/jphysiol.1996.sp021495.

Chlanda, Petr; Schraidt, Oliver; Kummer, Susann; Riches, James; Oberwinkler, Heike; Prinz, Simone et al. (2015): Structural Analysis of the Roles of Influenza A Virus Membrane-Associated Proteins in Assembly and Morphology. In: *Journal of virology* 89 (17), S. 8957–8966. DOI: 10.1128/JVI.00592-15.

Chlanda, Petr; Zimmerberg, Joshua (2016): Protein-lipid interactions critical to replication of the influenza A virus. In: *FEBS letters* 590 (13), S. 1940–1954. DOI: 10.1002/1873-3468.12118.

Cho, Wonhwa; Stahelin, Robert V. (2006): Membrane binding and subcellular targeting of C2 domains. In: *Biochimica et biophysica acta* 1761 (8), S. 838–849. DOI: 10.1016/j.bbalip.2006.06.014.

Choppin, P. W.; Tamm, I. (1960): Studies of two kinds of virus particles which comprise influenza A2 virus strains. I. Characterization of stable homogeneous substrains in reactions with specific antibody, mucoprotein inhibitors, and erythrocytes. In: *The Journal of experimental medicine* 112 (5), S. 895–920. DOI: 10.1084/jem.112.5.895.

Chukkapalli, Vineela; Inlora, Jingga; Todd, Gabrielle C.; Ono, Akira (2013): Evidence in support of RNA-mediated inhibition of phosphatidylserine-dependent HIV-1 Gag membrane binding in cells. In: *Journal of virology* 87 (12), S. 7155–7159. DOI: 10.1128/JVI.00075-13.

Cooke, Ira R.; Deserno, Markus (2006): Coupling between lipid shape and membrane curvature. In: *Biophysical journal* 91 (2), S. 487–495. DOI: 10.1529/biophysj.105.078683.

Cooper, Matthew A.; Try, Andrew C.; Carroll, Joe; Ellar, David J.; Williams, Dudley H. (1998): Surface plasmon resonance analysis at a supported lipid monolayer. In: *Biochimica et Biophysica Acta (BBA) - Biomembranes* 1373 (1), S. 101–111. DOI: 10.1016/S0005-2736(98)00091-1.

Crane, Jonathan M.; Tamm, Lukas K. (2004): Role of Cholesterol in the Formation and Nature of Lipid Rafts in Planar and Spherical Model Membranes. In: *Biophysical journal* 86 (5), S. 2965–2979.

Cros, Jerome F.; García-Sastre, Adolfo; Palese, Peter (2005): An unconventional NLS is critical for the nuclear import of the influenza A virus nucleoprotein and ribonucleoprotein. In: *Traffic (Copenhagen, Denmark)* 6 (3), S. 205–213. DOI: 10.1111/j.1600-0854.2005.00263.x.

Cui, Haosheng; Lyman, Edward; Voth, Gregory A. (2011): Mechanism of membrane curvature sensing by amphipathic helix containing proteins. In: *Biophysical journal* 100 (5), S. 1271–1279. DOI: 10.1016/j.bpj.2011.01.036.

Dadonaite, Bernadeta; Vijayakrishnan, Swetha; Fodor, Ervin; Bhella, David; Hutchinson, Edward C. (2016): Filamentous influenza viruses. In: *The Journal of general virology* 97 (8), S. 1755–1764. DOI: 10.1099/jgv.0.000535.

Das, Subash C.; Watanabe, Shinji; Hatta, Masato; Noda, Takeshi; Neumann, Gabrielle; Ozawa, Makoto; Kawaoka, Yoshihiro (2012): The highly conserved arginine residues at positions 76 through 78 of influenza A virus matrix protein M1 play an important role in viral replication by affecting the intracellular localization of M1. In: *Journal of virology* 86 (3), S. 1522–1530. DOI: 10.1128/JVI.06230-11.

Datta, Siddhartha A. K.; Zhao, Zhuojun; Clark, Patrick K.; Tarasov, Sergey; Alexandratos, Jerry N.; Campbell, Stephen J. et al. (2007): Interactions between HIV-1 Gag molecules in solution: an inositol phosphate-mediated switch. In: *Journal of molecular biology* 365 (3), S. 799–811. DOI: 10.1016/j.jmb.2006.10.072.

Dawson, John C.; Legg, John A.; Machesky, Laura M. (2006): Bar domain proteins: a role in tubulation, scission and actin assembly in clathrin-mediated endocytosis. In: *Trends in cell biology* 16 (10), S. 493–498. DOI: 10.1016/j.tcb.2006.08.004.

Deseri, Luca; Zurlo, Giuseppe (2013): The stretching elasticity of biomembranes determines their line tension and bending rigidity. In: *Biomechanics and modeling in mechanobiology* 12 (6), S. 1233–1242. DOI: 10.1007/s10237-013-0478-z.

Dharmalingam, Elavarasi; Haeckel, Akvile; Pinyol, Roser; Schwintzer, Lukas; Koch, Dennis; Kessels, Michael Manfred; Qualmann, Britta (2009): F-BAR proteins of the syndapin family shape the plasma membrane and are crucial for neuromorphogenesis. In: *The Journal of neuroscience : the official journal of the Society for Neuroscience* 29 (42), S. 13315–13327. DOI: 10.1523/JNEUROSCI.3973-09.2009.

Diaz-Rohrer, Blanca B.; Levental, Kandice R.; Simons, Kai; Levental, Ilya (2014): Membrane raft association is a determinant of plasma membrane localization. In: *Proceedings of the National Academy of Sciences of the United States of America* 111 (23), S. 8500–8505. DOI: 10.1073/pnas.1404582111.

Dick, Robert A.; Vogt, Volker M. (2014): Membrane interaction of retroviral Gag proteins. In: *Frontiers in microbiology* 5, S. 187. DOI: 10.3389/fmicb.2014.00187.

Dimova, Rumiana (2014): Recent developments in the field of bending rigidity measurements on membranes. In: *Advances in colloid and interface science* 208, S. 225–234. DOI: 10.1016/j.cis.2014.03.003.

Dix, James A.; Hom, Erik F. Y.; Verkman, A. S. (2006): Fluorescence correlation spectroscopy simulations of photophysical phenomena and molecular interactions: a molecular dynamics/monte carlo approach. In: *The journal of physical chemistry. B* 110 (4), S. 1896–1906. DOI: 10.1021/jp055840k.

Doktorova, M.; Harries, D.; Khelashvili, G. (2017): Determination of bending rigidity and tilt modulus of lipid membranes from real-space fluctuation analysis of molecular dynamics simulations. In: *Physical chemistry chemical physics : PCCP* 19 (25), S. 16806–16818. DOI: 10.1039/c7cp01921a.

Dou, Dan; Hernández-Neuta, Iván; Wang, Hao; Östbye, Henrik; Qian, Xiaoyan; Thiele, Swantje et al. (2017): Analysis of IAV Replication and Co-infection Dynamics by a Versatile RNA Viral Genome Labeling Method. In: *Cell reports* 20 (1), S. 251–263. DOI: 10.1016/j.celrep.2017.06.021.

Dou, Dan; Revol, Rebecca; Östbye, Henrik; Wang, Hao; Daniels, Robert (2018): Influenza A Virus Cell Entry, Replication, Virion Assembly and Movement. In: *Frontiers in immunology* 9, S. 1581. DOI: 10.3389/fimmu.2018.01581.

Drin, Guillaume; Antonny, Bruno (2010): Amphipathic helices and membrane curvature. In: *FEBS letters* 584 (9), S. 1840–1847. DOI: 10.1016/j.febslet.2009.10.022.

Drin, Guillaume; Casella, Jean-François; Gautier, Romain; Boehmer, Thomas; Schwartz, Thomas U.; Antonny, Bruno (2007): A general amphipathic alpha-helical motif for sensing membrane curvature. In: *Nature structural & molecular biology* 14 (2), S. 138–146. DOI: 10.1038/nsmb1194.

Du, Ruikun; Cui, Qinghua; Rong, Lijun (2019): Competitive Cooperation of Hemagglutinin and Neuraminidase during Influenza A Virus Entry. In: *Viruses* 11 (5). DOI: 10.3390/v11050458.

Dunsing, Valentin; Chiantia, Salvatore (2018): A Fluorescence Fluctuation Spectroscopy Assay of Protein-Protein Interactions at Cell-Cell Contacts. In: *Journal of visualized experiments : JoVE* (142). DOI: 10.3791/58582.

Dunsing, Valentin; Luckner, Madlen; Zühlke, Boris; Petazzi, Roberto A.; Herrmann, Andreas; Chiantia, Salvatore (2018): Optimal fluorescent protein tags for quantifying protein oligomerization in living cells. In: *Scientific reports* 8 (1), S. 10634. DOI: 10.1038/s41598-018-28858-0.

Dunsing, Valentin; Mayer, Magnus; Liebsch, Filip; Multhaup, Gerhard; Chiantia, Salvatore (2017): Direct evidence of amyloid precursor-like protein 1 trans interactions in cell-cell adhesion platforms investigated via fluorescence fluctuation spectroscopy. In: *Molecular biology of the cell* 28 (25), S. 3609–3620. DOI: 10.1091/mbc.E17-07-0459.

Edinger, Thomas O.; Pohl, Marie O.; Stertz, Silke (2014): Entry of influenza A virus: host factors and antiviral targets. In: *The Journal of general virology* 95 (Pt 2), S. 263–277. DOI: 10.1099/vir.0.059477-0.

Eggeling C, et al. 2009. Direct observation of the nanoscale dynamics of membrane lipids in a

living cell. In: *Nature* 457, 1159–1162.

Ekyalongo RC, Nakayama H, Kina K, Kaga N, Iwabuchi K. 2015. Organization and functions of glycolipid-enriched microdomains in phagocytes. In*: Biochim. Biophys. Acta* 1851, 90–97.

Elleman, C. J.; Barclay, W. S. (2004): The M1 matrix protein controls the filamentous phenotype of influenza A virus. In: *Virology* 321 (1), S. 144–153. DOI: 10.1016/j.virol.2003.12.009.

Elson, Elliot L. (2011): Fluorescence correlation spectroscopy: past, present, future. In: *Biophysical journal* 101 (12), S. 2855–2870. DOI: 10.1016/j.bpj.2011.11.012.

Elton, D.; Simpson-Holley, M.; Archer, K.; Medcalf, L.; Hallam, R.; McCauley, J.; Digard, P. (2001): Interaction of the influenza virus nucleoprotein with the cellular CRM1-mediated nuclear export pathway. In: *Journal of virology* 75 (1), S. 408–419. DOI: 10.1128/JVI.75.1.408-419.2001.

Elton, Debra; Bruce, Emily A.; Bryant, Neil; Wise, Helen M.; MacRae, Shona; Rash, Adam et al. (2013): The genetics of virus particle shape in equine influenza A virus. In: *Influenza and other respiratory viruses* 7 Suppl 4, S. 81–89. DOI: 10.1111/irv.12197.

Elton, Debra; Medcalf, Liz; Bishop, Konrad; Harrison, Deborah; Digard, Paul (1999): Identification of Amino Acid Residues of Influenza Virus Nucleoprotein Essential for RNA Binding. In: *Journal of virology* 73 (9), S. 7357–7367.

Ermilova, Inna; Lyubartsev, Alexander P. (2018): Cholesterol in phospholipid bilayers: positions and orientations inside membranes with different unsaturation degrees. In: *Soft matter* 15 (1), S. 78–93. DOI: 10.1039/c8sm01937a.

Farnoud, Amir M.; Toledo, Alvaro M.; Konopka, James B.; Del Poeta, Maurizio; London, Erwin (2015): Raft-like membrane domains in pathogenic microorganisms. In: *Current topics in membranes* 75, S. 233–268. DOI: 10.1016/bs.ctm.2015.03.005.

Farsad, K.; Ringstad, N.; Takei, K.; Floyd, S. R.; Rose, K.; Camilli, P. de (2001): Generation of high curvature membranes mediated by direct endophilin bilayer interactions. In: *The Journal of cell biology* 155 (2), S. 193–200. DOI: 10.1083/jcb.200107075.

Farsad, Khashayar; Camilli, Pietro de (2003): Mechanisms of membrane deformation. In: *Current Opinion in Cell Biology* 15 (4), S. 372–381. DOI: 10.1016/S0955-0674(03)00073-5.

Fontana, Juan; Cardone, Giovanni; Heymann, J. Bernard; Winkler, Dennis C.; Steven, Alasdair C. (2012): Structural changes in Influenza virus at low pH characterized by cryo-electron tomography. In: *Journal of virology* 86 (6), S. 2919–2929. DOI: 10.1128/JVI.06698-11.

Fontana, Juan; Steven, Alasdair C. (2013): At low pH, influenza virus matrix protein M1 undergoes a conformational change prior to dissociating from the membrane. In: *Journal of virology* 87 (10), S. 5621–5628. DOI: 10.1128/JVI.00276-13.

Fontana, Juan; Steven, Alasdair C. (2015): Influenza virus-mediated membrane fusion: Structural insights from electron microscopy. In: *Archives of biochemistry and*

biophysics 581, S. 86–97. DOI: 10.1016/j.abb.2015.04.011.

Ford, Marijn G. J.; Mills, Ian G.; Peter, Brian J.; Vallis, Yvonne; Praefcke, Gerrit J. K.; Evans, Philip R.; McMahon, Harvey T. (2002): Curvature of clathrin-coated pits driven by epsin. In: *Nature* 419 (6905), S. 361–366. DOI: 10.1038/nature01020.

Frensing, Timo; Kupke, Sascha Y.; Bachmann, Mandy; Fritzsche, Susanne; Gallo-Ramirez, Lili E.; Reichl, Udo (2016): Influenza virus intracellular replication dynamics, release kinetics, and particle morphology during propagation in MDCK cells. In: *Applied microbiology and biotechnology* 100 (16), S. 7181–7192. DOI: 10.1007/s00253-016-7542-4.

Frolov, Vadim A.; Shnyrova, Anna V.; Zimmerberg, Joshua (2011): Lipid polymorphisms and membrane shape. In: *Cold Spring Harbor perspectives in biology* 3 (11), a004747. DOI: 10.1101/cshperspect.a004747.

Frost, Adam; Perera, Rushika; Roux, Aurélien; Spasov, Krasimir; Destaing, Olivier; Egelman, Edward H. et al. (2008): Structural basis of membrane invagination by F-BAR domains. In: *Cell* 132 (5), S. 807–817. DOI: 10.1016/j.cell.2007.12.041.

Frostell, Asa; Vinterbäck, Lena; Sjöbom, Hans (2013): Protein-Ligand Interactions Using SPR Systems. In: *Methods in molecular biology (Clifton, N.J.)* 1008, S. 139–165. DOI: 10.1007/978-1-62703-398-5_6.

Fujiyoshi, Y.; Kume, N. P.; Sakata, K.; Sato, S. B. (1994): Fine structure of influenza A virus observed by electron cryo-microscopy. In: *The EMBO journal* 13 (2), S. 318–326.

Furukawa, Noriko; Mima, Joji (2014): Multiple and distinct strategies of yeast SNAREs to confer the specificity of membrane fusion. In: *Scientific reports* 4, S. 4277. DOI: 10.1038/srep04277.

Furuse, Yuki; Suzuki, Akira; Kamigaki, Taro; Oshitani, Hitoshi (2009): Evolution of the M gene of the influenza A virus in different host species: large-scale sequence analysis. In: *Virology journal* 6, S. 67. DOI: 10.1186/1743-422X-6-67.

G Mez-Puertas, P.; Mena, I.; Castillo, M.; Vivo, A.; P Rez-Pastrana, E.; Portela, A. (1999): Efficient formation of influenza virus-like particles: dependence on the expression levels of viral proteins. In: *The Journal of general virology* 80 (Pt 7), S. 1635–1645. DOI: 10.1099/0022-1317-80-7-1635.

Gallop, Jennifer L.; Jao, Christine C.; Kent, Helen M.; Butler, P. Jonathan G.; Evans, Philip R.; Langen, Ralf; McMahon, Harvey T. (2006): Mechanism of endophilin N-BAR domain-mediated membrane curvature. In: *The EMBO journal* 25 (12), S. 2898–2910. DOI: 10.1038/sj.emboj.7601174.

Gao, Shijuan; Wu, Jiaoxiang; Liu, Ran-Yi; Li, Jiandong; Song, Liping; Teng, Yan et al. (2015): Interaction of NS2 with AIMP2 facilitates the switch from ubiquitination to SUMOylation of M1 in influenza A virus-infected cells. In: *Journal of virology* 89 (1), S. 300–311. DOI: 10.1128/JVI.02170-14.

Garcia, Galo; Bertin, Aurelie; Li, Zhu; Song, Yi; McMurray, Michael A.; Thorner, Jeremy; Nogales, Eva (2011): Subunit-dependent modulation of septin assembly: budding yeast

septin Shs1 promotes ring and gauze formation. In: *The Journal of cell biology* 195 (6), S. 993–1004. DOI: 10.1083/jcb.201107123.

García-Sáez, Ana J.; Chiantia, Salvatore; Schwille, Petra (2007): Effect of line tension on the lateral organization of lipid membranes. In: *The Journal of biological chemistry* 282 (46), S. 33537–33544. DOI: 10.1074/jbc.M706162200.

Gassart, Aude de; Geminard, Charles; Fevrier, Benoit; Raposo, Graca; Vidal, Michel (2003): Lipid raft-associated protein sorting in exosomes. In: *Blood* 102 (13), S. 4336–4344. DOI: 10.1182/blood-2003-03-0871.

Gater, Deborah L.; Réat, Valérie; Czaplicki, Georges; Saurel, Olivier; Milon, Alain; Jolibois, Franck; Cherezov, Vadim (2013): Hydrogen bonding of cholesterol in the lipidic cubic phase. In: *Langmuir : the ACS journal of surfaces and colloids* 29 (25), S. 8031–8038. DOI: 10.1021/la401351w.

Gerhard, W.; Mozdzanowska, K.; Furchner, M.; Washko, G.; Maiese, K. (1997): Role of the B-cell response in recovery of mice from primary influenza virus infection. In: *Immunological reviews* 159, S. 95–103. DOI: 10.1111/j.1600-065x.1997.tb01009.x.

Gerl, Mathias J.; Sampaio, Julio L.; Urban, Severino; Kalvodova, Lucie; Verbavatz, Jean-Marc; Binnington, Beth et al. (2012): Quantitative analysis of the lipidomes of the influenza virus envelope and MDCK cell apical membrane. In: *The Journal of cell biology* 196 (2), S. 213–221. DOI: 10.1083/jcb.201108175.

Ghosh, Ujjayini; Xie, Li; Jia, Lihui; Liang, Shuang; Weliky, David P. (2015): Closed and Semiclosed Interhelical Structures in Membrane vs Closed and Open Structures in Detergent for the Influenza Virus Hemagglutinin Fusion Peptide and Correlation of Hydrophobic Surface Area with Fusion Catalysis. In: *Journal of the American Chemical Society* 137 (24), S. 7548–7551. DOI: 10.1021/jacs.5b04578.

Gómez-Puertas, P.; Albo, C.; Pérez-Pastrana, E.; Vivo, A.; Portela, A. (2000): Influenza virus matrix protein is the major driving force in virus budding. In: *Journal of virology* 74 (24), S. 11538–11547. DOI: 10.1128/jvi.74.24.11538-11547.2000.

Gong, Jianzhi; Xu, Wenfang; Zhang, Jie (2007): Structure and functions of influenza virus neuraminidase. In: *Current medicinal chemistry* 14 (1), S. 113–122. DOI: 10.2174/092986707779313444.

Göttlinger, Heinrich G. (2010): Influenza exits the cell without an ESCRT. In: *Cell* 142 (6), S. 839–841. DOI: 10.1016/j.cell.2010.08.036.

Graaf, Miranda de; Fouchier, Ron A. M. (2014): Role of receptor binding specificity in influenza A virus transmission and pathogenesis. In: *The EMBO journal* 33 (8), S. 823–841. DOI: 10.1002/embj.201387442.

Grantham, Michael L.; Stewart, Shaun M.; Lalime, Erin N.; Pekosz, Andrew (2010): Tyrosines in the influenza A virus M2 protein cytoplasmic tail are critical for production of infectious virus particles. In: *Journal of virology* 84 (17), S. 8765–8776. DOI: 10.1128/JVI.00853-10.

Gregoriades, A.; Frangione, B. (1981): Insertion of influenza M protein into the viral lipid bilayer and localization of site of insertion. In: *Journal of virology* 40 (1), S. 323–328.

Griot, C.; Hoop, R. (2007): Aviäre Influenza--die Sicht der Veterinärmedizin. In: *Therapeutische Umschau. Revue therapeutique* 64 (11), S. 621–628. DOI: 10.1024/0040-5930.64.11.621.

Gruenke, Jennifer A.; Armstrong, R. Todd; Newcomb, William W.; Brown, Jay C.; White, Judith M. (2002): New insights into the spring-loaded conformational change of influenza virus hemagglutinin. In: *Journal of virology* 76 (9), S. 4456–4466. DOI: 10.1128/jvi.76.9.4456-4466.2002.

Gruner, S. M.; Cullis, P. R.; Hope, M. J.; Tilcock, C. P. (1985): Lipid polymorphism: the molecular basis of nonbilayer phases. In: *Annual review of biophysics and biophysical chemistry* 14, S. 211–238. DOI: 10.1146/annurev.bb.14.060185.001235.

Grünwald, D.; Cardoso, M. C.; Leonhardt, H.; Buschmann, V. (2005): Diffusion and binding properties investigated by Fluorescence Correlation Spectroscopy (FCS). In: *Current pharmaceutical biotechnology* 6 (5), S. 381–386. DOI: 10.2174/138920105774370616.

Guckenberger, Achim; Gekle, Stephan (2017): Theory and algorithms to compute Helfrich bending forces: a review. In: *Journal of physics. Condensed matter : an Institute of Physics journal* 29 (20), S. 203001. DOI: 10.1088/1361-648X/aa6313.

Guo, Hongbo; Rabouw, Huib; Slomp, Anne; Dai, Meiling; van der Vegt, Floor; van Lent, Jan W. M. et al. (2018): Kinetic analysis of the influenza A virus HA/NA balance reveals contribution of NA to virus-receptor binding and NA-dependent rolling on receptor-containing surfaces. In: *PLoS pathogens* 14 (8), e1007233. DOI: 10.1371/journal.ppat.1007233.

Hac-Wydro, Katarzyna; Wydro, Paweł (2007): The influence of fatty acids on model cholesterol/phospholipid membranes. In: *Chemistry and physics of lipids* 150 (1), S. 66–81. DOI: 10.1016/j.chemphyslip.2007.06.213.

Halling, Katrin K.; Ramstedt, Bodil; Nyström, Joel H.; Slotte, J. Peter; Nyholm, Thomas K. M. (2008): Cholesterol interactions with fluid-phase phospholipids: effect on the lateral organization of the bilayer. In: *Biophysical journal* 95 (8), S. 3861–3871. DOI: 10.1529/biophysj.108.133744.

Hammond, Gerald R. V.; Balla, Tamas (2015): Polyphosphoinositide binding domains: Key to inositol lipid biology. In: *Biochimica et biophysica acta* 1851 (6), S. 746–758. DOI: 10.1016/j.bbalip.2015.02.013.

Hammond, Gerald R. V.; Fischer, Michael J.; Anderson, Karen E.; Holdich, Jon; Koteci, Ardita; Balla, Tamas; Irvine, Robin F. (2012): PI4P and PI(4,5)P2 are essential but independent lipid determinants of membrane identity. In: *Science (New York, N.Y.)* 337 (6095), S. 727–730. DOI: 10.1126/science.1222483.

Han, Qinglin; Chang, Chong; Li, Li; Klenk, Christoph; Cheng, Jinke; Chen, Yixin et al. (2014): Sumoylation of influenza A virus nucleoprotein is essential for intracellular trafficking and virus growth. In: *Journal of virology* 88 (16), S. 9379–9390. DOI: 10.1128/JVI.00509-14.

Hankins, Hannah M.; Baldridge, Ryan D.; Xu, Peng; Graham, Todd R. (2015): Role of flippases, scramblases and transfer proteins in phosphatidylserine subcellular distribution. In: *Traffic (Copenhagen, Denmark)* 16 (1), S. 35–47. DOI: 10.1111/tra.12233.

Hanzal-Bayer, Michael F.; Hancock, John F. (2007): Lipid rafts and membrane traffic. In: *FEBS letters* 581 (11), S. 2098–2104. DOI: 10.1016/j.febslet.2007.03.019.

Harris, A.; Forouhar, F.; Qiu, S.; Sha, B.; Luo, M. (2001): The crystal structure of the influenza matrix protein M1 at neutral pH: M1-M1 protein interfaces can rotate in the oligomeric structures of M1. In: *Virology* 289 (1), S. 34–44. DOI: 10.1006/viro.2001.1119.

Harris, A.; Sha, B.; Luo, M. (1999): Structural similarities between influenza virus matrix protein M1 and human immunodeficiency virus matrix and capsid proteins: an evolutionary link between negative-stranded RNA viruses and retroviruses. In: *The Journal of general virology* 80 (Pt 4), S. 863–869. DOI: 10.1099/0022-1317-80-4-863.

Harris, Audray; Cardone, Giovanni; Winkler, Dennis C.; Heymann, J. Bernard; Brecher, Matthew; White, Judith M.; Steven, Alasdair C. (2006): Influenza virus pleiomorphy characterized by cryoelectron tomography. In: *Proceedings of the National Academy of Sciences of the United States of America* 103 (50), S. 19123–19127. DOI: 10.1073/pnas.0607614103.

Hayase, Yukiharu; Uno, Fumio; Nii, Shiro (1995): Ultrahigh-Resolution Scanning Electron Microscopy of MDCK Cells Infected with Influenza Viruses. In: *J Electron Microsc (Tokyo)* 44 (5), S. 281–288. DOI: 10.1093/oxfordjournals.jmicro.a051177.

Heberle, Frederick A.; Feigenson, Gerald W. (2011): Phase separation in lipid membranes. In: *Cold Spring Harbor perspectives in biology* 3 (4). DOI: 10.1101/cshperspect.a004630.

Heimburg, Thomas; Angerstein, Brigitta; Marsh, Derek (1999): Binding of Peripheral Proteins to Mixed Lipid Membranes: Effect of Lipid Demixing upon Binding. In: *Biophysical journal* 76 (5), S. 2575–2586. DOI: 10.1016/S0006-3495(99)77410-2.

Heiny, A. T.; Miotto, Olivo; Srinivasan, Kellathur N.; Khan, Asif M.; Zhang, G. L.; Brusic, Vladimir et al. (2007): Evolutionarily conserved protein sequences of influenza a viruses, avian and human, as vaccine targets. In: *PloS one* 2 (11), e1190. DOI: 10.1371/journal.pone.0001190.

Helenius, Ari (1992): Unpacking the incoming influenza virus. In: *Cell* 69 (4), S. 577–578. DOI: 10.1016/0092-8674(92)90219-3.

Helfrich, W. (1973): Elastic properties of lipid bilayers: theory and possible experiments. In: *Zeitschrift fur Naturforschung. Teil C: Biochemie, Biophysik, Biologie, Virologie* 28 (11), S. 693–703. DOI: 10.1515/znc-1973-11-1209.

Helms, J. Bernd; Zurzolo, Chiara (2004): Lipids as targeting signals: lipid rafts and intracellular trafficking. In: *Traffic (Copenhagen, Denmark)* 5 (4), S. 247–254. DOI: 10.1111/j.1600-0854.2004.0181.x.

Henne, William Mike; Kent, Helen M.; Ford, Marijn G. J.; Hegde, Balachandra G.; Daumke, Oliver; Butler, P. Jonathan G. et al. (2007): Structure and analysis of FCHo2 F-BAR domain: a dimerizing and membrane recruitment module that effects membrane curvature. In: *Structure (London, England : 1993)* 15 (7), S. 839–852. DOI: 10.1016/j.str.2007.05.002.

Henrich, Erik; Peetz, Oliver; Hein, Christopher; Laguerre, Aisha; Hoffmann, Beate; Hoffmann, Jan et al. (2017): Analyzing native membrane protein assembly in nanodiscs by combined non-covalent mass spectrometry and synthetic biology. In: *eLife* 6. DOI: 10.7554/eLife.20954.

Henriksen, Jonas; Rowat, Amy C.; Ipsen, John H. (2004): Vesicle fluctuation analysis of the effects of sterols on membrane bending rigidity. In: *European biophysics journal : EBJ* 33 (8), S. 732–741. DOI: 10.1007/s00249-004-0420-5.

Heo, Won Do; Inoue, Takanari; Park, Wei Sun; Kim, Man Lyang; Park, Byung Ouk; Wandless, Thomas J.; Meyer, Tobias (2006): PI(3,4,5)P3 and PI(4,5)P2 lipids target proteins with polybasic clusters to the plasma membrane. In: *Science (New York, N.Y.)* 314 (5804), S. 1458–1461. DOI: 10.1126/science.1134389.

Hess, Samuel T.; Gould, Travis J.; Gudheti, Manasa V.; Maas, Sarah A.; Mills, Kevin D.; Zimmerberg, Joshua (2007): Dynamic clustered distribution of hemagglutinin resolved at 40 nm in living cell membranes discriminates between raft theories. In: *Proceedings of the National Academy of Sciences of the United States of America* 104 (44), S. 17370–17375. DOI: 10.1073/pnas.0708066104.

Hess, Samuel T.; Kumar, Mukesh; Verma, Anil; Farrington, Jane; Kenworthy, Anne; Zimmerberg, Joshua (2005): Quantitative electron microscopy and fluorescence spectroscopy of the membrane distribution of influenza hemagglutinin. In: *The Journal of cell biology* 169 (6), S. 965–976. DOI: 10.1083/jcb.200412058.

Hilsch, Malte; Goldenbogen, Björn; Sieben, Christian; Höfer, Chris T.; Rabe, Jürgen P.; Klipp, Edda et al. (2014): Influenza A matrix protein M1 multimerizes upon binding to lipid membranes. In: *Biophysical journal* 107 (4), S. 912–923. DOI: 10.1016/j.bpj.2014.06.042.

Hirama, Takashi; Lu, Stella M.; Kay, Jason G.; Maekawa, Masashi; Kozlov, Michael M.; Grinstein, Sergio; Fairn, Gregory D. (2017): Membrane curvature induced by proximity of anionic phospholipids can initiate endocytosis. In: *Nature communications* 8 (1), S. 1393. DOI: 10.1038/s41467-017-01554-9.

Ho, Chian Sing; Khadka, Nawal K.; She, Fengyu; Cai, Jianfeng; Pan, Jianjun (2016): Influenza M2 Transmembrane Domain Senses Membrane Heterogeneity and Enhances Membrane Curvature. In: *Langmuir : the ACS journal of surfaces and colloids* 32 (26), S. 6730–6738. DOI: 10.1021/acs.langmuir.6b00150.

Hoekstra, Dick; Maier, Olaf; van der Wouden, Johanna M.; Slimane, Tounsia Ait; van IJzendoorn, Sven C. D. (2003): Membrane dynamics and cell polarity: the role of sphingolipids. In: *Journal of lipid research* 44 (5), S. 869–877. DOI: 10.1194/jlr.R300003-JLR200.

Höfer, C. T.; Di Lella, S.; Dahmani, I.; Jungnick, N.; Bordag, N.; Bobone, S. et al. (2019a): Structural determinants of the interaction between influenza A virus matrix protein M1 and lipid membranes. In: *Biochimica et Biophysica Acta (BBA) - Biomembranes* 1861 (6), S. 1123–1134. DOI: 10.1016/j.bbamem.2019.03.013.

Höfer, C. T.; Di Lella, S.; Dahmani, I.; Jungnick, N.; Bordag, N.; Bobone, S. et al. (2019b): Structural determinants of the interaction between influenza A virus matrix protein M1 and lipid membranes. In: *Biochimica et biophysica acta. Biomembranes* 1861 (6), S. 1123–1134. DOI: 10.1016/j.bbamem.2019.03.013.

Hoffman, L. R.; Kuntz, I. D.; White, J. M. (1997): Structure-based identification of an inducer of the low-pH conformational change in the influenza virus hemagglutinin: irreversible inhibition of infectivity. In: *Journal of virology* 71 (11), S. 8808–8820.

Honda, A.; Endo, A.; Mizumoto, K.; Ishihama, A. (2001): Differential roles of viral RNA and cRNA in functional modulation of the influenza virus RNA polymerase. In: *The Journal of biological chemistry* 276 (33), S. 31179–31185. DOI: 10.1074/jbc.M102856200.

Hu, Junjie; Shibata, Yoko; Voss, Christiane; Shemesh, Tom; Li, Zongli; Coughlin, Margaret et al. (2008): Membrane proteins of the endoplasmic reticulum induce high-curvature tubules. In: *Science (New York, N.Y.)* 319 (5867), S. 1247–1250. DOI: 10.1126/science.1153634.

Huang, Qiang; Korte, Thomas; Rachakonda, P. Sivaramakrishna; Knapp, Ernst-Walter; Herrmann, Andreas (2009): Energetics of the loop-to-helix transition leading to the coiled-coil structure of influenza virus hemagglutinin HA2 subunits. In: *Proteins* 74 (2), S. 291–303. DOI: 10.1002/prot.22157.

Ibricevic, Aida; Pekosz, Andrew; Walter, Michael J.; Newby, Celeste; Battaile, John T.; Brown, Earl G. et al. (2006): Influenza virus receptor specificity and cell tropism in mouse and human airway epithelial cells. In: *Journal of virology* 80 (15), S. 7469–7480. DOI: 10.1128/JVI.02677-05.

Isas, J. Mario; Ambroso, Mark R.; Hegde, Prabhavati B.; Langen, Jennifer; Langen, Ralf (2015): Tubulation by amphiphysin requires concentration-dependent switching from wedging to scaffolding. In: *Structure (London, England : 1993)* 23 (5), S. 873–881. DOI: 10.1016/j.str.2015.02.014.

Israelachvili, J. N.; Marcelja, S.; Horn, R. G. (1980): Physical principles of membrane organization. In: *Quarterly reviews of biophysics* 13 (2), S. 121–200. DOI: 10.1017/s0033583500001645.

Israelachvili, Jacob N.; Wennerstroem, Haakan (1992): Entropic forces between amphiphilic surfaces in liquids. In: *J. Phys. Chem.* 96 (2), S. 520–531. DOI: 10.1021/j100181a007.

Ito, T.; Gorman, O. T.; Kawaoka, Y.; Bean, W. J.; Webster, R. G. (1991): Evolutionary analysis of the influenza A virus M gene with comparison of the M1 and M2 proteins. In: *Journal of virology* 65 (10), S. 5491–5498.

Itoh, Toshiki; Erdmann, Kai S.; Roux, Aurelien; Habermann, Bianca; Werner, Hauke; Camilli, Pietro de (2005): Dynamin and the actin cytoskeleton cooperatively regulate plasma membrane invagination by BAR and F-BAR proteins. In: *Developmental cell* 9 (6), S. 791–804. DOI: 10.1016/j.devcel.2005.11.005.

Itoh, Yasushi; Shinya, Kyoko; Kiso, Maki; Watanabe, Tokiko; Sakoda, Yoshihiro; Hatta, Masato et al. (2009): In vitro and in vivo characterization of new swine-origin H1N1 influenza viruses. In: *Nature* 460 (7258), S. 1021–1025. DOI: 10.1038/nature08260.

Ivanova, Pavlina T.; Myers, David S.; Milne, Stephen B.; McClaren, Jennifer L.; Thomas, Paul G.; Brown, H. Alex (2015): Lipid composition of viral envelope of three strains of influenza virus - not all viruses are created equal. In: *ACS infectious diseases* 1 (9), S. 399–452. DOI: 10.1021/acsinfecdis.5b00040.

Iwatsuki-Horimoto, Kiyoko; Horimoto, Taisuke; Noda, Takeshi; Kiso, Maki; Maeda, Junko; Watanabe, Shinji et al. (2006): The Cytoplasmic Tail of the Influenza A Virus M2 Protein Plays a Role in Viral Assembly. In: *Journal of virology* 80 (11), S. 5233–5240. DOI: 10.1128/JVI.00049-06.

Jackson, Meyer B. (2010): SNARE complex zipping as a driving force in the dilation of proteinaceous fusion pores. In: *The Journal of membrane biology* 235 (2), S. 89–100. DOI: 10.1007/s00232-010-9258-1.

Janmey, P. A.; Kinnunen, P. K. J. (2006): Biophysical properties of lipids and dynamic membranes. In: *Trends in cell biology* 16 (10), S. 538–546. DOI: 10.1016/j.tcb.2006.08.009.

Jao, Christine C.; Hegde, Balachandra G.; Gallop, Jennifer L.; Hegde, Prabhavati B.; McMahon, Harvey T.; Haworth, Ian S.; Langen, Ralf (2010): Roles of amphipathic helices and the bin/amphiphysin/rvs (BAR) domain of endophilin in membrane curvature generation. In: *The Journal of biological chemistry* 285 (26), S. 20164–20170. DOI: 10.1074/jbc.M110.127811.

Jarsch, Iris K.; Daste, Frederic; Gallop, Jennifer L. (2016a): Membrane curvature in cell biology: An integration of molecular mechanisms. In: *The Journal of cell biology* 214 (4), S. 375–387. DOI: 10.1083/jcb.201604003.

Jarsch, Iris K.; Daste, Frederic; Gallop, Jennifer L. (2016b): Membrane curvature in cell biology: An integration of molecular mechanisms. In: *The Journal of cell biology* 214 (4), S. 375–387. DOI: 10.1083/jcb.201604003.

Jin, H.; Leser, G. P.; Zhang, J.; Lamb, R. A. (1997): Influenza virus hemagglutinin and neuraminidase cytoplasmic tails control particle shape. In: *The EMBO journal* 16 (6), S. 1236–1247. DOI: 10.1093/emboj/16.6.1236.

Johnson, Kristen A.; Taghon, Geoffrey J. F.; Scott, Jordan L.; Stahelin, Robert V. (2016): The Ebola Virus matrix protein, VP40, requires phosphatidylinositol 4,5-bisphosphate (PI(4,5)P2) for extensive oligomerization at the plasma membrane and viral egress. In: *Scientific reports* 6, S. 19125. DOI: 10.1038/srep19125.

Kegulian, Natalie C.; Sankhagowit, Shalene; Apostolidou, Melania; Jayasinghe, Sajith A.; Malmstadt, Noah; Butler, Peter C.; Langen, Ralf (2015): Membrane Curvature-sensing and Curvature-inducing Activity of Islet Amyloid Polypeptide and Its Implications for Membrane Disruption. In: *The Journal of biological chemistry* 290 (43), S. 25782–25793. DOI: 10.1074/jbc.M115.659797.

Kerviel, Adeline; Dash, Shantoshini; Moncorgé, Olivier; Panthu, Baptiste; Prchal, Jan; Décimo, Didier et al. (2016): Involvement of an Arginine Triplet in M1 Matrix Protein Interaction with Membranes and in M1 Recruitment into Virus-Like Particles of the Influenza A(H1N1)pdm09 Virus. In: *PloS one* 11 (11), e0165421. DOI: 10.1371/journal.pone.0165421.

Kesimer, Mehmet; Kirkham, Sara; Pickles, Raymond J.; Henderson, Ashley G.; Alexis, Neil E.; Demaria, Genevieve et al. (2009): Tracheobronchial air-liquid interface cell culture: a model for innate mucosal defense of the upper airways? In: *American journal of physiology. Lung cellular and molecular physiology* 296 (1), L92-L100. DOI: 10.1152/ajplung.90388.2008.

Khatibzadeh, Nima; Spector, Alexander A.; Brownell, William E.; Anvari, Bahman (2013): Effects of plasma membrane cholesterol level and cytoskeleton F-actin on cell protrusion mechanics. In: *PloS one* 8 (2), e57147. DOI: 10.1371/journal.pone.0057147.

Khelashvili, George; Harries, Daniel; Weinstein, Harel (2009): Modeling membrane deformations and lipid demixing upon protein-membrane interaction: the BAR dimer adsorption. In: *Biophysical journal* 97 (6), S. 1626–1635. DOI: 10.1016/j.bpj.2009.07.006.

Kido, Hiroshi (2015): Influenza virus pathogenicity regulated by host cellular proteases, cytokines and metabolites, and its therapeutic options. In: *Proceedings of the Japan Academy. Series B, Physical and biological sciences* 91 (8), S. 351–368. DOI: 10.2183/pjab.91.351.

Kilbourne, E. D.; Murphy, J. S. (1960): Genetic studies of influenza viruses. I. Viral morphology and growth capacity as exchangeable genetic traits. Rapid in ovo adaptation of early passage Asian strain isolates by combination with PR8. In: *The Journal of experimental medicine* 111, S. 387–406. DOI: 10.1084/jem.111.3.387.

Kim, Paul; Jang, Yo Han; Kwon, Soon Bin; Lee, Chung Min; Han, Gyoonhee; Seong, Baik Lin (2018): Glycosylation of Hemagglutinin and Neuraminidase of Influenza A Virus as Signature for Ecological Spillover and Adaptation among Influenza Reservoirs. In: *Viruses* 10 (4). DOI: 10.3390/v10040183.

Kirchhausen, Tom (2012): Bending membranes. In: *Nature cell biology* 14 (9), S. 906–908. DOI: 10.1038/ncb2570.

Klemm, Robin W.; Ejsing, Christer S.; Surma, Michal A.; Kaiser, Hermann-Josef; Gerl, Mathias J.; Sampaio, Julio L. et al. (2009): Segregation of sphingolipids and sterols during formation of secretory vesicles at the trans-Golgi network. In: *The Journal of cell biology* 185 (4), S. 601–612. DOI: 10.1083/jcb.200901145.

Kolomenskii, A. A.; Gershon, P. D.; Schuessler, H. A. (1997): Sensitivity and detection limit of concentration and adsorption measurements by laser-induced surface-plasmon resonance. In: *Applied optics* 36 (25), S. 6539–6547. DOI: 10.1364/ao.36.006539.

Kolpe, Annasaheb; Arista-Romero, Maria; Schepens, Bert; Pujals, Silvia; Saelens, Xavier; Albertazzi, Lorenzo (2019): Super-resolution microscopy reveals significant impact of M2e-specific monoclonal antibodies on influenza A virus filament formation at the host cell surface. In: *Scientific reports* 9 (1), S. 4450. DOI: 10.1038/s41598-019-41023-5.

Kordyukova, Larisa V.; Shtykova, Eleonora V.; Baratova, Lyudmila A.; Svergun, Dmitri I.; Batishchev, Oleg V. (2019): Matrix proteins of enveloped viruses: a case study of Influenza A virus M1 protein. In: *Journal of biomolecular structure & dynamics* 37 (3), S. 671–690. DOI: 10.1080/07391102.2018.1436089.

Kozlov, Michael M.; Campelo, Felix; Liska, Nicole; Chernomordik, Leonid V.; Marrink, Siewert J.; McMahon, Harvey T. (2014): Mechanisms shaping cell membranes. In: *Current Opinion in Cell Biology* 29, S. 53–60. DOI: 10.1016/j.ceb.2014.03.006.

Kozlov, Michael M.; McMahon, Harvey T.; Chernomordik, Leonid V. (2010): Protein-driven membrane stresses in fusion and fission. In: *Trends in biochemical sciences* 35 (12), S. 699–706. DOI: 10.1016/j.tibs.2010.06.003.

Krabben, Ludwig; Fassio, Anna; Bhatia, Vikram Kjøller; Pechstein, Arndt; Onofri, Franco; Fadda, Manuela et al. (2011): Synapsin I senses membrane curvature by an amphipathic lipid packing sensor motif. In: *The Journal of neuroscience: the official journal of the Society for Neuroscience* 31 (49), S. 18149–18154. DOI: 10.1523/JNEUROSCI.4345-11.2011.

Kraft, Mary L. (2016): Sphingolipid Organization in the Plasma Membrane and the Mechanisms That Influence It. In: *Frontiers in cell and developmental biology* 4, S. 154. DOI: 10.3389/fcell.2016.00154.

Kretzschmar, E.; Bui, M.; Rose, J. K. (1996): Membrane association of influenza virus matrix protein does not require specific hydrophobic domains or the viral glycoproteins. In: *Virology* 220 (1), S. 37–45. DOI: 10.1006/viro.1996.0283.

Ksenofontov, A. L.; Dobrov, E. N.; Fedorova, N. V.; Radyukhin, V. A.; Badun, G. A.; Arutyunyan, A. M. et al. (2011): Intrinsically unstructured regions in the C domain of the influenza virus M1 protein. In: *Mol Biol* 45 (4), S. 634–640. DOI: 10.1134/S0026893311030071.

Kutateladze, Tatiana G. (2010): Translation of the phosphoinositide code by PI effectors. In: *Nature chemical biology* 6 (7), S. 507–513. DOI: 10.1038/nchembio.390.

Kuzmin, Peter I.; Akimov, Sergey A.; Chizmadzhev, Yuri A.; Zimmerberg, Joshua; Cohen, Fredric S. (2005): Line tension and interaction energies of membrane rafts calculated from lipid splay and tilt. In: *Biophysical journal* 88 (2), S. 1120–1133. DOI: 10.1529/biophysj.104.048223.

Lai, Chun-Liang; Jao, Christine C.; Lyman, Edward; Gallop, Jennifer L.; Peter, Brian J.; McMahon, Harvey T. et al. (2012): Membrane binding and self-association of the epsin N-terminal homology domain. In: *Journal of molecular biology* 423 (5), S. 800–817. DOI: 10.1016/j.jmb.2012.08.010.

Lakadamyali, Melike; Rust, Michael J.; Zhuang, Xiaowei (2004): Endocytosis of influenza viruses. In: *Microbes and infection* 6 (10), S. 929–936. DOI: 10.1016/j.micinf.2004.05.002.

Latham, T.; Galarza, J. M. (2001): Formation of wild-type and chimeric influenza virus-like particles following simultaneous expression of only four structural proteins. In: *Journal of virology* 75 (13), S. 6154–6165. DOI: 10.1128/JVI.75.13.6154-6165.2001.

Lee, Anthony G. (2005): How lipids and proteins interact in a membrane: a molecular approach. In: *Molecular bioSystems* 1 (3), S. 203–212. DOI: 10.1039/b504527d.

Lee, Kelly K. (2010): Architecture of a nascent viral fusion pore. In: *The EMBO journal* 29 (7), S. 1299–1311. DOI: 10.1038/emboj.2010.13.

LeGoff, Jérome; Rousset, Dominique; Abou-Jaoudé, Georges; Scemla, Anne; Ribaud, Patricia; Mercier-Delarue, Séverine et al. (2012): I223R mutation in influenza A(H1N1)pdm09 neuraminidase confers reduced susceptibility to oseltamivir and zanamivir and enhanced resistance with H275Y. In: *PloS one* 7 (8), e37095. DOI: 10.1371/journal.pone.0037095.

Leiding, Thom; Wang, Jun; Martinsson, Jonas; DeGrado, William F.; Arsköld, Sindra Peterson (2010): Proton and cation transport activity of the M2 proton channel from influenza A virus. In: *Proceedings of the National Academy of Sciences of the United States of America* 107 (35), S. 15409–15414. DOI: 10.1073/pnas.1009997107.

Lentz, M. R.; Webster, R. G.; Air, G. M. (1987): Site-directed mutation of the active site of influenza neuraminidase and implications for the catalytic mechanism. In: *Biochemistry* 26 (17), S. 5351–5358. DOI: 10.1021/bi00391a020.

Leser, George P.; Lamb, Robert A. (2005): Influenza virus assembly and budding in raft-derived microdomains: a quantitative analysis of the surface distribution of HA, NA and M2 proteins. In: *Virology* 342 (2), S. 215–227. DOI: 10.1016/j.virol.2005.09.049.

Leser, George P.; Lamb, Robert A. (2017): Lateral Organization of Influenza Virus Proteins in the Budozone Region of the Plasma Membrane. In: *Journal of virology* 91 (9). DOI: 10.1128/JVI.02104-16.

Leventis, Peter A.; Grinstein, Sergio (2010): The distribution and function of phosphatidylserine in cellular membranes. In: *Annual review of biophysics* 39, S. 407–427. DOI: 10.1146/annurev.biophys.093008.131234.

Li, S.; Schulman, J.; Itamura, S.; Palese, P. (1993): Glycosylation of neuraminidase determines the neurovirulence of influenza A/WSN/33 virus. In: *Journal of virology* 67 (11), S. 6667–6673.

Lin, Xingcheng; Eddy, Nathanial R.; Noel, Jeffrey K.; Whitford, Paul C.; Wang, Qinghua; Ma, Jianpeng; Onuchic, José N. (2014): Order and disorder control the functional rearrangement of influenza hemagglutinin. In: *Proceedings of the National Academy of Sciences of the United States of America* 111 (33), S. 12049–12054. DOI: 10.1073/pnas.1412849111.

Lipowsky, Reinhard (2014): Coupling of bending and stretching deformations in vesicle membranes. In: *Advances in colloid and interface science* 208, S. 14–24. DOI: 10.1016/j.cis.2014.02.008.

Liu, Teresa; Ye, Zhiping (2002): Restriction of viral replication by mutation of the influenza virus matrix protein. In: *Journal of virology* 76 (24), S. 13055–13061. DOI: 10.1128/jvi.76.24.13055-13061.2002.

Liu, Teresa; Ye, Zhiping (2004): Introduction of a temperature-sensitive phenotype into influenza A/WSN/33 virus by altering the basic amino acid domain of influenza virus matrix protein. In: *Journal of virology* 78 (18), S. 9585–9591. DOI: 10.1128/JVI.78.18.9585-9591.2004.

Liu, Xiaoling; Sun, Lei; Yu, Maorong; Wang, Zengfu; Xu, Chongfeng; Xue, Qinghua et al. (2009): Cyclophilin A interacts with influenza A virus M1 protein and impairs the early stage of the viral replication. In: *Cellular microbiology* 11 (5), S. 730–741. DOI: 10.1111/j.1462-5822.2009.01286.x.

Lloren, Khristine Kaith S.; Lee, Taehyung; Kwon, Jin Jung; Song, Min-Suk (2017): Molecular Markers for Interspecies Transmission of Avian Influenza Viruses in Mammalian Hosts. In: *International journal of molecular sciences* 18 (12). DOI: 10.3390/ijms18122706.

Löfås, Stefan; Malmqvist, Magnus; Rönnberg, Inger; Stenberg, Esa; Liedberg, Bo; Lundström, Ingemar (1991): Bioanalysis with surface plasmon resonance. In: *Sensors and Actuators B: Chemical* 5 (1-4), S. 79–84. DOI: 10.1016/0925-4005(91)80224-8.

Londrigan, Sarah L.; Short, Kirsty R.; Ma, Joel; Gillespie, Leah; Rockman, Steven P.; Brooks, Andrew G.; Reading, Patrick C. (2015): Infection of Mouse Macrophages by Seasonal Influenza Viruses Can Be Restricted at the Level of Virus Entry and at a Late Stage in the Virus Life Cycle. In: *Journal of virology* 89 (24), S. 12319–12329. DOI: 10.1128/JVI.01455-15.

Lorieau, Justin L.; Louis, John M.; Bax, Ad (2011): Helical hairpin structure of influenza hemagglutinin fusion peptide stabilized by charge-dipole interactions between the N-terminal amino group and the second helix. In: *Journal of the American Chemical Society* 133 (9), S. 2824–2827. DOI: 10.1021/ja1099775.

Lorieau, Justin L.; Louis, John M.; Schwieters, Charles D.; Bax, Adriaan (2012): pH-triggered, activated-state conformations of the influenza hemagglutinin fusion peptide revealed by NMR. In: *Proceedings of the National Academy of Sciences of the United States of America* 109 (49), S. 19994–19999. DOI: 10.1073/pnas.1213801109.

Luchini, Alessandra; Vitiello, Giuseppe (2019): Understanding the Nano-bio Interfaces: Lipid-Coatings for Inorganic Nanoparticles as Promising Strategy for Biomedical Applications. In: *Frontiers in Chemistry* 7. DOI: 10.3389/fchem.2019.00343.

Macdonald, Patrick J.; Chen, Yun; Wang, Xiao; Chen, Yan; Mueller, Joachim D. (2010): Brightness analysis by Z-scan fluorescence fluctuation spectroscopy for the study of protein interactions within living cells. In: *Biophysical journal* 99 (3), S. 979–988. DOI: 10.1016/j.bpj.2010.05.017.

Madsen, Jesper J.; Grime, John M. A.; Rossman, Jeremy S.; Voth, Gregory A. (2018): Entropic forces drive clustering and spatial localization of influenza A M2 during viral budding. In: *Proceedings of the National Academy of Sciences of the United States of America* 115 (37), E8595-E8603. DOI: 10.1073/pnas.1805443115.

Maekawa, Masashi; Fairn, Gregory D. (2015): Complementary probes reveal that phosphatidylserine is required for the proper transbilayer distribution of cholesterol. In: *Journal of cell science* 128 (7), S. 1422–1433. DOI: 10.1242/jcs.164715.

Magee, Anthony I.; Parmryd, Ingela (2003): Detergent-resistant membranes and the protein composition of lipid rafts. In: *Genome biology* 4 (11), S. 234. DOI: 10.1186/gb-2003-4-11-234.

Mair, Caroline M.; Ludwig, Kai; Herrmann, Andreas; Sieben, Christian (2014): Receptor binding and pH stability - how influenza A virus hemagglutinin affects host-specific virus infection. In: *Biochimica et biophysica acta* 1838 (4), S. 1153–1168. DOI: 10.1016/j.bbamem.2013.10.004.

Makarkov, Alexander I.; Golizeh, Makan; Ruiz-Lancheros, Elizabeth; Gopal, Angelica A.; Costas-Cancelas, Ian N.; Chierzi, Sabrina et al. (2019): Plant-derived virus-like particle vaccines drive cross-presentation of influenza A hemagglutinin peptides by human monocyte-derived macrophages. In: *NPJ vaccines* 4, S. 17. DOI: 10.1038/s41541-019-0111-y.

Maldonado, Reynaldo L.; Blough, Herbert A. (1980): A comparative study of the lipids of plasma membranes of normal cells and those infected and transformed by rous sarcoma virus. In: *Virology* 102 (1), S. 62–70. DOI: 10.1016/0042-6822(80)90070-7.

Manca, Fabio; Pincet, Frederic; Truskinovsky, Lev; Rothman, James E.; Foret, Lionel; Caruel, Matthieu (2019): SNARE machinery is optimized for ultrafast fusion. In:

Proceedings of the National Academy of Sciences of the United States of America 116 (7), S. 2435–2442. DOI: 10.1073/pnas.1820394116.

Manzoor, Rashid; Igarashi, Manabu; Takada, Ayato (2017): Influenza A Virus M2 Protein: Roles from Ingress to Egress. In: *International journal of molecular sciences* 18 (12). DOI: 10.3390/ijms18122649.

Marquardt, Drew; Kučerka, Norbert; Wassall, Stephen R.; Harroun, Thad A.; Katsaras, John (2016): Cholesterol's location in lipid bilayers. In: *Chemistry and physics of lipids* 199, S. 17–25. DOI: 10.1016/j.chemphyslip.2016.04.001.

Marsh, Derek (2006): Elastic curvature constants of lipid monolayers and bilayers. In: *Chemistry and physics of lipids* 144 (2), S. 146–159. DOI: 10.1016/j.chemphyslip.2006.08.004.

Marsh, Derek (2007): Lateral Pressure Profile, Spontaneous Curvature Frustration, and the Incorporation and Conformation of Proteins in Membranes. In: *Biophysical Journal* 93 (11), S. 3884–3899. DOI: 10.1529/biophysj.107.107938.

Martinez-Seara, Hector; Róg, Tomasz; Pasenkiewicz-Gierula, Marta; Vattulainen, Ilpo; Karttunen, Mikko; Reigada, Ramon (2008): Interplay of unsaturated phospholipids and cholesterol in membranes: effect of the double-bond position. In: *Biophysical journal* 95 (7), S. 3295–3305. DOI: 10.1529/biophysj.108.138123.

Martyna, Agnieszka; Bahsoun, Basma; Badham, Matthew D.; Srinivasan, Saipraveen; Howard, Mark J.; Rossman, Jeremy S. (2017): Membrane remodeling by the M2 amphipathic helix drives influenza virus membrane scission. In: *Scientific reports* 7, S. 44695. DOI: 10.1038/srep44695.

Martyna, Agnieszka; Gómez-Llobregat, Jordi; Lindén, Martin; Rossman, Jeremy S. (2016): Curvature Sensing by a Viral Scission Protein. In: *Biochemistry* 55 (25), S. 3493–3496. DOI: 10.1021/acs.biochem.6b00539.

Matrosovich, M. N.; Gambaryan, A. S.; Tuzikov, A. B.; Byramova, N. E.; Mochalova, L. V.; Golbraikh, A. A. et al. (1993): Probing of the receptor-binding sites of the H1 and H3 influenza A and influenza B virus hemagglutinins by synthetic and natural sialosides. In: *Virology* 196 (1), S. 111–121. DOI: 10.1006/viro.1993.1459.

McAuley, J. L.; Corcilius, L.; Tan, H-X; Payne, R. J.; McGuckin, M. A.; Brown, L. E. (2017): The cell surface mucin MUC1 limits the severity of influenza A virus infection. In: *Mucosal immunology* 10 (6), S. 1581–1593. DOI: 10.1038/mi.2017.16.

McCauley, J. W.; Mahy, B. W. (1983): Structure and function of the influenza virus genome. In: *The Biochemical journal* 211 (2), S. 281–294. DOI: 10.1042/bj2110281.

McCown, Matthew F.; Pekosz, Andrew (2005): The influenza A virus M2 cytoplasmic tail is required for infectious virus production and efficient genome packaging. In: *Journal of virology* 79 (6), S. 3595–3605. DOI: 10.1128/JVI.79.6.3595-3605.2005.

McCown, Matthew F.; Pekosz, Andrew (2006): Distinct domains of the influenza a virus M2 protein cytoplasmic tail mediate binding to the M1 protein and facilitate infectious

virus production. In: *Journal of virology* 80 (16), S. 8178–8189. DOI: 10.1128/JVI.00627-06.

McKimm-Breschkin, Jennifer L. (2013): Influenza neuraminidase inhibitors: antiviral action and mechanisms of resistance. In: *Influenza and other respiratory viruses* 7 Suppl 1, S. 25–36. DOI: 10.1111/irv.12047.

McLaughlin, Stuart; Murray, Diana (2005): Plasma membrane phosphoinositide organization by protein electrostatics. In: *Nature* 438 (7068), S. 605–611. DOI: 10.1038/nature04398.

McLaughlin, Stuart; Wang, Jiyao; Gambhir, Alok; Murray, Diana (2002): PIP(2) and proteins: interactions, organization, and information flow. In: *Annual review of biophysics and biomolecular structure* 31, S. 151–175. DOI: 10.1146/annurev.biophys.31.082901.134259.

McMahon, Harvey T.; Boucrot, Emmanuel (2015): Membrane curvature at a glance. In: *Journal of cell science* 128 (6), S. 1065–1070. DOI: 10.1242/jcs.114454.

McMahon, Harvey T.; Gallop, Jennifer L. (2005): Membrane curvature and mechanisms of dynamic cell membrane remodelling. In: *Nature* 438 (7068), S. 590–596. DOI: 10.1038/nature04396.

Melen, Krister; Fagerlund, Riku; Franke, Jacqueline; Kohler, Matthias; Kinnunen, Leena; Julkunen, Ilkka (2003): Importin alpha nuclear localization signal binding sites for STAT1, STAT2, and influenza A virus nucleoprotein. In: *The Journal of biological chemistry* 278 (30), S. 28193–28200. DOI: 10.1074/jbc.M303571200.

Mertens, Haydyn D. T.; Svergun, Dmitri I. (2010): Structural characterization of proteins and complexes using small-angle X-ray solution scattering. In: *Journal of structural biology* 172 (1), S. 128–141. DOI: 10.1016/j.jsb.2010.06.012.

Mim, Carsten; Unger, Vinzenz M. (2012): Membrane curvature and its generation by BAR proteins. In: *Trends in biochemical sciences* 37 (12), S. 526–533. DOI: 10.1016/j.tibs.2012.09.001.

Moravcevic, Katarina; Oxley, Camilla L.; Lemmon, Mark A. (2012): Conditional peripheral membrane proteins: facing up to limited specificity. In: *Structure (London, England : 1993)* 20 (1), S. 15–27. DOI: 10.1016/j.str.2011.11.012.

Mosier, Philip D.; Chiang, Meng-Jung; Lin, Zhengshi; Gao, Yamei; Althufairi, Bashayer; Zhou, Qibing et al. (2016): Broad Spectrum Anti-Influenza Agents by Inhibiting Self-Association of Matrix Protein 1. In: *Scientific reports* 6, S. 32340. DOI: 10.1038/srep32340.

Mosley, V. M.; Wyckoff, R. W. G. (1946): Electron micrography of the virus of influenza. In: *Nature* 157, S. 263. DOI: 10.1038/157263a0.

Moules, V.; Ferraris, O.; Terrier, O.; Giudice, E.; Yver, M.; Rolland, J. P. et al. (2010): In vitro characterization of naturally occurring influenza H3NA- viruses lacking the NA

gene segment: toward a new mechanism of viral resistance? In: *Virology* 404 (2), S. 215–224. DOI: 10.1016/j.virol.2010.04.030.

Mountford, Carolyn E.; Grossman, George; Hampson, Alan W.; Holmes, Kerry T. (1982): Influenza virus: An NMR study of mechanisms involved in infection. In: *Biochimica et Biophysica Acta (BBA) - Molecular Cell Research* 720 (1), S. 65–74. DOI: 10.1016/0167-4889(82)90039-8.

Muftuoglu, Yagmur; Xue, Yi; Gao, Xiang; Wu, Dianqing; Ha, Ya (2016): Mechanism of substrate specificity of phosphatidylinositol phosphate kinases. In: *Proceedings of the National Academy of Sciences of the United States of America* 113 (31), S. 8711–8716. DOI: 10.1073/pnas.1522112113.

Muraki, Yasushi; Washioka, Hiroshi; Sugawara, Kanetsu; Matsuzaki, Yoko; Takashita, Emi; Hongo, Seiji (2004): Identification of an amino acid residue on influenza C virus M1 protein responsible for formation of the cord-like structures of the virus. In: *The Journal of general virology* 85 (Pt 7), S. 1885–1893. DOI: 10.1099/vir.0.79937-0.

Nakajima, Noriko; Hata, Satoru; Sato, Yuko; Tobiume, Minoru; Katano, Harutaka; Kaneko, Keiko et al. (2010): The first autopsy case of pandemic influenza (A/H1N1pdm) virus infection in Japan: detection of a high copy number of the virus in type II alveolar epithelial cells by pathological and virological examination. In: *Japanese journal of infectious diseases* 63 (1), S. 67–71.

Nara, Peter L.; Tobin, Gregory J.; Chaudhuri, A. Ray; Trujillo, Jessie D.; Lin, George; Cho, Michael W. et al. (2010): How can vaccines against influenza and other viral diseases be made more effective? In: *PLoS biology* 8 (12), e1000571. DOI: 10.1371/journal.pbio.1000571.

Nayak, Debi P.; Balogun, Rilwan A.; Yamada, Hiroshi; Zhou, Z. Hong; Barman, Subrata (2009): Influenza virus morphogenesis and budding. In: *Virus research* 143 (2), S. 147–161. DOI: 10.1016/j.virusres.2009.05.010.

Nayak, Debi P.; Hui, Eric Ka-Wai; Barman, Subrata (2004): Assembly and budding of influenza virus. In: *Virus research* 106 (2), S. 147–165. DOI: 10.1016/j.virusres.2004.08.012.

Needham, D.; Nunn, R. S. (1990): Elastic deformation and failure of lipid bilayer membranes containing cholesterol. In: *Biophysical journal* 58 (4), S. 997–1009. DOI: 10.1016/S0006-3495(90)82444-9.

Neumann, G.; Castrucci, M. R.; Kawaoka, Y. (1997): Nuclear import and export of influenza virus nucleoprotein. In: *Journal of virology* 71 (12), S. 9690–9700.

Nishimura, Hidekazu; Hara, Masahiro; Sugawara, Kanetsu; Kitame, Fumio; Takiguchi, Kazuhiko; Umetsu, Yoriko et al. (1990): Characterization of the cord-like structures emerging from the surface of influenza C virus-infected cells. In: *Virology* 179 (1), S. 179–188. DOI: 10.1016/0042-6822(90)90287-2.

Noda, Takeshi; Kawaoka, Yoshihiro (2010): Structure of influenza virus ribonucleoprotein complexes and their packaging into virions. In: *Reviews in medical virology* 20 (6), S. 380–391. DOI: 10.1002/rmv.666.

Noton, Sarah L.; Medcalf, Elizabeth; Fisher, Dawn; Mullin, Anne E.; Elton, Debra; Digard, Paul (2007): Identification of the domains of the influenza A virus M1 matrix protein required for NP binding, oligomerization and incorporation into virions. In: *The Journal of general virology* 88 (Pt 8), S. 2280–2290. DOI: 10.1099/vir.0.82809-0.

Oh, Hana; Mohler, Emile R.; Tian, Aiwei; Baumgart, Tobias; Diamond, Scott L. (2009): Membrane cholesterol is a biomechanical regulator of neutrophil adhesion. In: *Arteriosclerosis, thrombosis, and vascular biology* 29 (9), S. 1290–1297. DOI: 10.1161/ATVBAHA.109.189571.

Ohkura, Takashi; Momose, Fumitaka; Ichikawa, Reiko; Takeuchi, Kaoru; Morikawa, Yuko (2014): Influenza A virus hemagglutinin and neuraminidase mutually accelerate their apical targeting through clustering of lipid rafts. In: *Journal of virology* 88 (17), S. 10039–10055. DOI: 10.1128/JVI.00586-14.

Ohvo-Rekilä, Henna; Ramstedt, Bodil; Leppimäki, Petra; Slotte, J. Peter (2002): Cholesterol interactions with phospholipids in membranes. In: *Progress in lipid research* 41 (1), S. 66–97. DOI: 10.1016/s0163-7827(01)00020-0.

Olsen, Anne S. B.; Færgeman, Nils J. (2017): Sphingolipids: membrane microdomains in brain development, function and neurological diseases. In: *Open biology* 7 (5). DOI: 10.1098/rsob.170069.

Olsen, Brett N.; Bielska, Agata A.; Lee, Tiffany; Daily, Michael D.; Covey, Douglas F.; Schlesinger, Paul H. et al. (2013): The Structural Basis of Cholesterol Accessibility in Membranes. In: *Biophysical journal* 105 (8), S. 1838–1847. DOI: 10.1016/j.bpj.2013.08.042.

Ono, A.; Demirov, D.; Freed, E. O. (2000): Relationship between human immunodeficiency virus type 1 Gag multimerization and membrane binding. In: *Journal of virology* 74 (11), S. 5142–5150. DOI: 10.1128/jvi.74.11.5142-5150.2000.

O'Shannessy, D. J.; Brigham-Burke, M.; Soneson, K. K.; Hensley, P.; Brooks, I. (1993): Determination of rate and equilibrium binding constants for macromolecular interactions using surface plasmon resonance: use of nonlinear least squares analysis methods. In: *Analytical biochemistry* 212 (2), S. 457–468. DOI: 10.1006/abio.1993.1355.

Pal, Sangita; Santos, Andres; Rosas, Juan M.; Ortiz-Guzman, Joshua; Rosas-Acosta, Germán (2011): Influenza A virus interacts extensively with the cellular SUMOylation system during infection. In: *Virus research* 158 (1-2), S. 12–27. DOI: 10.1016/j.virusres.2011.02.017.

Pan, Jianjun; Mills, Thalia T.; Tristram-Nagle, Stephanie; Nagle, John F. (2008): Cholesterol perturbs lipid bilayers nonuniversally. In: *Physical review letters* 100 (19), S. 198103. DOI: 10.1103/PhysRevLett.100.198103.

Pan, Jianjun; Tristram-Nagle, Stephanie; Nagle, John F. (2009): Effect of cholesterol on structural and mechanical properties of membranes depends on lipid chain saturation. In: *Physical review. E, Statistical, nonlinear, and soft matter physics* 80 (2 Pt 1), S. 21931.

Pandit, Sagar A.; Chiu, See-Wing; Jakobsson, Eric; Grama, Ananth; Scott, H. L. (2008): Cholesterol packing around lipids with saturated and unsaturated chains: a simulation study. In: *Langmuir : the ACS journal of surfaces and colloids* 24 (13), S. 6858–6865. DOI: 10.1021/la8004135.

Peter, Brian J.; Kent, Helen M.; Mills, Ian G.; Vallis, Yvonne; Butler, P. Jonathan G.; Evans, Philip R.; McMahon, Harvey T. (2004): BAR domains as sensors of membrane curvature: the amphiphysin BAR structure. In: *Science (New York, N.Y.)* 303 (5657), S. 495–499. DOI: 10.1126/science.1092586.

Pichler, Harald; Emmerstorfer-Augustin, Anita (2018): Modification of membrane lipid compositions in single-celled organisms - From basics to applications. In: *Methods (San Diego, Calif.)* 147, S. 50–65. DOI: 10.1016/j.ymeth.2018.06.009.

Pielak, Rafal M.; Chou, James J. (2010): Kinetic analysis of the M2 proton conduction of the influenza virus. In: *Journal of the American Chemical Society* 132 (50), S. 17695–17697. DOI: 10.1021/ja108458u.

Pike, Linda J. (2009): The challenge of lipid rafts. In: *Journal of lipid research* 50 (Suppl), S323-8. DOI: 10.1194/jlr.R800040-JLR200.

Pinto, Lawrence H.; Holsinger, Leslie J.; Lamb, Robert A. (1992): Influenza virus M2 protein has ion channel activity. In: *Cell* 69 (3), S. 517–528. DOI: 10.1016/0092-8674(92)90452-I.

Pizzorno, Andrés; Abed, Yacine; Bouhy, Xavier; Beaulieu, Edith; Mallett, Corey; Russell, Rupert; Boivin, Guy (2012): Impact of mutations at residue I223 of the neuraminidase protein on the resistance profile, replication level, and virulence of the 2009 pandemic influenza virus. In: *Antimicrobial agents and chemotherapy* 56 (3), S. 1208–1214. DOI: 10.1128/AAC.05994-11.

Plant, Anne L. (1993): Self-assembled phospholipid/alkanethiol biomimetic bilayers on gold. In: *Langmuir* 9 (11), S. 2764–2767. DOI: 10.1021/la00035a004.

Polozov, Ivan V.; Bezrukov, Ludmila; Gawrisch, Klaus; Zimmerberg, Joshua (2008): Progressive ordering with decreasing temperature of the phospholipids of influenza virus. In: *Nature chemical biology* 4 (4), S. 248–255. DOI: 10.1038/nchembio.77.

R T Avalos; Z Yu; D P Nayak (1997): Association of influenza virus NP and M1 proteins with cellular cytoskeletal elements in influenza virus-infected cells. In: *Journal of virology* 71 (4), S. 2947–2958. Online verfügbar unter https://jvi.asm.org/content/71/4/2947.short.

Reinhardt, Jens; Wolff, Thorsten (2000): The influenza A virus M1 protein interacts with the cellular receptor of activated C kinase (RACK) 1 and can be phosphorylated by

protein kinase C. In: *Veterinary Microbiology* 74 (1-2), S. 87–100. DOI: 10.1016/S0378-1135(00)00169-3.

Richnau, Ninna; Fransson, Asa; Farsad, Khashayar; Aspenström, Pontus (2004): RICH-1 has a BIN/Amphiphysin/Rvsp domain responsible for binding to membrane lipids and tubulation of liposomes. In: *Biochemical and biophysical research communications* 320 (3), S. 1034–1042. DOI: 10.1016/j.bbrc.2004.05.221.

Ries, Jonas; Schwille, Petra (2006): Studying slow membrane dynamics with continuous wave scanning fluorescence correlation spectroscopy. In: *Biophysical journal* 91 (5), S. 1915–1924. DOI: 10.1529/biophysj.106.082297.

Ritacco, Hernán; Langevin, Dominique; Diamant, Haim; Andelman, David (2011): Dynamic surface tension of aqueous solutions of ionic surfactants: role of electrostatics. In: *Langmuir : the ACS journal of surfaces and colloids* 27 (3), S. 1009–1014. DOI: 10.1021/la103039v.

Roberts, Kari L.; Leser, George P.; Ma, Chunlong; Lamb, Robert A. (2013): The amphipathic helix of influenza A virus M2 protein is required for filamentous bud formation and scission of filamentous and spherical particles. In: *Journal of virology* 87 (18), S. 9973–9982. DOI: 10.1128/JVI.01363-13.

Roberts, P. C.; Compans, R. W. (1998): Host cell dependence of viral morphology. In: *Proceedings of the National Academy of Sciences of the United States of America* 95 (10), S. 5746–5751. DOI: 10.1073/pnas.95.10.5746.

Roberts, P. C.; Lamb, R. A.; Compans, R. W. (1998): The M1 and M2 proteins of influenza A virus are important determinants in filamentous particle formation. In: *Virology* 240 (1), S. 127–137. DOI: 10.1006/viro.1997.8916.

Róg, Tomasz; Pasenkiewicz-Gierula, Marta; Vattulainen, Ilpo; Karttunen, Mikko (2007): What happens if cholesterol is made smoother: importance of methyl substituents in cholesterol ring structure on phosphatidylcholine-sterol interaction. In: *Biophysical journal* 92 (10), S. 3346–3357. DOI: 10.1529/biophysj.106.095497.

Romero-Beltran, Lesly; Baker, Steven F.; Puerto-Solís, Marylin; González-Losa, Refugio; Conde-Ferraez, Laura; Alvarez-Sánchez, Leidi C. et al. (2016): Mutations at highly conserved residues in influenza A(H1N1)pdm09 virus affect neuraminidase activity. In: *Virus research* 225, S. 1–9. DOI: 10.1016/j.virusres.2016.09.002.

Rossman, Jeremy S.; Jing, Xianghong; Leser, George P.; Balannik, Victoria; Pinto, Lawrence H.; Lamb, Robert A. (2010a): Influenza virus m2 ion channel protein is necessary for filamentous virion formation. In: *Journal of virology* 84 (10), S. 5078–5088. DOI: 10.1128/JVI.00119-10.

Rossman, Jeremy S.; Jing, Xianghong; Leser, George P.; Lamb, Robert A. (2010b): Influenza virus M2 protein mediates ESCRT-independent membrane scission. In: *Cell* 142 (6), S. 902–913. DOI: 10.1016/j.cell.2010.08.029.

Rossman, Jeremy S.; Lamb, Robert A. (2011): Influenza virus assembly and budding. In: *Virology* 411 (2), S. 229–236. DOI: 10.1016/j.virol.2010.12.003.

Rossman, Jeremy S.; Lamb, Robert A. (2013): Viral membrane scission. In: *Annual review of cell and developmental biology* 29, S. 551–569. DOI: 10.1146/annurev-cellbio-101011-155838.

Rossman, Jeremy S.; Leser, George P.; Lamb, Robert A. (2012): Filamentous influenza virus enters cells via macropinocytosis. In: *Journal of virology* 86 (20), S. 10950–10960. DOI: 10.1128/JVI.05992-11.

Roux, Aurélien; Cuvelier, Damien; Nassoy, Pierre; Prost, Jacques; Bassereau, Patricia; Goud, Bruno (2005): Role of curvature and phase transition in lipid sorting and fission of membrane tubules. In: *The EMBO journal* 24 (8), S. 1537–1545. DOI: 10.1038/sj.emboj.7600631.

Roy, A. M.; Parker, J. S.; Parrish, C. R.; Whittaker, G. R. (2000): Early stages of influenza virus entry into Mv-1 lung cells: involvement of dynamin. In: *Virology* 267 (1), S. 17–28. DOI: 10.1006/viro.1999.0109.

Ruigrok, R. W.; Barge, A.; Durrer, P.; Brunner, J.; Ma, K.; Whittaker, G. R. (2000a): Membrane interaction of influenza virus M1 protein. In: *Virology* 267 (2), S. 289–298. DOI: 10.1006/viro.1999.0134.

Ruigrok, R. W.; Schoehn, G.; Dessen, A.; Forest, E.; Volchkov, V.; Dolnik, O. et al. (2000b): Structural characterization and membrane binding properties of the matrix protein VP40 of Ebola virus. In: *Journal of molecular biology* 300 (1), S. 103–112. DOI: 10.1006/jmbi.2000.3822.

Ruigrok, Rob W.H.; Calder, Lesley J.; Wharton, Stephen A. (1989): Electron microscopy of the influenza virus submembranal structure. In: *Virology* 173 (1), S. 311–316. DOI: 10.1016/0042-6822(89)90248-1.

Russell, R. J.; Stevens, D. J.; Haire, L. F.; Gamblin, S. J.; Skehel, J. J. (2006): Avian and human receptor binding by hemagglutinins of influenza A viruses. In: *Glycoconjugate journal* 23 (1-2), S. 85–92. DOI: 10.1007/s10719-006-5440-1.

Rust, Michael J.; Lakadamyali, Melike; Zhang, Feng; Zhuang, Xiaowei (2004): Assembly of endocytic machinery around individual influenza viruses during viral entry. In: *Nature structural & molecular biology* 11 (6), S. 567–573. DOI: 10.1038/nsmb769.

Rusten, Tor Erik; Stenmark, Harald (2006): Analyzing phosphoinositides and their interacting proteins. In: *Nature methods* 3 (4), S. 251–258. DOI: 10.1038/nmeth867.

Saeedimasine, Marzieh; Montanino, Annaclaudia; Kleiven, Svein; Villa, Alessandra (2019): Role of lipid composition on the structural and mechanical features of axonal membranes: a molecular simulation study. In: *Scientific reports* 9 (1), S. 8000. DOI: 10.1038/s41598-019-44318-9.

Safo, Martin K.; Musayev, Faik N.; Mosier, Philip D.; Zhou, Qibing; Xie, Hang; Desai, Umesh R. (2014): Crystal structures of influenza A virus matrix protein M1: variations on a theme. In: *PloS one* 9 (10), e109510. DOI: 10.1371/journal.pone.0109510.

Saletti, David; Radzimanowski, Jens; Effantin, Gregory; Midtvedt, Daniel; Mangenot, Stéphanie; Weissenhorn, Winfried et al. (2017): The Matrix protein M1 from influenza C virus induces tubular membrane invaginations in an in vitro cell membrane model. In: *Scientific reports* 7. DOI: 10.1038/srep40801.

Sanyal, Sumana; Menon, Anant K. (2009): Flipping lipids: why an' what's the reason for? In: *ACS chemical biology* 4 (11), S. 895–909. DOI: 10.1021/cb900163d.

Scheiffele, P.; Rietveld, A.; Wilk, T.; Simons, K. (1999): Influenza viruses select ordered lipid domains during budding from the plasma membrane. In: *The Journal of biological chemistry* 274 (4), S. 2038–2044. DOI: 10.1074/jbc.274.4.2038.

Scheiffele, P.; Roth, M. G.; Simons, K. (1997): Interaction of influenza virus haemagglutinin with sphingolipid-cholesterol membrane domains via its transmembrane domain. In: *The EMBO journal* 16 (18), S. 5501–5508. DOI: 10.1093/emboj/16.18.5501.

Schmidt, Nathan W.; Mishra, Abhijit; Wang, Jun; DeGrado, William F.; Wong, Gerard C. L. (2013): Influenza virus A M2 protein generates negative Gaussian membrane curvature necessary for budding and scission. In: *Journal of the American Chemical Society* 135 (37), S. 13710–13719. DOI: 10.1021/ja400146z.

Schmitt, Anthony P.; Lamb, Robert A. (2005): Influenza Virus Assembly and Budding at the Viral Budozone. In: Karl Maramorosch, Aaron J. Shatkin und Polly Roy (Hg.): Advances in virus research, Bd. 64. San Diego, Calif., London: Elsevier Academic (Advances in Virus Research), S. 383–416.

Schowalter, Rachel M.; Chang, Andres; Robach, Jessica G.; Buchholz, Ursula J.; Dutch, Rebecca Ellis (2009): Low-pH triggering of human metapneumovirus fusion: essential residues and importance in entry. In: *Journal of virology* 83 (3), S. 1511–1522. DOI: 10.1128/JVI.01381-08.

Schuck, Sebastian; Simons, Kai (2004): Polarized sorting in epithelial cells: raft clustering and the biogenesis of the apical membrane. In: *Journal of cell science* 117 (Pt 25), S. 5955–5964. DOI: 10.1242/jcs.01596.

Schulze, I. T. (1997): Effects of glycosylation on the properties and functions of influenza virus hemagglutinin. In: *The Journal of infectious diseases* 176 Suppl 1, S24-8. DOI: 10.1086/514170.

Schweitzer, Yonatan; Kozlov, Michael M. (2015): Membrane-mediated interaction between strongly anisotropic protein scaffolds. In: *PLoS computational biology* 11 (2), e1004054. DOI: 10.1371/journal.pcbi.1004054.

Seladi-Schulman, Jill; Steel, John; Lowen, Anice C. (2013): Spherical influenza viruses have a fitness advantage in embryonated eggs, while filament-producing strains are

selected in vivo. In: *Journal of virology* 87 (24), S. 13343–13353. DOI: 10.1128/JVI.02004-13.

Sergei L. Kosakovsky Pond, Art F.Y. Poon, Simon D.W. Frost (Hg.) (2007): Estimating selection pressures on alignments of coding sequences. Analyses using HyPhy. Online verfügbar unter https://www.ccg.unam.mx/~vinuesa/tlem/docs/hyphybook2007.pdf, zuletzt aktualisiert am 28.04.2020.000Z, zuletzt geprüft am 28.04.2020.

Sezgin, Erdinc; Levental, Ilya; Mayor, Satyajit; Eggeling, Christian (2017): The mystery of membrane organization: composition, regulation and physiological relevance of lipid rafts. In: *Nature reviews. Molecular cell biology* 18 (6), S. 361–374. DOI: 10.1038/nrm.2017.16.

Sha, B.; Luo, M. (1997a): Crystallization and preliminary X-ray crystallographic studies of type A influenza virus matrix protein M1. In: *Acta crystallographica. Section D, Biological crystallography* 53 (Pt 4), S. 458–460. DOI: 10.1107/S0907444997000152.

Sha, B.; Luo, M. (1997b): Structure of a bifunctional membrane-RNA binding protein, influenza virus matrix protein M1. In: *Nature structural biology* 4 (3), S. 239–244. DOI: 10.1038/nsb0397-239.

Shimbo, K.; Brassard, D. L.; Lamb, R. A.; Pinto, L. H. (1996): Ion selectivity and activation of the M2 ion channel of influenza virus. In: *Biophysical journal* 70 (3), S. 1335–1346. DOI: 10.1016/S0006-3495(96)79690-X.

Shin, Hye-Won; Takatsu, Hiroyuki; Nakayama, Kazuhisa (2012): Mechanisms of membrane curvature generation in membrane traffic. In: *Membranes* 2 (1), S. 118–133. DOI: 10.3390/membranes2010118.

Shishkov, A. V.; Goldanskii, V. I.; Baratova, L. A.; Fedorova, N. V.; Ksenofontov, A. L.; Zhirnov, O. P.; Galkin, A. V. (1999): The in situ spatial arrangement of the influenza A virus matrix protein M1 assessed by tritium bombardment. In: *Proceedings of the National Academy of Sciences of the United States of America* 96 (14), S. 7827–7830. DOI: 10.1073/pnas.96.14.7827.

Shishkov, Alexander; Bogacheva, Elena; Fedorova, Natalia; Ksenofontov, Alexander; Badun, Gennadii; Radyukhin, Victor et al. (2011): Spatial structure peculiarities of influenza A virus matrix M1 protein in an acidic solution that simulates the internal lysosomal medium. In: *The FEBS journal* 278 (24), S. 4905–4916. DOI: 10.1111/j.1742-4658.2011.08392.x.

Shishkov, Alexander V.; Bogacheva, Elena N.; Dolgov, Alexey A.; Chulichkov, Alexey L.; Knyazev, Denis G.; Fedorova, Natalia V. et al. (2009): The in situ structural characterization of the influenza A virus matrix M1 protein within a virion. In: *Protein and peptide letters* 16 (11), S. 1407–1413. DOI: 10.2174/092986609789353682.

Shortridge, K. F.; Zhou, N. N.; Guan, Y.; Gao, P.; Ito, T.; Kawaoka, Y. et al. (1998): Characterization of avian H5N1 influenza viruses from poultry in Hong Kong. In: *Virology* 252 (2), S. 331–342. DOI: 10.1006/viro.1998.9488.

Shtykova, Eleonora V.; Baratova, Lyudmila A.; Fedorova, Natalia V.; Radyukhin, Victor A.; Ksenofontov, Alexander L.; Volkov, Vladimir V. et al. (2013): Structural analysis of influenza A virus matrix protein M1 and its self-assemblies at low pH. In: *PloS one* 8 (12), e82431. DOI: 10.1371/journal.pone.0082431.

Shtykova, Eleonora V.; Dadinova, Liubov A.; Fedorova, Natalia V.; Golanikov, Andrey E.; Bogacheva, Elena N.; Ksenofontov, Alexander L. et al. (2017): Influenza virus Matrix Protein M1 preserves its conformation with pH, changing multimerization state at the priming stage due to electrostatics. In: *Scientific reports* 7 (1), S. 16793. DOI: 10.1038/s41598-017-16986-y.

Shtyrya, Y. A.; Mochalova, L. V.; Bovin, N. V. (2009): Influenza Virus Neuraminidase: Structure and Function. In: *Acta Naturae* 1 (2), S. 26–32.

Sieczkarski, Sara B.; Whittaker, Gary R. (2002): Influenza virus can enter and infect cells in the absence of clathrin-mediated endocytosis. In: *Journal of virology* 76 (20), S. 10455–10464. DOI: 10.1128/jvi.76.20.10455-10464.2002.

Simons, Kai; Gerl, Mathias J. (2010): Revitalizing membrane rafts: new tools and insights. In: *Nature reviews. Molecular cell biology* 11 (10), S. 688–699. DOI: 10.1038/nrm2977.

Simons, K.; Ikonen, E. Functional rafts in cell membranes. *Nature* 1997, *387*, 569–572, DOI: 10.1038/42408

Simons, Kai; Sampaio, Julio L. (2011): Membrane organization and lipid rafts. In: *Cold Spring Harbor perspectives in biology* 3 (10), a004697. DOI: 10.1101/cshperspect.a004697.

Simons K*,* Toomre D*.* Lipid rafts and signal transduction*. Nat Rev Mol Cell Biol.* 2000*;1(1):*31-39

Simpson-Holley, Martha; Ellis, Darren; Fisher, Dawn; Elton, Debra; McCauley, John; Digard, Paul (2002): A functional link between the actin cytoskeleton and lipid rafts during budding of filamentous influenza virions. In: *Virology* 301 (2), S. 212–225. DOI: 10.1006/viro.2002.1595.

Simunovic, Mijo; Voth, Gregory A.; Callan-Jones, Andrew; Bassereau, Patricia (2015): When Physics Takes Over: BAR Proteins and Membrane Curvature. In: *Trends in cell biology* 25 (12), S. 780–792. DOI: 10.1016/j.tcb.2015.09.005.

Smrt, Sean T.; Draney, Adrian W.; Lorieau, Justin L. (2015): The influenza hemagglutinin fusion domain is an amphipathic helical hairpin that functions by inducing membrane curvature. In: *The Journal of biological chemistry* 290 (1), S. 228–238. DOI: 10.1074/jbc.M114.611657.

Song, J.; Waugh, R. E. (1990): Bilayer membrane bending stiffness by tether formation from mixed PC-PS lipid vesicles. In: *Journal of biomechanical engineering* 112 (3), S. 235–240. DOI: 10.1115/1.2891178.

Soni, Smita P.; Adu-Gyamfi, Emmanuel; Yong, Sylvia S.; Jee, Clara S.; Stahelin, Robert V. (2013): The Ebola virus matrix protein deeply penetrates the plasma membrane: an

important step in viral egress. In: *Biophysical journal* 104 (9), S. 1940–1949. DOI: 10.1016/j.bpj.2013.03.021.

Stachowiak, Jeanne C.; Hayden, Carl C.; Sasaki, Darryl Y. (2010): Steric confinement of proteins on lipid membranes can drive curvature and tubulation. In: *Proceedings of the*

National Academy of Sciences of the United States of America 107 (17), S. 7781–7786. DOI: 10.1073/pnas.0913306107.

Stachowiak, Jeanne C.; Schmid, Eva M.; Ryan, Christopher J.; Ann, Hyoung Sook; Sasaki, Darryl Y.; Sherman, Michael B. et al. (2012): Membrane bending by protein-protein crowding. In: *Nature cell biology* 14 (9), S. 944–949. DOI: 10.1038/ncb2561.

Stahelin, Robert V. (2013): Surface plasmon resonance: a useful technique for cell biologists to characterize biomolecular interactions. In: *Molecular biology of the cell* 24 (7), S. 883–886. DOI: 10.1091/mbc.E12-10-0713.

Stauffer, Sarah; Feng, Yuehan; Nebioglu, Firat; Heilig, Rosalie; Picotti, Paola; Helenius, Ari (2014): Stepwise priming by acidic pH and a high K+ concentration is required for efficient uncoating of influenza A virus cores after penetration. In: *Journal of virology* 88 (22), S. 13029–13046. DOI: 10.1128/JVI.01430-14.

Steinhauer, D. A. (1999): Role of hemagglutinin cleavage for the pathogenicity of influenza virus. In: *Virology* 258 (1), S. 1–20. DOI: 10.1006/viro.1999.9716.

Stevens, James; Blixt, Ola; Tumpey, Terrence M.; Taubenberger, Jeffery K.; Paulson, James C.; Wilson, Ian A. (2006): Structure and receptor specificity of the hemagglutinin from an H5N1 influenza virus. In: *Science (New York, N.Y.)* 312 (5772), S. 404–410. DOI: 10.1126/science.1124513.

Su, Bin; Wurtzer, Sébastien; Rameix-Welti, Marie-Anne; Dwyer, Dominic; van der Werf, Sylvie; Naffakh, Nadia et al. (2009): Enhancement of the influenza A hemagglutinin (HA)-mediated cell-cell fusion and virus entry by the viral neuraminidase (NA). In: *PloS one* 4 (12), e8495. DOI: 10.1371/journal.pone.0008495.

Su, Wen-Chi; Yu, Wen-Ya; Huang, Shih-Han; Lai, Michael M. C. (2018): Ubiquitination of the Cytoplasmic Domain of Influenza A Virus M2 Protein Is Crucial for Production of Infectious Virus Particles. In: *Journal of virology* 92 (4). DOI: 10.1128/JVI.01972-17.

Subczynski, Witold K.; Pasenkiewicz-Gierula, Marta; Widomska, Justyna; Mainali, Laxman; Raguz, Marija (2017): High cholesterol/low cholesterol: Effects in biological membranes Review. In: *Cell biochemistry and biophysics* 75 (3-4), S. 369–385. DOI: 10.1007/s12013-017-0792-7.

Sun, Mingzhai; Northup, Nathan; Marga, Francoise; Huber, Tamas; Byfield, Fitzroy J.; Levitan, Irena; Forgacs, Gabor (2007): The effect of cellular cholesterol on membrane-cytoskeleton adhesion. In: *Journal of cell science* 120 (Pt 13), S. 2223–2231. DOI: 10.1242/jcs.001370.

Sun, Xiangjie; Whittaker, Gary R. (2007): Role of the actin cytoskeleton during influenza virus internalization into polarized epithelial cells. In: *Cellular microbiology* 9 (7), S. 1672–1682. DOI: 10.1111/j.1462-5822.2007.00900.x.

Suzuki, Y.; Gojobori, T. (1999): A method for detecting positive selection at single amino acid sites. In: *Molecular biology and evolution* 16 (10), S. 1315–1328. DOI: 10.1093/oxfordjournals.molbev.a026042.

Suzuki, Y.; Ito, T.; Suzuki, T.; Holland, R. E.; Chambers, T. M.; Kiso, M. et al. (2000): Sialic acid species as a determinant of the host range of influenza A viruses. In: *Journal of virology* 74 (24), S. 11825–11831. DOI: 10.1128/jvi.74.24.11825-11831.2000.

Takeda, Makoto; Leser, George P.; Russell, Charles J.; Lamb, Robert A. (2003): Influenza virus hemagglutinin concentrates in lipid raft microdomains for efficient viral fusion. In: *Proceedings of the National Academy of Sciences of the United States of America* 100 (25), S. 14610–14617. DOI: 10.1073/pnas.2235620100.

Takei, K.; Slepnev, V. I.; Haucke, V.; Camilli, P. de (1999): Functional partnership between amphiphysin and dynamin in clathrin-mediated endocytosis. In: *Nature cell biology* 1 (1), S. 33–39. DOI: 10.1038/9004.

Tang, Yijun; Zeng, Xiangqun; Liang, Jennifer (2010): Surface Plasmon Resonance: An Introduction to a Surface Spectroscopy Technique. In: *Journal of chemical education* 87 (7), S. 742–746. DOI: 10.1021/ed100186y.

Tao, Yitzhi Jane; Zheng, Wenjie (2012): Biochemistry. Visualizing the influenza genome. In: *Science (New York, N.Y.)* 338 (6114), S. 1545–1546. DOI: 10.1126/science.1231588.

Taubenberger, Jeffery K.; Morens, David M. (2008): The pathology of influenza virus infections. In: *Annual review of pathology* 3, S. 499–522. DOI: 10.1146/annurev.pathmechdis.3.121806.154316.

Terrettaz, Samuel; Stora, Thierry; Duschl, Claus; Vogel, Horst (1993): Protein binding to supported lipid membranes: investigation of the cholera toxin-ganglioside interaction by simultaneous impedance spectroscopy and surface plasmon resonance. In: *Langmuir* 9 (5), S. 1361–1369. DOI: 10.1021/la00029a033.

Thaa, Bastian; Herrmann, Andreas; Veit, Michael (2009): The polybasic region is not essential for membrane binding of the matrix protein M1 of influenza virus. In: *Virology* 383 (1), S. 150–155. DOI: 10.1016/j.virol.2008.10.001.

Treanor, J. J.; Tierney, E. L.; Zebedee, S. L.; Lamb, R. A.; Murphy, B. R. (1990): Passively transferred monoclonal antibody to the M2 protein inhibits influenza A virus replication in mice. In: *Journal of virology* 64 (3), S. 1375–1377.

Trebbien, Ramona; Larsen, Lars E.; Viuff, Birgitte M. (2011): Distribution of sialic acid receptors and influenza A virus of avian and swine origin in experimentally infected pigs. In: *Virology journal* 8, S. 434. DOI: 10.1186/1743-422X-8-434.

Tsfasman, Tatyana; Kost, Vladimir; Markushin, Stanislav; Lotte, Vera; Koptiaeva, Irina; Bogacheva, Elena et al. (2015): Amphipathic alpha-helices and putative cholesterol binding domains of the influenza virus matrix M1 protein are crucial for virion structure organisation. In: *Virus research* 210, S. 114–118. DOI: 10.1016/j.virusres.2015.07.017.

Tsukamoto, Manami; Kuroda, Kenichi; Ramamoorthy, Ayyalusamy; Yasuhara, Kazuma (2014): Modulation of raft domains in a lipid bilayer by boundary-active curcumin. In: *Chemical communications (Cambridge, England)* 50 (26), S. 3427–3430. DOI: 10.1039/c3cc47738j.

van Meer, Gerrit; Kroon, Anton I. P. M. de (2011): Lipid map of the mammalian cell. In: *Journal of cell science* 124 (Pt 1), S. 5–8. DOI: 10.1242/jcs.071233.

Vance, J. E. (1990): Phospholipid synthesis in a membrane fraction associated with mitochondria. In: *The Journal of biological chemistry* 265 (13), S. 7248–7256.

Vance, Jean E. (2008): Phosphatidylserine and phosphatidylethanolamine in mammalian cells: two metabolically related aminophospholipids. In: *Journal of lipid research* 49 (7), S. 1377–1387. DOI: 10.1194/jlr.R700020-JLR200.

Vanni, Stefano; Vamparys, Lydie; Gautier, Romain; Drin, Guillaume; Etchebest, Catherine; Fuchs, Patrick F. J.; Antonny, Bruno (2013): Amphipathic lipid packing sensor motifs: probing bilayer defects with hydrophobic residues. In: *Biophysical journal* 104 (3), S. 575–584. DOI: 10.1016/j.bpj.2012.11.3837.

Veatch, Sarah L.; Keller, Sarah L. (2003): Separation of Liquid Phases in Giant Vesicles of Ternary Mixtures of Phospholipids and Cholesterol. In: *Biophysical journal* 85 (5), S. 3074–3083. DOI: 10.1016/S0006-3495(03)74726-2.

Veit, Michael; Thaa, Bastian (2011): Association of influenza virus proteins with membrane rafts. In: *Advances in virology* 2011, S. 370606. DOI: 10.1155/2011/370606.

Verma, Dileep Kumar; Gupta, Dinesh; Lal, Sunil Kumar (2018): Host Lipid Rafts Play a Major Role in Binding and Endocytosis of Influenza A Virus. In: *Viruses* 10 (11). DOI: 10.3390/v10110650.

Vijayakrishnan, Swetha; Loney, Colin; Jackson, David; Suphamungmee, Worawit; Rixon, Frazer J.; Bhella, David (2013): Cryotomography of budding influenza A virus reveals filaments with diverse morphologies that mostly do not bear a genome at their distal end. In: *PLoS pathogens* 9 (6), e1003413. DOI: 10.1371/journal.ppat.1003413.

Vivek Darapaneni (2015): Large-scale Analysis of Influenza A Virus Sequences Reveals Universally Conserved Residues of Matrix Proteins. In: *American Journal of Current Microbiology* 3 (1), S. 1–13.

Voeltz, Gia K.; Prinz, William A.; Shibata, Yoko; Rist, Julia M.; Rapoport, Tom A. (2006): A class of membrane proteins shaping the tubular endoplasmic reticulum. In: *Cell* 124 (3), S. 573–586. DOI: 10.1016/j.cell.2005.11.047.

Vries, Erik de; Tscherne, Donna M.; Wienholts, Marleen J.; Cobos-Jiménez, Viviana; Scholte, Florine; García-Sastre, Adolfo et al. (2011): Dissection of the influenza A virus endocytic routes reveals macropinocytosis as an alternative entry pathway. In: *PLoS pathogens* 7 (3), e1001329. DOI: 10.1371/journal.ppat.1001329.

Wallace, Elizabeth J.; Hooper, Nigel M.; Olmsted, Peter D. (2006): Effect of hydrophobic mismatch on phase behavior of lipid membranes. In: *Biophysical journal* 90 (11), S. 4104–4118. DOI: 10.1529/biophysj.105.062778.

Wang, Chang; Krause, Martin R.; Regen, Steven L. (2015): Push and pull forces in lipid raft formation: the push can be as important as the pull. In: *Journal of the American Chemical Society* 137 (2), S. 664–666. DOI: 10.1021/ja5115437.

Wang, Dan; Harmon, Aaron; Jin, Jing; Francis, David H.; Christopher-Hennings, Jane; Nelson, Eric et al. (2010): The lack of an inherent membrane targeting signal is responsible for the failure of the matrix (M1) protein of influenza A virus to bud into virus-like particles. In: *Journal of virology* 84 (9), S. 4673–4681. DOI: 10.1128/JVI.02306-09.

Wang, Jiyao; Gambhir, Alok; Hangyás-Mihályné, Gyöngyi; Murray, Diana; Golebiewska, Urszula; McLaughlin, Stuart (2002): Lateral sequestration of phosphatidylinositol 4,5-bisphosphate by the basic effector domain of myristoylated alanine-rich C kinase substrate is due to nonspecific electrostatic interactions. In: *The Journal of biological chemistry* 277 (37), S. 34401–34412. DOI: 10.1074/jbc.M203954200.

Wang, Jun; Qiu, Jade Xiaoyan; Soto, Cinque; DeGrado, William F. (2011): Structural and dynamic mechanisms for the function and inhibition of the M2 proton channel from influenza A virus. In: *Current opinion in structural biology* 21 (1), S. 68–80. DOI: 10.1016/j.sbi.2010.12.002.

Wang, Shanshan; Zhao, Zhendong; Bi, Yuhai; Sun, Lei; Liu, Xiaoling; Liu, Wenjun (2013): Tyrosine 132 phosphorylation of influenza A virus M1 protein is crucial for virus replication by controlling the nuclear import of M1. In: *Journal of virology* 87 (11), S. 6182–6191. DOI: 10.1128/JVI.03024-12.

Wang, Zhen; Schey, Kevin L. (2015): Proteomic Analysis of Lipid Raft-Like Detergent-Resistant Membranes of Lens Fiber Cells. In: *Investigative ophthalmology & visual science* 56 (13), S. 8349–8360. DOI: 10.1167/iovs.15-18273.

Wang, Zheng; Daum, Luke T.; Vora, Gary J.; Metzgar, David; Walter, Elizabeth A.; Canas, Linda C. et al. (2006): Identifying influenza viruses with resequencing microarrays. In: *Emerging infectious diseases* 12 (4), S. 638–646. DOI: 10.3201/eid1204.051441.

Ward, Colin W.; Colman, Peter M.; Laver, W.Graeme (1983): The disulphide bonds of an Asian influenza virus neuraminidase. In: *FEBS letters* 153 (1), S. 29–33. DOI: 10.1016/0014-5793(83)80113-6.

Wasilewski, Sebastian; Calder, Lesley J.; Grant, Tim; Rosenthal, Peter B. (2012): Distribution of surface glycoproteins on influenza A virus determined by electron cryotomography. In: *Vaccine* 30 (51), S. 7368–7373. DOI: 10.1016/j.vaccine.2012.09.082.

Waugh, R. E.; Song, J.; Svetina, S.; Zeks, B. (1992): Local and nonlocal curvature elasticity in bilayer membranes by tether formation from lecithin vesicles. In: *Biophysical journal* 61 (4), S. 974–982. DOI: 10.1016/S0006-3495(92)81904-5.

Weber, Friedemann; Elliott, Richard M. (2002): Antigenic drift, antigenic shift and interferon antagonists: how bunyaviruses counteract the immune system. In: *Virus research* 88 (1-2), S. 129–136. DOI: 10.1016/S0168-1702(02)00125-9.

Wharton, S. A.; Belshe, R. B.; Skehel, J. J.; Hay, A. J. (1994): Role of virion M2 protein in influenza virus uncoating: specific reduction in the rate of membrane fusion between

virus and liposomes by amantadine. In: *The Journal of general virology* 75 (Pt 4), S. 945–948. DOI: 10.1099/0022-1317-75-4-945.

Wikramaratna, Paul S.; Sandeman, Michi; Recker, Mario; Gupta, Sunetra (2013): The antigenic evolution of influenza: drift or thrift? In: *Philosophical transactions of the Royal Society of London. Series B, Biological sciences* 368 (1614), S. 20120200. DOI: 10.1098/rstb.2012.0200.

Wilson, Robert L.; Frisz, Jessica F.; Klitzing, Haley A.; Zimmerberg, Joshua; Weber, Peter K.; Kraft, Mary L. (2015): Hemagglutinin clusters in the plasma membrane are not enriched with cholesterol and sphingolipids. In: *Biophysical journal* 108 (7), S. 1652–1659. DOI: 10.1016/j.bpj.2015.02.026.

Wohlgemuth, Nicholas; Lane, Andrew P.; Pekosz, Andrew (2018): Influenza A Virus M2 Protein Apical Targeting Is Required for Efficient Virus Replication. In: *Journal of virology* 92 (22). DOI: 10.1128/JVI.01425-18.

Woods, Parker S.; Doolittle, Lauren M.; Rosas, Lucia E.; Joseph, Lisa M.; Calomeni, Edward P.; Davis, Ian C. (2016): Lethal H1N1 influenza A virus infection alters the murine alveolar type II cell surfactant lipidome. In: *American journal of physiology. Lung cellular and molecular physiology* 311 (6), L1160-L1169. DOI: 10.1152/ajplung.00339.2016.

Worch, Remigiusz (2014): Structural biology of the influenza virus fusion peptide. In: *Acta biochimica Polonica* 61 (3), S. 421–426.

Wu, Chung-Yi; Jeng, King-Song; Lai, Michael M-C (2011): The SUMOylation of matrix protein M1 modulates the assembly and morphogenesis of influenza A virus. In: *Journal of virology* 85 (13), S. 6618–6628. DOI: 10.1128/JVI.02401-10.

Xu, Rui; Wilson, Ian A. (2011): Structural characterization of an early fusion intermediate of influenza virus hemagglutinin. In: *Journal of virology* 85 (10), S. 5172–5182. DOI: 10.1128/JVI.02430-10.

Yamada, Shinya; Suzuki, Yasuo; Suzuki, Takashi; Le, Mai Q.; Nidom, Chairul A.; Sakai-Tagawa, Yuko et al. (2006): Haemagglutinin mutations responsible for the binding of H5N1 influenza A viruses to human-type receptors. In: *Nature* 444 (7117), S. 378–382. DOI: 10.1038/nature05264.

Yamamoto-Goshima, F.; Maeno, K. (1994): Approach to the involvement of influenza B neuraminidase in the cleavage of HA by host cell protease using low pH-induced cell fusion reaction. In: *Microbiology and immunology* 38 (10), S. 819–822. DOI: 10.1111/j.1348-0421.1994.tb01864.x.

Yandrapalli, Naresh; Lubart, Quentin; Tanwar, Hanumant S.; Picart, Catherine; Mak, Johnson; Muriaux, Delphine; Favard, Cyril (2016): Self assembly of HIV-1 Gag protein on lipid membranes generates PI(4,5)P2/Cholesterol nanoclusters. In: *Scientific reports* 6, S. 39332. DOI: 10.1038/srep39332.

Yang, Xiaoyun; Steukers, Lennert; Forier, Katrien; Xiong, Ranhua; Braeckmans, Kevin; van Reeth, Kristien; Nauwynck, Hans (2014): A beneficiary role for neuraminidase in influenza virus penetration through the respiratory mucus. In: *PloS one* 9 (10), e110026. DOI: 10.1371/journal.pone.0110026.

Yánguez, Emilio; Hunziker, Annika; Dobay, Maria Pamela; Yildiz, Soner; Schading, Simon; Elshina, Elizaveta et al. (2018): Phosphoproteomic-based kinase profiling early in influenza virus infection identifies GRK2 as antiviral drug target. In: *Nature communications* 9 (1), S. 3679. DOI: 10.1038/s41467-018-06119-y.

Ye, Z. P.; Pal, R.; Fox, J. W.; Wagner, R. R. (1987): Functional and antigenic domains of the matrix (M1) protein of influenza A virus. In: *Journal of virology* 61 (2), S. 239–246.

Ye, Zhiping; Liu, Teresa; Offringa, Daniel P.; McInnis, Jonathan; Levandowski, Roland A. (1999): Association of Influenza Virus Matrix Protein with Ribonucleoproteins. In: *Journal of virology* 73 (9), S. 7467–7473.

Yeung, Tony; Gilbert, Gary E.; Shi, Jialan; Silvius, John; Kapus, Andras; Grinstein, Sergio (2008): Membrane phosphatidylserine regulates surface charge and protein localization. In: *Science (New York, N.Y.)* 319 (5860), S. 210–213. DOI: 10.1126/science.1152066.

Yu, Kuo-Long; Torri, Albert F.; Luo, Guangxiang; Cianci, Christopher; Grant-Young, Katharine; Danetz, Stephanie et al. (2002): Structure–activity relationships for a series of thiobenzamide influenza fusion inhibitors derived from 1,3,3-Trimethyl-5-hydroxy-cyclohexylmethylamine. In: *Bioorganic & Medicinal Chemistry Letters* 12 (23), S. 3379–3382. DOI: 10.1016/S0960-894X(02)00761-8.

Yu, Maorong; Liu, Xiaoling; Cao, Shuai; Zhao, Zhendong; Zhang, Ke; Xie, Qing et al. (2012): Identification and characterization of three novel nuclear export signals in the influenza A virus nucleoprotein. In: *Journal of virology* 86 (9), S. 4970–4980. DOI: 10.1128/JVI.06159-11.

Yu, Qiuhong; Sun, Jianbo; Huang, Siqi; Chang, Haojing; Bai, Qingwen; Chen, Yong-Xiang; Liang, Dehai (2018): Inward Budding and Endocytosis of Membranes Regulated by de Novo Designed Peptides. In: *Langmuir : the ACS journal of surfaces and colloids* 34 (21), S. 6183–6193. DOI: 10.1021/acs.langmuir.8b00882.

Yuan, Shuofeng; Chu, Hin; Chan, Jasper Fuk-Woo; Ye, Zi-Wei; Wen, Lei; Yan, Bingpeng et al. (2019): SREBP-dependent lipidomic reprogramming as a broad-spectrum antiviral target. In: *Nature communications* 10 (1), S. 120. DOI: 10.1038/s41467-018-08015-x.

Zhang, Jie; Pekosz, Andrew; Lamb, Robert A. (2000): Influenza Virus Assembly and Lipid Raft Microdomains: a Role for the Cytoplasmic Tails of the Spike Glycoproteins. In: *Journal of virology* 74 (10), S. 4634–4644.

Zhang, Ke; Wang, Zhao; Fan, Gui-Zhen; Wang, Juan; Gao, Shengyan; Li, Yun et al. (2015): Two polar residues within C-terminal domain of M1 are critical for the formation of influenza A Virions. In: *Cellular microbiology* 17 (11), S. 1583–1593. DOI: 10.1111/cmi.12457.

Zhang, Ke; Wang, Zhao; Liu, Xiaoling; Yin, Changcheng; Basit, Zeshan; Xia, Bin; Liu, Wenjun (2012): Dissection of influenza A virus M1 protein: pH-dependent oligomerization of N-terminal domain and dimerization of C-terminal domain. In: *PloS one* 7 (5), e37786. DOI: 10.1371/journal.pone.0037786.

Zhang, Lei; Zhao, Lisha; Ouyang, Ping-Kai; Chen, Pu (2019): Insight into the role of cholesterol in modulation of morphology and mechanical properties of CHO-K1 cells: An in situ AFM study. In: *Front. Chem. Sci. Eng.* 13 (1), S. 98–107. DOI: 10.1007/s11705-018-1775-y.

Zhang, Wenting; Zheng, Wenjie; Toh, Yukimatsu; Betancourt-Solis, Miguel A.; Tu, Jiagang; Fan, Yanlin et al. (2017): Crystal structure of an orthomyxovirus matrix protein reveals mechanisms for self-polymerization and membrane association. In: *Proceedings of the National Academy of Sciences of the United States of America* 114 (32), S. 8550–8555. DOI: 10.1073/pnas.1701747114.

Zhang, Xinsheng; Oglesbee, Michael (2003): Use of surface plasmon resonance for the measurement of low affinity binding interactions between HSP72 and measles virus nucleocapsid protein. In: *Biological procedures online* 5, S. 170–181. DOI: 10.1251/bpo59.

Zhao, Hongxia; Michelot, Alphée; Koskela, Essi V.; Tkach, Vadym; Stamou, Dimitrios; Drubin, David G.; Lappalainen, Pekka (2013): Membrane-sculpting BAR domains generate stable lipid microdomains. In: *Cell reports* 4 (6), S. 1213–1223. DOI: 10.1016/j.celrep.2013.08.024.

Zhirnov, O. P. (1990): Solubilization of matrix protein M1/M from virions occurs at different pH for orthomyxo- and paramyxoviruses. In: *Virology* 176 (1), S. 274–279. DOI: 10.1016/0042-6822(90)90253-N.

Zhirnov, O. P. (1992): Isolation of matrix protein M1 from influenza viruses by acid-dependent extraction with nonionic detergent. In: *Virology* 186 (1), S. 324–330. DOI: 10.1016/0042-6822(92)90090-C.

Zimmerberg, Joshua; Kozlov, Michael M. (2006): How proteins produce cellular membrane curvature. In: *Nature reviews. Molecular cell biology* 7 (1), S. 9–19. DOI: 10.1038/nrm1784.

List of Figures

144

Acknowledgments

Eidesstattliche Erklärung

und Einverständniserklärung

nach § 6 Abs. 2 Nr. 5, 6 und 7 der Promotionsordnung der Wirtschafts- und Sozialwissenschaftlichen Fakultät der Universität Potsdam vom 10.07.2013

Von:

Name: Dahmani

Vorname(n):   Ismail

Hiermit versichere ich an Eides statt, dass

- meine hinsichtlich der früheren Teilnahme an Promotionsverfahren gemachten Angaben richtig sind;
- die eingereichte Arbeit oder wesentliche Teile derselben in keinem anderen Verfahren zur Erlangung eines akademischen Grades vorgelegt worden sind;
- bei der Anfertigung der Dissertation die Grundsätze zur Sicherung guter wissenschaftlicher Praxis der DFG eingehalten wurden, die Dissertation selbständig und ohne fremde Hilfe verfasst wurde, andere als die von mir angegebenen Quellen und Hilfsmittel nicht benutzt worden sind und die den benutzten Werken wörtlich oder sinngemäß entnommenen Stellen als solche kenntlich gemacht wurden.

Einer Überprüfung der eingereichten Dissertationsschrift bzw. der an deren Stelle eingereichten Schriften mittels einer Plagiatssoftware stimme ich zu.

_____   _____

Ort/Datum   Unterschrift